ELSEVIER

Contents lists available at ScienceDirect

Powder Technology

journal homepage: www.journals.elsevier.com/powder-technology





Synergistic approach to colloidal stability and thermophysical optimisation of multi-walled carbon nanotubes, aluminium nitride, and silver-based hybrid nanofluids

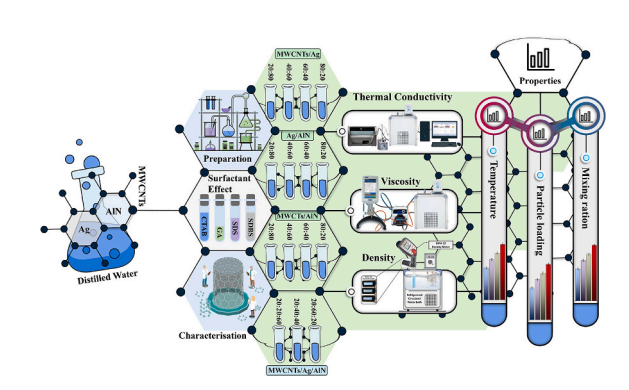
Hamza Babar ^{a,*}, Hongwei Wu ^{a,*}, Wenbin Zhang ^b, Muhammad Asim ^c, Ali Koşar ^{d,e,f}

- ^a School of Physics, Engineering and Computer Science, University of Hertfordshire, Hatfield AL10 9AB, United Kingdom
- ^b School of Science and Technology, Nottingham Trent University, Clifton Lane, Nottingham NG11 8NS, United Kingdom
- ^c Division of Science, Engineering, and Health Studies (SEHS), School of Professional Education & Executive Development, The Hong Kong Polytechnic University, Hong Kong
- ^d Faculty of Engineering and Natural Sciences, Sabanci University, Istanbul 34956, Turkey
- ^e Sabanci University Nanotechnology and Applications Center (SUNUM), Sabanci University, Tuzla, Istanbul 34956, Turkey
- f Center of Excellence for Functional Surfaces and Interfaces for Nano-Diagnostics (EFSUN), Sabanci University, Istanbul 34956, Turkey

HIGHLIGHTS

- Tri-hybrid nanofluids balanced thermal performance, stability, and costeffectiveness.
- Surfactant choice and pH optimisation proved critical for sustained colloidal stability.
- Synergistic nanoparticle interactions improved thermal conductivity and redispersion ability.
- SDBS-enhanced dispersion reduced sedimentation and agglomeration for long-term stability.
- Statistical models accurately predicted nanofluid properties across varying compositions.

G R A P H I C A L A B S T R A C T



ARTICLE INFO

Keywords:
Hybrid nanofluid
Stability
Surfactant
Thermophysical properties
Heat transfer

ABSTRACT

Efficient thermal management is essential for high-performance applications such as electronics cooling, electric vehicles, and energy systems, where conventional coolants often fail to meet performance demands. This study aims to address the limitations of conventional coolants by formulating and evaluating advanced hybrid and tri-hybrid nanofluids composed of multi-walled carbon nanotubes (MWCNTs), silver (Ag), and aluminium nitride (AlN). A two-step preparation method was employed to formulate various nanofluid formulations and investigate the effects of nanoparticle volumetric ratios and different surfactants, including sodium dodecyl sulfate (SDS), cetyltrimethylammonium bromide (CTAB), gum arabic (GA), and sodium dodecyl benzene sulfonate (SDBS) on colloidal stability, heat transfer characteristics, and cost-effectiveness. Nanofluid formulations were prepared using volumetric ratios of 80:20, 60:40, 40:60, and 20:80 for hybrid combinations, and 20/20/60, 20/40/40, and 20/60/20 for tri-hybrid mixtures, and analysed over a temperature range of 20 to 45 °C. Experimental results revealed that SDBS consistently outperformed the others, by maintaining a stable suspension and thus preserving

E-mail addresses: h.babar@herts.ac.uk (H. Babar), h.wu6@herts.ac.uk (H. Wu).

^{*} Corresponding authors.

the enhanced thermal properties over extended periods. Among all tested nanofluids, MWCNTs exhibited the highest thermal conductivity enhancement of $8.57\,\%$. The tri-hybrid formulation with a $20/60/20\,\text{MWCNTs/Ag/AlN}$ ratio achieved a comparable enhancement of $8.14\,\%$, demonstrating that optimised combinations of nanoparticles can simultaneously deliver high thermal performance, good stability, and reasonable cost-efficiency. However, this tri-hybrid formulation also showed the highest viscosity increase noted to be $5.55\,\%$, compared to a $4.43\,\%$ increase for simple Ag nanofluids. Additionally, the highest density increase was $0.25\,\%$ for Ag, while the highest among hybrid combinations was $0.22\,\%$ for the $80/20\,\text{Ag/AlN}$ mixture. Finally, among tri-hybrid formulations, the $20/60/20\,$ ratio showed the highest increase of $0.19\,\%$, whereas the $20/40/40\,$ ratio exhibited a more moderate increase. Cost analysis indicated that the tri-hybrid nanofluid with a $20/40/40\,$ ratio is the most cost-effective option when cost considerations are as important as thermal performance. However, for applications where maximising thermal performance is crucial, the tri-hybrid with a $20/60/20\,$ ratio is the preferred choice. This work contributes new insights into the development of multifunctional nanofluids and presents comprehensive investigations into MWCNTs, Ag, and AlN-based tri-hybrid formulations.

1. Introduction

The increasing demand for efficient thermal management in highperformance systems has driven the exploration of innovative cooling fluids with superior heat transfer capabilities. In recent years, rapid advancements in artificial intelligence (AI) technologies have further intensified the need for compact and highly effective thermal management systems, capable of handling the substantial heat generated by high-performance computing. According to the International Energy Agency (IEA), in 2022, global data centre electricity consumption was estimated to be between 240 and 340 TWh [1]. The other industry gaining attention is electric vehicles (EVs) which brought heightened attention to the automotive sector, where effective thermal management is essential for improving performance, safety, and extending battery life. The electric vehicle market is projected to experience substantial growth in the coming years, IEA reported that the global stock of EVs surpassed 10 million in 2022, a significant increase from 3 million in 2019 [2]. This growth places additional pressure on the development of efficient battery cooling systems, as improper thermal management can lead to critical failures such as thermal runaway. As industries move towards more compact and energy-efficient designs, there is a critical need to develop thermal solutions that not only manage heat effectively but also reduce energy consumption. Traditional coolants, such as water (W) and ethylene glycol (EG), often fall short in meeting the heat dissipation needs of advanced technologies, leading to the growing interest in nanofluids (NFs).

Researchers are actively exploring hybrid systems that combine different cooling strategies to optimise heat transfer efficiency [3–5]. Alongside efforts to design more efficient heat sinks, there has been a continuous push to develop thermal coolants with improved thermophysical properties. Among these, nanofluids have gained attention due to their enhanced thermal performance compared to conventional fluids. Hybrid nanofluids (HNFs), which incorporate two or more types of nanoparticles, offer even greater potential by combining the distinct properties of different materials to improve heat transfer.

This study focuses on a comprehensive exploration of the thermophysical characteristics of the hybrid and tri-hybrid nanofluids containing MWCNTs, AlN, and Ag nanoparticles. These nanoparticles, known for their unique properties, offer a synergistic effect when combined, potentially delivering superior thermal conductivity (TC), stability, and overall heat transfer capability. Understanding the behaviour of such complex nanofluids under varying conditions is crucial for optimising their application in high-performance cooling systems for electronics, data centres, and energy storage systems.

The field of nanofluids is inherently complex, as their thermophysical properties are influenced by a multitude of factors. Stability remains a significant challenge in the effective application of nanofluids, as agglomeration and sedimentation can severely hinder performance. Therefore, experimental investigations have become increasingly vital to understanding and optimising these materials. By systematically analysing the effects of various additives, surfactants, and preparation

methods, researchers aim to enhance the stability and heat transfer characteristics of nanofluids, paving the way for their successful integration into advanced thermal management solutions. Xian et al. [6] examined the influence of various surfactants and ultrasonication duration on the stability and thermophysical properties of HNFs, using the two-step method to disperse titania (TiO2) and graphene nanoplatelets (GnPs) in a water/ethylene glycol (W/EG) mixture. Their findings revealed that the addition of hexadecyltrimethylammonium bromide (CTAB) significantly enhanced stability, with minimal sedimentation observed over a 40-day period. The study also varied the sonication time between 15 and 90 min, revealing that longer sonication times further enhanced stability. Furthermore, thermal conductivity measurements exhibited a maximum enhancement of 23.74 % when 0.1 wt% of carboxyl-functionalised GnPs was incorporated at 60 °C, demonstrating that hybrid nanofluids outperformed their mono counterparts across varying concentrations and temperatures. Their findings suggested that the hybrid nanofluids possess promising properties for applications in heat transfer systems. Tiwari et al. [7] conducted an experimental study on CeO2-MWCNT/water hybrid nanofluid, examining synthesis, surfactant, sonication, and stability (4S consideration). The nanofluid was prepared using a two-step method, with varying ultrasonication times (30 to 180 min) and six different surfactants (anionic, cationic, and polymeric) tested at different nanoparticle-tosurfactant ratios. They concluded that optimal conditions for longterm stability included a surfactant-to-nanoparticle ratio of 3:2, a pH of 9.5, and 90 min of sonication, which produced the highest zeta potential. The CTAB surfactant provided the best stability for up to 30 days, while the sodium dodecyl benzenesulfonate (SDBS) surfactant exhibited superior stability beyond that timeframe. A correlation between hybrid stabilization and thermal conductivity was observed, indicating that excessive surfactant reduced conductivity. Additionally, the impact of surfactants on surface tension was also investigated and proposed a correlation for predicting thermal conductivity values. Babar et al. [8] conducted a comprehensive investigation into the thermophysical properties and stability of hybrid nanofluids formulated by dispersing silver, beryllium oxide, and silicon carbide nanoparticles in water. Their study demonstrated that the use of surfactants significantly enhanced the stability of these nanofluids, while the specific mixing ratios of nanoparticles played a crucial role in optimising both thermal conductivity and overall performance. The results showed that hybrid nanofluids, particularly Ag/SiC at a 60:40 ratio, achieved up to a 7.43 % improvement in thermal conductivity compared to water, while maintaining manageable increases in viscosity and density. The study concluded that careful selection of nanoparticle combinations allowed for the optimisation of both performance and cost, with Ag-SiC hybrids providing an effective balance for advanced heat transfer applications.

Kumar et al. [9] prepared the hybrid nanofluid intending to improve the thermal conductivity of CuO/water nanofluids, which suffer from poor conductivity due to the stability and morphology of CuO nanoparticles. They proposed a novel strategy of mixing polyhedron-shaped MgO nanoparticles with CuO nanoparticles to enhance the thermal conductivity of the resulting nanofluid. The study used a CuO/MgO with a weight ratio of 7:3 and investigated volume fractions ranging from 0.25 % to 1.5 % in water at temperatures between 30 °C and 55 °C. A two-step approach was adopted for nanofluid preparation and conducted various analyses, including XRD and stability examinations, to characterise the nanoparticles and ensure the quality of the nanofluid. The findings demonstrated a notable improvement in thermal conductivity, particularly at higher temperatures, with a 12.5 % increase observed at 55 °C and a volume fraction of 1.5 %. Mane et al. [10] studied the electrical conductivity of water-based nanofluids containing CuO, Fe₃O₄, and hybrid CuO/Fe₃O₄ nanoparticles, stabilised with biopolymer dispersants (gum arabica and chitosan) and a synthetic dispersant (SDBS). Nanofluids were prepared with a 0.1 wt% nanoparticle concentration and dispersant concentrations of 0.05 and 0.5 wt %, and electrical conductivity was measured over a temperature range of 25 °C to 40 °C. The results showed dispersants significantly influenced conductivity, while nanoparticle type had little effect. SDBS-stabilised nanofluids at 0.5 wt% showed conductivity 708.7 times more than the base fluid, while chitosan and gum arabic-stabilised nanofluids exhibited conductivities 144.2 and 12.8 times higher, respectively. Additionally, quadratic nonlinear polynomial equations were developed using response surface methodology (RSM) to predict conductivity, offering key insights into the electrical behaviour of biopolymer-stabilised nanofluids. Adam et al. [11] investigated the optical properties and colloid stability of SiO2-water nanofluids for hybrid thermal/photovoltaic applications at elevated temperatures. Different nanoparticle volume fractions were synthesised, ranging from 0.0011 % to 0.0367 %, and factors such as sonication temperature, nanoparticle concentration, exposure temperature, and exposure time were examined. Their findings exhibited that reducing the temperature during sonication while preparing the fluid improved stability, with 30 °C yielding the best results. The absorptance of the nanofluids decreased with increasing exposure temperatures from 25 °C to 90 °C, with higher temperatures resulting in increased agglomeration. Their study also assessed the energy performance of a concentrating photovoltaic/thermal (CPVT) system using the NFs as optical filters instead of water. Despite some stability challenges at elevated temperatures, the SiO2-H2O HNFs showed promise for enhancing the efficiency of CPVT devices, providing valuable insights into the temperature-dependent behaviour of nanofluids for solar energy applications. Duan et al. [12] numerically analysed transient natural convection and entropy generation in a 3D cylindrical microtube filled with a hybrid nanofluid composed of Al₂O₃ and Cu nanoparticles suspended in water, targeting biomedical applications such as targeted drug delivery and microfluidic heat exchangers. According to the results, the addition of nanoparticles enhanced the effective thermal conductivity and heat capacity of the working fluid, leading to higher average Nusselt numbers and more efficient heat transfer. This improvement is particularly beneficial for biomedical microdevices, where precise thermal management is essential. However, the increased nanoparticle concentration also resulted in higher viscosity, which can raise the pressure drop within the system. This study, while primarily focused on heat transfer characteristics, also acknowledged the significance of pressure drop augmentation and emphasised the need to consider it in future microfluidic system designs. A numerical study conducted by Karouei et al. [13] evaluated the thermal performance of Ag-graphene (HEG)/water and MWCNT-Fe₃O₄/water hybrid nanofluids in a helical double-pipe heat exchanger equipped with an innovative curved conical turbulator. The results indicated that both nanofluids significantly enhanced heat transfer relative to pure water, with Ag-HEG/water delivering superior performance at lower mass flow rates. Maximum thermal efficiency was achieved at the highest tested nanoparticle concentration of 0.7 %, highlighting the critical role of volume fraction in optimising thermal performance.

Artificial neural networks (ANN) have been widely implemented across various research fields, including nanofluids, to predict their properties and heat transfer characteristics for diverse applications.

Kumar et al. [14] carried out an experimental and artificial neural network (ANN) analysis on the thermophysical properties of oxide-MWCNT water hybrid nanofluids. HNFs were prepared by mixing water-based metal oxide nanofluids (ZnO, Al₂O₃, CeO₂, and TiO₂) with MWCNT nanofluids in an 80:20 volumetric ratio. The study tested nanofluid concentrations from 0.25 % to 2.0 % and temperatures ranging from 25 °C to 50 °C and measured key thermophysical properties such as dynamic viscosity, density, thermal conductivity, and specific heat. According to the results, the MWCNT-CeO2/water HNF showed the best performance, with superior thermophysical properties and the highest Mouromtseff number. This highlights the significance of selecting the appropriate pair of nanoparticles. In addition, to predict the properties, a hyperparameter-optimised ANN model was developed, which showed excellent accuracy when compared to experimental data, with correlation coefficients over 0.999, mean square errors below 0.001, and deviations within ± 5 %. Jalili et al. [15] conducted a detailed thermal analysis of magnetohydrodynamic (MHD) hybrid nanofluid flow confined between two parallel plates, using a novel suspension of MWCNTs and Ag nanoparticles dispersed in a 50:50 ethylene glycol-water mixture. The study introduces the use of Homotopy Perturbation Method (HPM) and Akbari-Ganji Method (AGM) in Python (via SymPy and SciPy) to solve highly non-linear coupled differential equations, validated against Runge-Kutta numerical solutions. The analysis demonstrated that the hybrid nanofluid significantly outperformed conventional and mono-nanoparticle fluids in thermal performance. It was found that the use of MWCNT-Ag hybrid nanoparticles led to an improvement of approximately 11 % in temperature distribution compared to base fluids with single nanoparticles.

Said et al. [16] investigated the synthesis, thermophysical properties, and stability of HNFs composed of Fe₃O₄-coated MWCNTs through an AI approach for predictive modelling. The researchers employed an in-situ growth method combined with chemical reduction to synthesise the Fe₃O₄-coated MWCNTs, and they validated their findings using X-ray diffraction, vibrating sample magnetometry, and scanning electron microscopy (SEM) techniques. They found that the highest zeta potential value of -48 mV was achieved at a 0.05 % concentration. At 0.3 % concentration, thermal conductivity improved by 13.78 % and 28.33 % at 20 $^{\circ}\text{C}$ and 60 $^{\circ}\text{C}$, respectively, compared to water, while viscosity rose by 27.83 % and 50 %, respectively. Multi-Layer Perceptron ANN was utilised to model the relationships between temperature, concentration, and thermophysical properties. The model demonstrated high accuracy, effectively replicating experimental results across various conditions and highlighting the potential of AI in advancing the understanding of hybrid nanofluids for enhanced thermal management solutions.

The realm of nanofluid investigation has witnessed a noteworthy expansion in the last twenty years, as demonstrated by data in publications from the Scopus database, as shown in Fig. 1. In 2005, there were only 63 studies, but by 2023, this number had soared to 4666. This exponential growth trajectory is not merely a numbers game; it reflects the scientific community's recognition of nanofluids' enhanced thermal properties and their potential to revolutionise various applications. The steady rise in nanofluid publications suggests that investigators are still in the process of unlocking their full potential. Each new study seems to push the boundaries, whether it's optimising performance, exploring new application areas, or addressing challenges like cost, long-term stability, and scalability.

This study has not been confined to a single type of nanofluid but has expanded to include various categories: silver belonging to the metallic group, aluminium nitride from the category of nitrides, and multiwalled carbon nanotubes derived from carbon materials, each with its unique properties, limitations, and potential uses. Fig. 2(a) illustrates the global distribution of studies focused on the nanofluids under consideration. India emerges as a leading country, following Iran, with significant research activity concentrated in Asian countries. Additionally, a considerable number of researchers from the United States, Europe, the United Kingdom, Canada, and other regions are engaged in

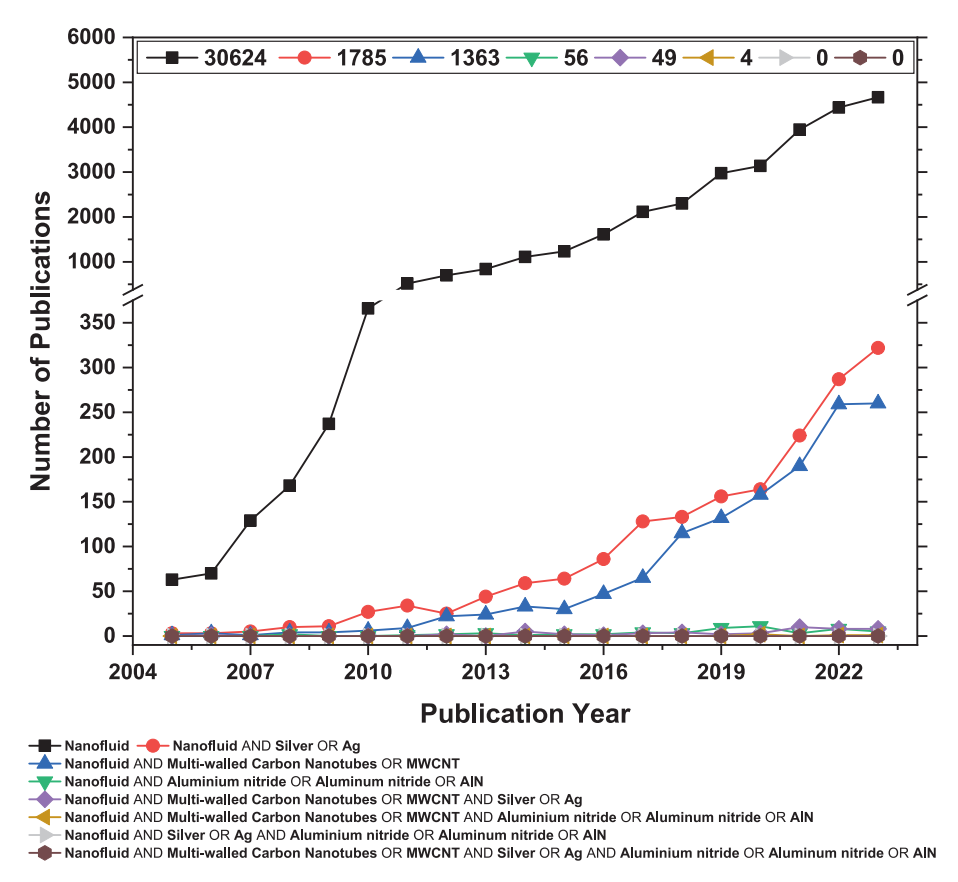


Fig. 1. Number of nanofluid publications from 2004 to 2022 based on the Scopus database.

this field. These researchers are interconnected, underscoring the collaborative efforts to explore the potential of nanofluids and address challenges for their commercial application. Fig. 2(b) presents a bibliometric analysis conducted using VOSviewer, which visualises the network of researchers actively involved in the field of nanofluids [17]. This analysis highlights key groups and individuals, illustrating their collaborations and connections. The visualization reveals distinct clusters of researchers who frequently work together, indicating strong collaborative networks within the field. Such interconnected efforts are crucial for advancing the research and development of nanofluids, ultimately facilitating their commercial application across various industries. The collaborative nature of this research enhances the potential for innovative solutions and accelerates the practical use of these advanced fluids.

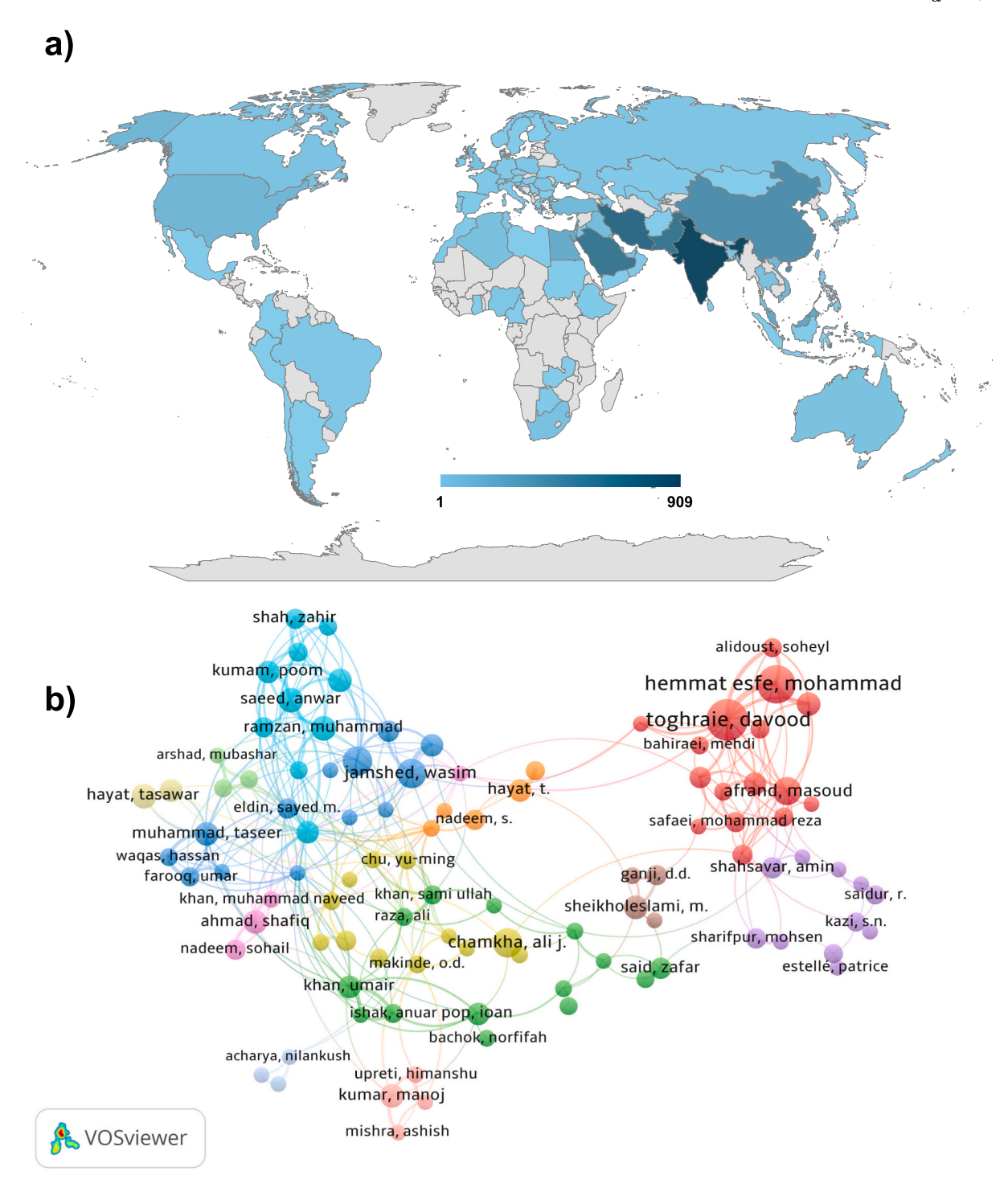
Silver nanoparticles are considered to be investigated in this study for their excellent thermal conductivity and antimicrobial properties, making them suitable for applications in thermal management and biomedical fields. As per statistics from Scopus, further filtered with "Silver" or "Ag" it was noticed that the Ag nanofluid gained significant attention over the years, with research publications increasing from 3 in 2005 to 322 in 2023. The steady rise in publications suggests ongoing exploration and optimisation of silver nanofluids to enhance their performance and broaden their application scope. Multi-walled carbon nanotubes are known for their superior thermal conductivity and lower density, which can significantly enhance the heat transfer capabilities of nanofluids. In 2005, only one research study was documented on MWCNT's, however, by 2023, the number of studies had surged to 260, indicating a substantial rise in researchers' interest. Despite their superior thermal conductivity, MWCNTs face limitations, including high production costs and challenges with percolation network formation. The costliness of MWCNTs and the difficulty in breaking their percolation networks can hinder their practical application in nanofluids.

Aluminium Nitride (AlN) nanofluids have also been a subject of

research, with the number of studies peaking at 11 in 2020 before slightly decreasing to 5 in 2023. AlN nanoparticles offer high thermal conductivity compared to oxides and many other nitrides and carbides, lower density, and are cost-effective, making these particles ideal as one of the potential candidates for hybrid nanofluids. These particles could be used in combination with particles that have higher thermal conductivity but face issues with stability and high cost. This underscores the significance of hybrid nanofluids, which combine particles with complementary properties to overcome individual limitations. Table 1 offers an overview of additional studies on nanofluids, highlighting the different nanoparticles, base fluids, and surfactants investigated, along with the objectives and key findings of each research effort.

The introduction of hybrid nanofluids marks a novel approach in nanofluid research, offer versatility, tunability, and potential for improved thermal management by tailoring nanoparticle combinations. Finally, the results were further refined to include multiple particle types for analysing hybrid nanofluids. According to the findings, only a few studies have reported on MWCNTs-Ag hybrid nanofluids, while some have examined AlN and MWCNTs individually but not their hybrid combination. To date, there is no study reported on the Ag-AlN hybrid and tri-hybrid of MWCNT-Ag-AlN. This study aims to bridge the existing research gap by thoroughly investigating the thermal conductivity, viscosity, and density of nanofluids in both simple and hybrid forms, with the goal of improving thermal properties and stability while reducing costs.

By overcoming the limitations of individual nanoparticles, this research will explore their synergistic behaviour in hybrid and tri-hybrid combinations. The results will highlight the critical role of nanoparticle type, concentration, and mixing ratio in optimising the thermophysical properties of these fluids. This research is expected to contribute significantly to the body of knowledge in the field, providing practical insights that can be applied across various scientific and engineering disciplines. The findings could have a far-reaching impact, offering



 $\textbf{Fig. 2.} \ \ \textbf{Global distribution and research network visualization in nanofluid studies.}$

solutions that enhance both theoretical understanding and real-world applications.

Unlike many previous studies that limit their scope to thermal enhancement or basic formulation, this work adopts a more holistic approach that combines stability optimisation, thermophysical evaluation, and cost-performance analysis of hybrid and tri-hybrid nanofluids. The methodology begins with a systematic comparison of widely used surfactants (SDS, CTAB, GA, and SDBS) across different nanoparticle types to determine the most effective stabilizing agent for long-term dispersion. In addition to surfactant screening, a detailed study was conducted to examine the effects of varying particle concentrations

(0.01–0.03 vol%) on both the pH behaviour and colloidal stability of the nanofluids over time. This allowed for the identification of optimal concentrations that balance thermal enhancement with long-term suspension stability, an often neglected but critical aspect for real-world deployment. Moving beyond simple or binary formulations, this study introduces novel tri-hybrid nanofluids (MWCNTs/Ag/AlN), enabling the exploitation of synergistic interactions among different nanoparticles to simultaneously improve thermal conductivity, stability, and cost-effectiveness. The prepared fluids were comprehensively characterized not only for thermal conductivity but also for viscosity, density, and pH within a practical temperature range. A comparative cost-performance

Table 1
Summary of the nanofluid research, highlighting the nanoparticles, base fluid, surfactants studied, objectives, and key findings.

Reference	Nanofluid investigated		Surfactant studied	Objective	Findings
	Nanoparticles	Basefluid			
Rehman et al. [18]	Al ₂ O ₃ -TiO ₂ hybrid	W-EG mixture (60:40)	CTAB, SDS Poly (vinyl alcohol), Polyvinylpyrrolidone (PVP), Polyethylene glycol (PEG), Oleic acid (OA)	Identify the best surfactant for long-term heat transfer applications. Investigate surfactant effects on nanofluid stability, viscosity,	PVP is the most suitable surfactant for hybrid nanofluids. PVP enhances thermal conductivity and stability for long-term applications.
Wusiman et al. [19]	MWCNTs	Water	SDS, SDBS	and thermal conductivity (TC). Investigate thermal conductivity and study the effect of surfactants	MWCNTs with SDBS showed better thermal conductivity enhancement (TCE). SDS had a negative impact on thermal conductivity of MWCNTs. Optimum pH value was found to be around 9.
Mehta et al. [20]	$\mathrm{Al}_2\mathrm{O}_3$	Water	СТАВ	Prepare stable Al ₂ O ₃ -water nanofluid using CTAB surfactant Enhance thermophysical properties and stability of nanofluid	The use of CTAB as a surfactant significantly improves the stability of ${\rm Al_2O_3}$ -water nanofluids. With CTAB, the mean particle sizes after one month were 80 nm, compared to 536 nm without surfactant, leading to better thermal conductivity and dynamic viscosity improvements of 8.5 % and 76.2 % respectively at a 1 % volume concentration.
Saraswat and Sengwa [21]	ZnO	EG-glycerol (90:10)	PVP	Analyse optical, dielectric, and rheological properties	Alcohol mixture based nanofluids show improved optical, dielectric, and rheological properties.
Yalçın et al. [22]	Graphite	Water	Gum Arabic, Cetrimonium bromide, Ammonium citrate	Investigate how different surfactants affect nanofluid viscosity.	Surfactant types and proportions affect nanofluid viscosity differently. Different surfactant usages distinctly change nanofluid dynamic viscosity.
Poloju et al. [23]	SiO ₂ , ZnO, and TiO ₂ ternary	Water	SDBS	Investigate TC and dispersion properties of SDBS nanofluid. Analyse impacts of sonication time, surfactant inclusion, and ageing.	SDBS decorated ternary nanofluid showed enhanced thermal conductivity. Surfactant inclusion, sonication time, and ageing affected dispersion properties.
Borode et al. [24]	Graphene nanoplatelets (GNP)	Water	SDBS, SDS, GA, and Tween 80	Study effects of surfactants on GNP nanofluids properties. Analyse stability, thermal, electrical conductivity, and viscosity of nanofluids.	SDBS-based nanofluids showed the best dispersion and stabilization. Electrical and thermal conductivity increased with surfactant addition.
Wang et al. [25]	Fe ₃ O ₄ , CNT, Fe ₃ O ₄ -CNT hybrid	Water	Colace, Trisodium citrate dihydrate (TSC), PVP, CTAB, Tetramethylammonium hydroxide (TMAH), Acacia Senegal, SDBS, SDS, and Sodium lauryl sulfonate (SLS)	Investigate the effect of surfactants on stability and thermo-physical properties. Propose empirical formulas for nanofluid viscosity predictions	Nanoparticle size, volume fraction, and temperature affect nanofluid viscosity. Surfactants TMAH, SDS, and SLS improve stability and TC.
Dalkılıç et al. [26]	$\mathrm{CNT} ext{-}\mathrm{SiO}_2$ hybrid	Water	No surfactant was used for 0.1 %, 0.5 %, and 1 % concentrations Gum Arabic used as surfactant only for 2 % concentration samples	Measure and analyse the TCE of water-based CNT-SiO ₂ hybrid nanofluids at different concentrations, temperatures, and CNT:SiO ₂ ratios.	Hybrid nanofluid exhibited better TCE compared to individual nanoparticles. Gum Arabic surfactant enhanced stability but at the cost of increased
Esfahani et al. [27]	ZnO-Ag (50%–50 %) hybrid	Water	-	Study the effect of particle loading (0.125–2 vol%) and temperature (25–50 °C) on TC and develop a new correlation.	viscosity. At higher temperatures, increasing volume fraction had a greater effect on TC due to enhanced Brownian motion. A new correlation was developed to predict the TC, with a margin of deviation of 1.3 % compared to experimental results.
Dezfulizadeh et al. [28]	Cu-SiO ₂ -MWCNT ternary hybrid	Water		Investigate the dynamic viscosity and TC of the ternary hybrid at different temperatures and nanoparticle concentrations.	The ternary formulation exhibited Newtonian behaviour. The nanofluid sample showed greater TC and dynamic viscosity enhancements compared to mono and binary nanofluids. Mathematical correlations estimate the TC and dynamic viscosity, with maximum errors of 1.167 % and 1.327 % respectively.
Adun et al. [29]	Al ₂ O ₃ -ZnO- Fe ₃ O ₄ ternary hybrid	Water	-	Investigate the thermal properties and examine the effects of temperature, volume	Optimum TCE of 36.018 % recorded at 1.25 % volume concentration at 65 °C (continued on next page)

(continued on next page)

Powder Technology 465 (2025) 121348

Table 1 (continued)

Reference	Nanofluid investigated		Surfactant studied	Objective	Findings
	Nanoparticles	Basefluid			
				concentration, and mixture ratio (1:1:1, 1:2:1, and 1:1:2) Develop a machine learning model for accurate prediction of properties	Gaussian process regression showed excellent prediction
Sepehrnia et al. [30]	Fe ₃ O ₄ , TiO ₂ , and graphene oxide (GO)	Hydraulic oil HLP 68	-	Improve the efficiency of hydraulic systems with nano-additives.	Dynamic viscosity increases significantly with nano-additives and lower temperatures.
Ajeena et al. [31]	ZrO ₂ (Zirconium Dioxide) and SiC (Silicon Carbide) in a 50–50 ratio	Distilled water	-	Determine the dynamic viscosity by studying its rheology. Assess the characteristics and stability of the ZrO ₂ and SiC nanoparticles in the base fluid.	The hybrid samples displayed Newtonian fluid behaviour across a range of temperatures, demonstrating their suitability for use in various devices as a Newtonian fluid.
Qu et al. [32]	${\rm SiO_2\text{-}Al_2O_3\text{-}MWCNTs}$	Water	-	Examine the effect of nanoparticle loading and temperature. Develop a new model for viscosity prediction using nonlinear curve fitting techniques.	Viscosity rose from 1.55 to 3.26 cP when the volume fraction increased from 0.1 % to 0.5 %. Viscosity decreases with increasing temperature. At 0.3 % volume fraction, the viscosity reduced from 3.3 to 1.73 cP when temperature increased from 20 °C to 60 °C
Mande et al. [33]	${ m TiO_2\text{-}CuO}$ hybrid	Water	-	Investigate thermal transport properties of TiO ₂ /CuO hybrid nanofluids. Study morphological characteristics using SEM, XRD, and EDX.	Thermal conductivity was enhanced with particle loading. Density and viscosity increased while specific heat decreased with concentration.
Ghafouri and Toghraie [34]	ZnO-SiC hybrid	Ethylene glycol	СТАВ	Evaluate TC of SiC-ZnO hybrid nanofluid. Analyses the effects of nanoparticle size, temperature, and volume fraction.	Thermal conductivity enhanced by 15.91 % at optimal conditions. New multivariate correlation accurately predicts thermal conductivity.

analysis was also conducted, providing valuable insights into the economic viability of each formulation. Altogether, the methodology established in this study offers a robust and transferable framework for the development of advanced nanofluids, making it highly relevant for next-generation thermal management applications in electronics, energy systems, and transportation technologies.

2. Nanofluid preparation

Literature reports two primary methods for preparing nanofluids: single-step method and two-step method. The single-step method, which includes techniques such as laser ablation and vapour deposition, involves complex processes and specialised equipment. This complexity presents challenges, particularly in scaling up to produce large quantities of nanofluids. In contrast, the two-step method has emerged as a preferred approach due to its efficiency, cost-effectiveness, and capacity to produce substantial volumes of nanofluids [35]. Consequently, the two-step method was employed in this study to prepare various simple, hybrid, and tri-hybrid nanofluid samples. However, prior to formulating the samples to analyse their thermophysical properties, a comprehensive study was carried out to examine the effects of different surfactants and particle concentrations on the stability of Ag, AlN, and MWCNT's nanofluids. This preliminary investigation was conducted to select the most appropriate surfactant and particle concentration for subsequent experiments.

To investigate the impact of surfactants, initial samples of Ag, AlN, and MWCNT nanofluids were prepared with a particle concentration of 0.01 vol%. In the subsequent phase, particle concentrations were varied from 0.01 vol% to 0.03 vol% and observed sedimentation over time. Following the selection of suitable surfactants and particle concentrations, simple, hybrid, and trihybrid nanofluid samples were prepared. These samples were then used to further investigate thermal and rheological properties at various temperatures. The nanoparticles used in

this experimental investigation were purchased from well-known suppliers, Sigma-Aldrich and Alfa Aesar. Table 2 provides detailed information on their cost, size, density, thermal conductivity, and purity. To ensure homogeneity and stability, a series of preparation processes were employed. These processes included magnetic stirring, surfactant addition, bath sonication, and high-intensity probe sonication.

To measure the amount of nanoparticles against the particle concentration (φ) , the well-known volume fraction equation was used, as represented in Eq. (1). Analytical balance was used to weigh the particles prior to adding them in the basefluid water while continuously performing the stirring operation. At this stage, the surfactant was also introduced in an amount equal to that of the particles. The solution was stirred for 1 h using a magnetic stirrer, followed by sonication in a bath for another hour. Subsequently, the processed solution was ultrasonicated for 1.5 h using a SONICS probe sonicator, set to 50 % amplitude with a pulse sequence of 3 s ON and 2 s OFF. As the nanoparticles are suspended in the fluid, they tend to agglomerate and form clusters. The sonication process helps to break up these clusters while stirring ensures a more uniform suspension. To prevent an increase in temperature due to sonication, the sample was kept in a water bath.

For hybrid and tri-hybrid nanofluids, each component fluid was prepared separately following the above steps, then the measured volumes were mixed while stirring. The hybrid solution was further ultrasonicated for 30 min with a probe sonicator to ensure a more homogeneous suspension. Fig. 3 illustrates the steps followed to prepare the simple and hybrid nanofluid samples.

$$\varphi = \begin{bmatrix} \frac{m_{np}}{\rho_{np}} \\ \frac{m_{np}}{\rho_{np}} + \frac{m_{bf}}{\rho_{bf}} \end{bmatrix} \tag{1}$$

where m_{np} represents the mass of the nanoparticles, while ρ_{np} stands for the density of the nanoparticles. However, m_{bf} refers to the mass of the

Table 2 Properties of the particles.

Nanoparticle	Formula	Density (g/cm3)	Size	Purity	Thermal Conductivity (W/m.K)	Cost (£)*	Quantity (g)	Reference
Carbon nanotube, multi- walled	MWCNT's	2.1	O.D. $ imes$ L 6–13 nm $ imes$ 2.5–20 μ m	> 98 %	3000	1590	10	[36]
Silver	Ag	10.5	10-40 nm	99.9 %	429	386	10	[37,38]
Aluminium nitride	AlN	3.26	< 100 nm		285	119	10	[39,40]

^{*} Prices as of June 12th, 2024.

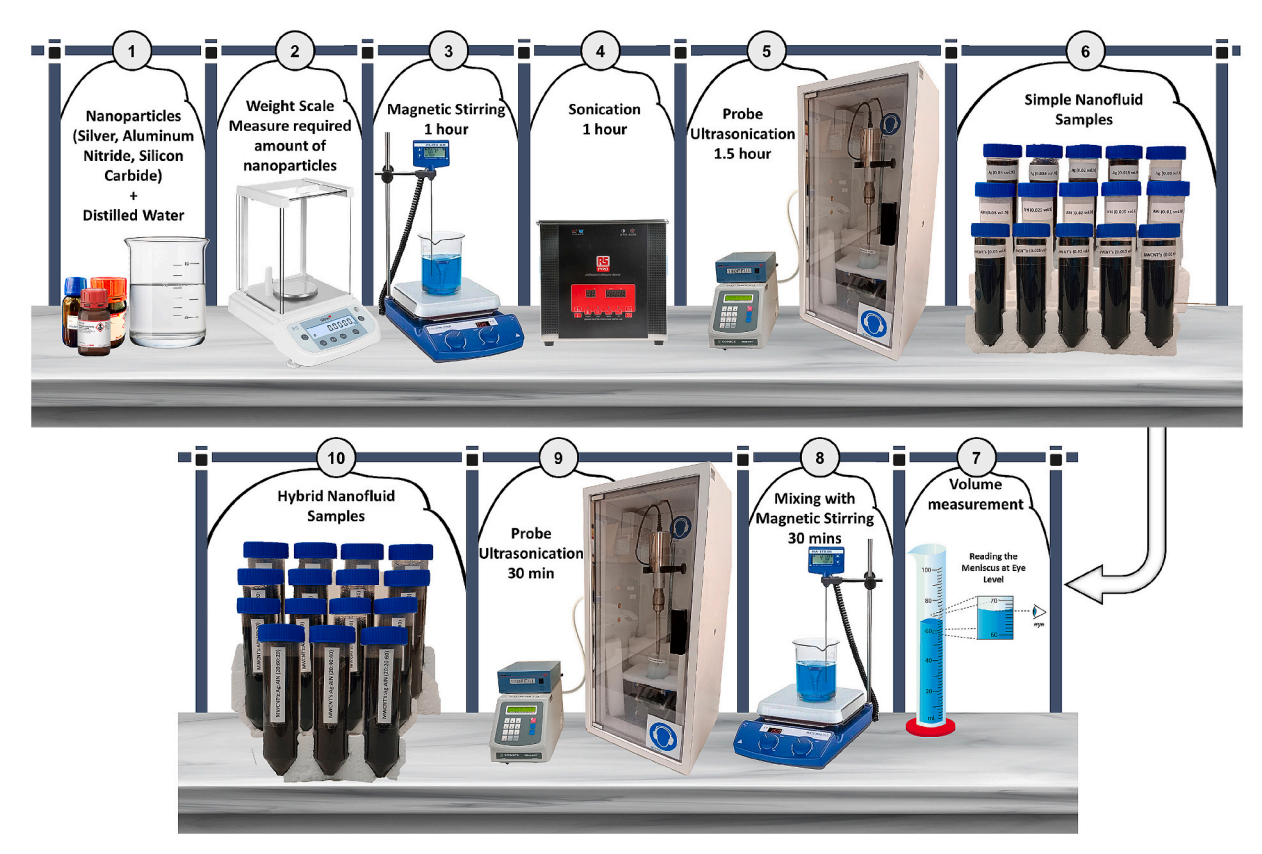


Fig. 3. Schematic diagram of nanofluid preparation steps for simple and hybrid samples.

base fluid, and ρ_{bf} indicates the density of the base fluid.

3. Stability and pH characteristics

3.1. Effect of surfactants

To select a suitable surfactant and concentration for preparing both simple and hybrid samples, a study was conducted to assess the stability of AlN, MWCNTs, and Ag nanofluids across various concentrations and introducing different surfactants. Four types of surfactants SDS, GA, SDBA, and CTAB were chosen to investigate their impact on sample stability. Surfactants are known for their ability to induce electrostatic or steric repulsion forces among nanoparticles, which effectively prevent their undesirable agglomeration. This strategic use of surfactants plays a crucial role in maintaining the stability of nanofluid systems. A number of studies reported that the use of appropriate surfactant can improve the stability of the nanofluids.

This phase of the study involved monitoring the settling of particles in the base fluid over time. Furthermore, changes in pH values were analysed following the addition of surfactants and varying particle concentrations. To measure the pH value, a Hanna pH meter (Model HI 98128) was utilised, accompanied by its calibration certificate. Additional calibration steps were undertaken to ensure precise pH

measurements. The calibration involved immersing the pH meter's probe in cleaning solution to cleanse the temperature sensor and electrode. Subsequently, the meter was calibrated using buffer solutions of pH 4.01 and 7.01. After each immersion, the meter recorded the corresponding pH values. Following calibration, pH measurements of a neutral solution were conducted to validate accuracy.

To mitigate the influence of temperature fluctuations on pH measurements, each sample was kept in a thermal bath maintained at a constant temperature of 20 $^{\circ}$ C, as depicted in Fig. 4. This controlled environment ensured consistent temperature conditions for accurate pH readings. Additionally, to minimise measurement variability, pH values were recorded three times for each sample.

The preparation of nanofluid samples involved rigorous processes including magnetic stirring and sonication, conducted within a fume cabinet to maintain safety and minimise contamination. These procedures exposed the fluid to atmospheric air. The setup for pH value determination was also conducted in an open environment. Under these conditions, the pH of the distilled water typically ranged between 5.4 and 5.7 [41]. As anticipated, in this study, pH of the base fluid was found to be 5.69 \pm 0.01.

To study the impact of various surfactants on the stability, AlN, MWCNTs, and Ag nanofluids were prepared with a particle concentration of 0.01 vol%. It was observed that the addition of nanoparticles significantly affected the pH of the fluid, and the surfactants interacted

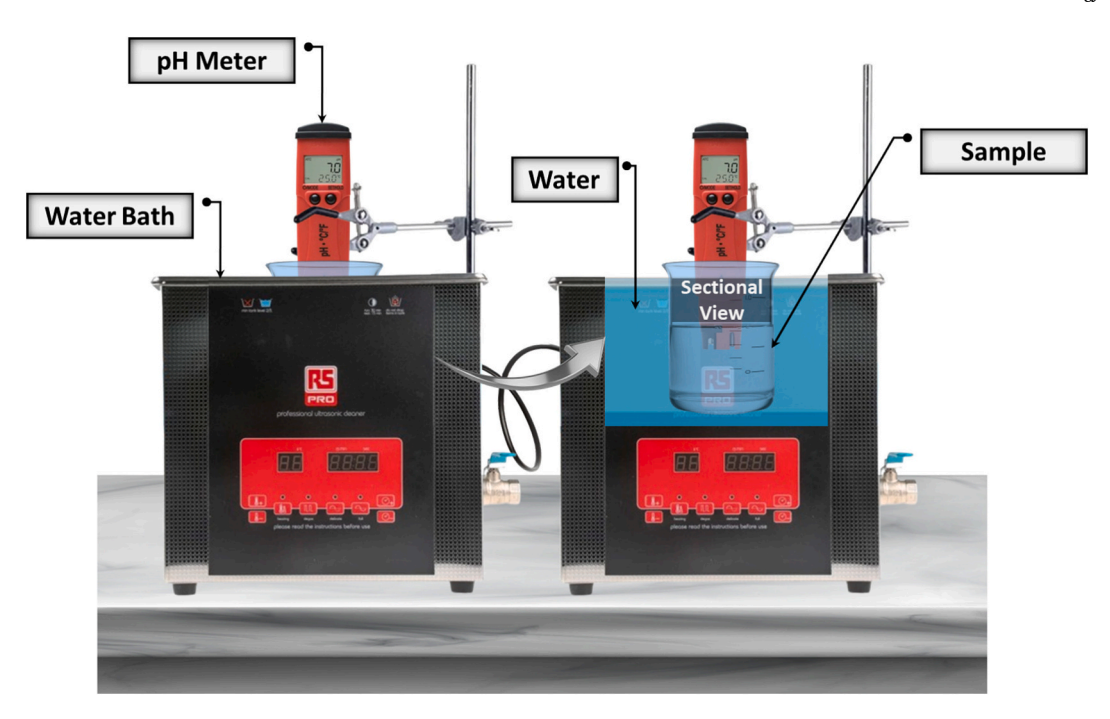


Fig. 4. Setup for pH measurement of nanofluid samples in a thermal bath.

differently with various particles, as shown in Fig. 5. Distilled water, used as the baseline in this study, exhibited an initial pH of 5.69. The introduction of silver nanoparticles increased the pH to 6.24. The addition of surfactants to the silver nanofluid further modified the pH, demonstrating the unique interactions between the surfactants and the nanoparticles. CTAB and SDS slightly lowered the pH to 6.1 and 5.85 respectively, while GA caused a more significant drop to 5.58. Notably,

SDBS exhibited a unique behaviour by dramatically increasing the pH to 7.2, thereby making the silver nanofluid the most alkaline among those tested.

The AlN nanofluid demonstrated a markedly different behaviour compared to the silver nanofluid. Without any surfactants, the AlN nanofluid had a notably high pH of 8.04. CTAB raised the pH to 8.45, while SDS pushed it slightly higher to 8.6. GA had the most pronounced

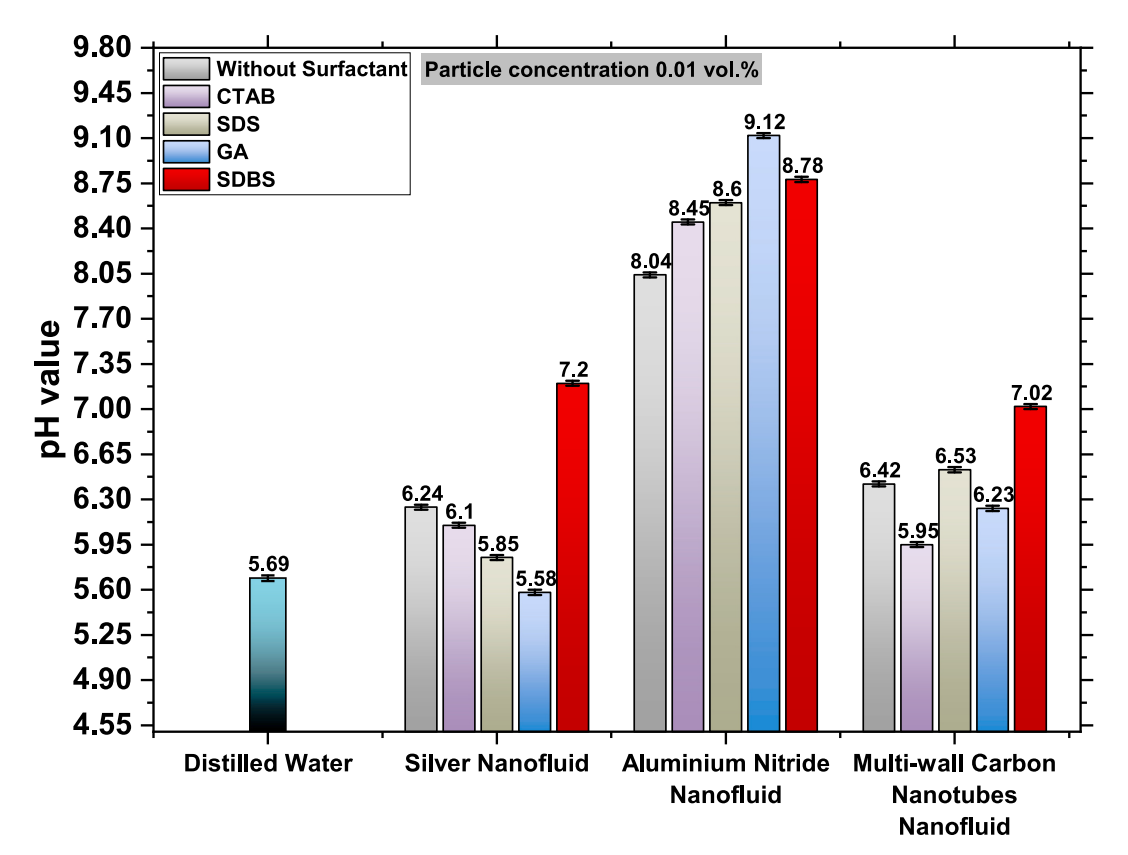


Fig. 5. pH values of AlN, MWCNT, and Ag nanofluids with different surfactants at 0.01 vol% concentration.

effect, elevating the pH substantially to 9.12. SDBS also significantly increased the alkalinity of the AlN nanofluid, though not to the extent of GA, reaching a pH of 8.78. The MWCNT nanofluid presented another distinct pH profile, highlighting the diverse behaviour of different nanomaterials in aqueous solutions. The solution had pH value measured to be 6.42 notably higher than the basefluid distilled water, however, like Ag and AlN the introduction of surfactants altered this pH in various ways. CTAB and GA lowered the pH value to 5.95 and 6.23 respectively, while SDS slightly increased it to 6.53. SDBS, consistent

with its behaviour in the silver nanofluid, significantly increased the pH to 7.02. This alkalizing effect of SDBS across different nanomaterials was a notable trend, possibly related to its strong anionic character and its unique interaction with various nanoparticle surfaces. Consistent with its behaviour in the silver nanofluid, SDBS significantly increased the pH of the MWCNT nanofluid to 7.02, highlighting its strong alkaline effect.

The surfactant study revealed that while some surfactants improved the stability of the nanofluid, others had an adverse effect, reducing particle suspension stability. Over the course of a week, the nanofluid

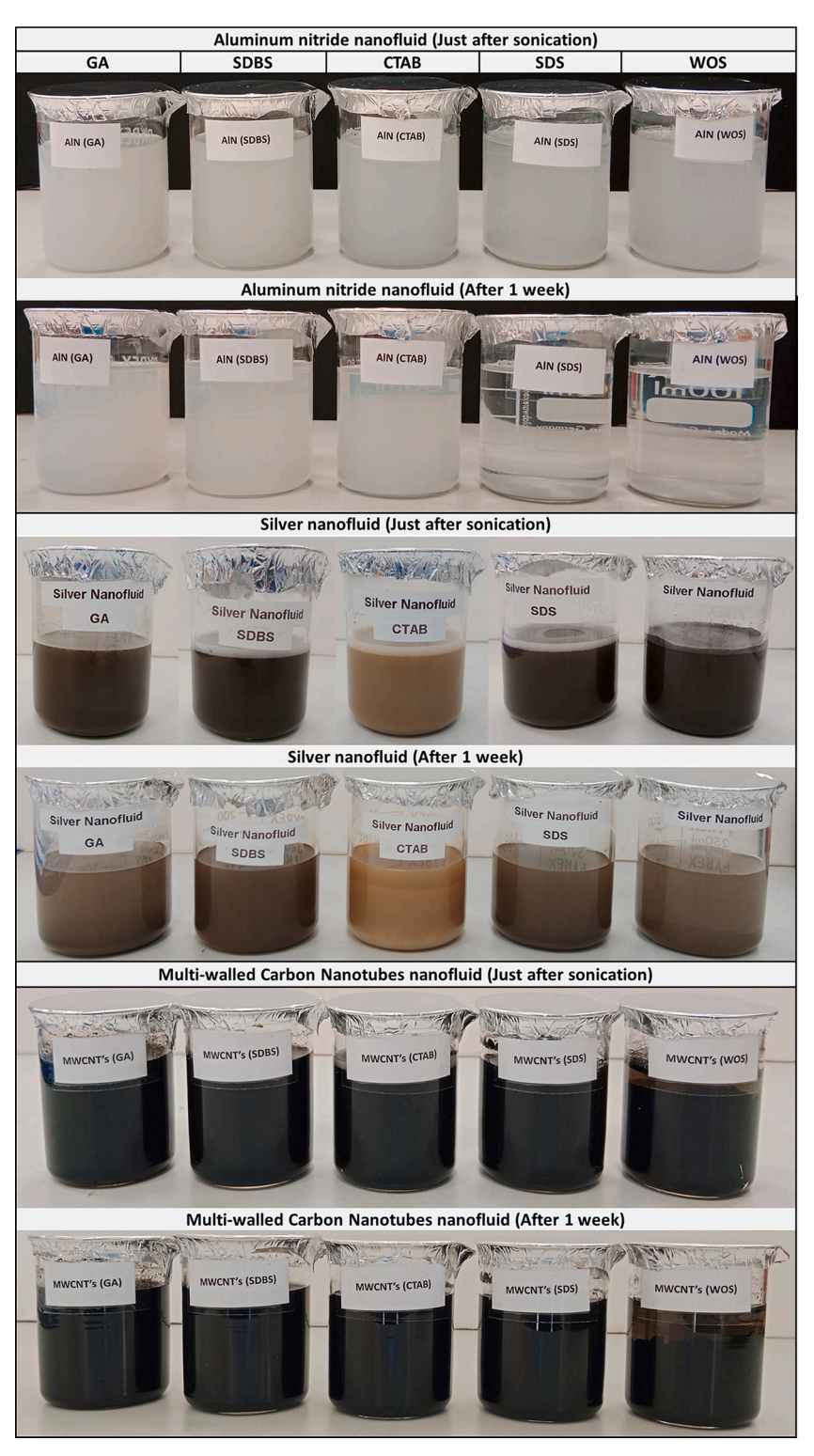


Fig. 6. Sedimentation observation of nanofluid samples with different surfactants.

samples were examined to analyse particle sedimentation behaviour with the addition of different surfactants. It was observed that AlN nanosheets tended to agglomerate and form clusters, which began to settle after 24 h. By the end of the observation period, complete particle settling had occurred in these samples, leading to the conclusion that SDS was unsuitable for use with AlN nanopowder. Furthermore, the sample with CTAB surfactant showed signs of instability. The top layers of this sample began to clarify as the particles started to settle down, as shown in Fig. 6. The sample with GA surfactant showed improved stability over CTAB and SDS, however, the AlN sample containing SDBS surfactant outperformed all and exhibited better stability. The particles in this sample remained suspended for a longer duration, indicating that SDBS can enhance the stability of AlN nanofluids. For this study, samples were processed with 30 min of stirring and 1 h of probe sonication to specifically examine the effects of surfactants. It is important to note that fluids prepared for property studies were processed for a longer duration.

For silver nanofluid, it was observed that sample without surfactant exhibited relatively poor stability. When comparing various surfactants, samples prepared with SDS and GA showed particles starting to settle down earlier than others. Introducing cationic surfactants resulted in a noticeable change in the fluid's colour and a significant decrease in pH value. Among the surfactants tested, CTAB demonstrated an improvement in the stability of the nanofluid. However, SDBS outperformed all other surfactants, maintaining the suspension's stability for a longer period. Thus, SDBS proved to be the most effective surfactant in enhancing the stability of the silver nanofluid.

The significance of surfactants is further underscored by the poor stability observed in MWCNT sample prepared without surfactant. The settling of particles is easily observed in the sample without surfactant, as the fluid's top layers start to clear. However, due to the dark colour of the suspension, it is somewhat challenging to observe sedimentation and agglomeration of particles in the samples containing surfactants. A glass pipette observation method was used to examine the aggregation of particles at this stage, as depicted in Fig. 7. Additionally, TEM analysis was employed to assess the aggregation of particles in the subsequent section.

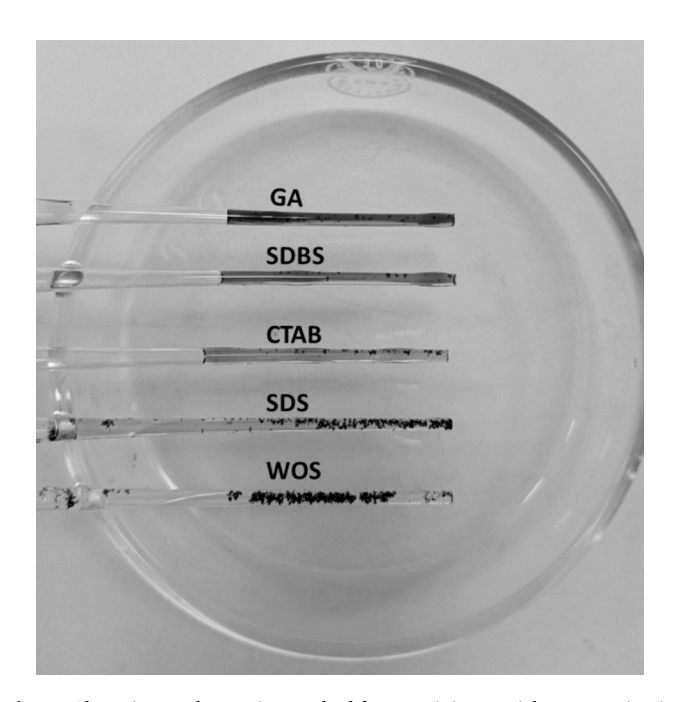


Fig. 7. Glass pipette observation method for examining particle aggregation in MWCNT samples.

Among the surfactants tested, SDS demonstrated inadequate performance in stabilizing the particles, whereas SDBS and GA significantly enhanced suspension stability and reduced aggregate formation. The CTAB surfactant offered better stability than SDS, but it was not as effective as SDBS and GA. Prolonged observation further confirmed that SDBS is the most suitable surfactant for improving the stability of MWCNT suspensions. Additionally, the density of MWCNTs is relatively low, which allows small aggregates to remain suspended in the fluid rather than settling at the bottom. This low density contributes to the stability of the suspension, as the lighter aggregates are less prone to sedimentation. Conversely, Ag nanoparticles have a density that is approximately five times greater than that of MWCNTs. This significant difference in density means that silver nanoparticles have a much stronger tendency to settle at the bottom of the base fluid. This difference in density and the resultant sedimentation tendencies highlight the importance of considering particle characteristics.

Importantly, it has been observed that after the sedimentation or aggregation of particles in the base fluid, the solution containing AlN and MWCNTs requires significantly more sonication processing time to achieve uniform suspension compared to a solution containing silver nanoparticles. This increased sonication time is necessary due to the stronger bonding interactions between AlN and MWCNT particles. These interactions are largely influenced by the shapes of the particles involved.

The findings underscore the significant effects of different surfactants on the pH and stability of various nanofluids, which are essential for customizing their properties for specific applications. By selecting and optimising surfactants, researchers can improve nanofluid stability over time, which is crucial for applications in electronics cooling, automotive systems, and renewable energy technologies. This understanding paves the way for tailored solutions that enhance the efficiency of thermal management systems across various industries.

3.2. Effect of particles loading

In the second phase of the study focusing on stability and pH characteristics, nanofluids containing Ag, AlN, and MWCNTs were meticulously prepared across varying particle concentrations (0.01–0.03 vol%) utilizing SDBS as a surfactant to enhance suspension stability. The investigation aimed to elucidate the interplay between particle concentration and pH values within each nanofluid type. It was observed that, while all three nanofluids exhibited a rise in pH with increasing particle concentration, the extent of change varies, as shown in Fig. 8. The study's findings revealed distinct pH characteristics among the nanofluids studied. The Ag and MWCNTs solutions were observed to be nearly neutral to slightly basic, while AlN nanofluids exhibited a basic nature that intensified with increasing particle concentration. For Ag nanofluids, pH levels showed a slight increase from 7.2 at 0.01 vol% to 7.38 at 0.03 vol%, indicating modest pH variation with concentration. In contrast, AlN nanofluids displayed a more pronounced elevation in pH levels as particle concentration increased, it varied significantly from 8.78 at 0.01 vol% to 10.21 at 0.03 vol%. Certain fuel cell technologies, such as anion exchange membrane fuel cells, utilise alkaline electrolytes. AlN nanofluids, if carefully engineered, hold promise for enhancing heat transfer within these cells, thereby boosting efficiency and overall performance. Moreover, the inherent alkalinity of AlN nanofluids makes them well-suited for the alkaline electrolyte environment typical of such fuel cell technologies [42]. This synergy suggests that AlN nanofluids not only improve thermal management but also contribute positively to the operational conditions required for optimal fuel cell performance. Meanwhile, MWCNT's nanofluids maintained relatively lower pH values across the concentration range compared to both Ag and AlN. The pH varied marginally from 7.02 to 7.17, suggesting minimal influence on pH by varying concentration.

In the context of nanofluid stability, the concentration of particles plays a crucial role. The study observed that MWCNTs maintained

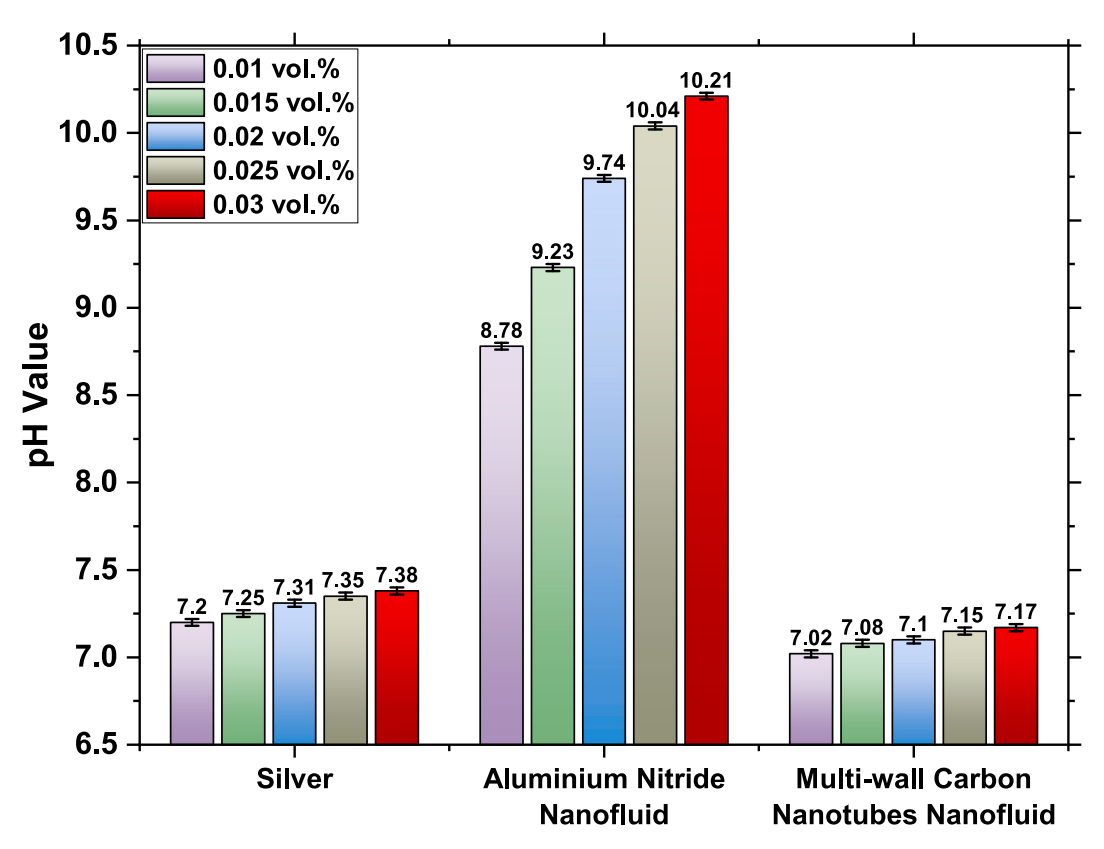


Fig. 8. pH variation with particle concentration for Ag, AlN, and MWCNT nanofluids.

stability throughout the examination period across all concentrations. It was revealed that for MWCNTs, the probability of nanotube aggregation is higher than sedimentation due to their lower density, which is closer to that of the base fluid (water) compared to other nanoparticles such as AlN and Ag. Additionally, it was noted that some dispersed tubes became entangled like ropes, making them difficult to break or separate, while tubes connected at their ends were easier to break. In contrast, AlN nanofluids exhibited different stability characteristics, samples with concentrations above 0.02 vol% began to settle after 72 h. The AlN particles agglomerated, forming densely packed clusters that were difficult to break and disperse. Upon extended observation, it was found that the settled particles in the conical test tube conformed to the shape of the tube bottom, forming a pellet that required high-frequency ultrasonic waves to disperse. This indicates that the attractive forces among these particles are strong, and even the addition of surfactants failed to sufficiently reduce these forces to maintain uniform suspension in the fluid for a longer period. This effect was more pronounced at higher particle concentrations. It is concluded that AlN nanoparticles are not an appropriate choice for use as a single particle to prepare nanofluids due to their tendency to form hard-to-disperse aggregates. However, they could potentially be utilised in combination with other particles or after specific surface treatments to enhance their dispersion stability. Researchers are encouraged to further explore the complex behaviour of AlN nanoparticles to develop more effective stabilization strategies. Silver nanoparticles (Ag) exhibit distinct sedimentation behaviour compared to both MWCNTs and AlN nanoparticles. Silver nanoparticles, despite their small size, face challenges in maintaining uniform suspension due to their relatively higher density. Specifically, the sample prepared with a concentration of 0.03 vol% began to clear the upper layer of the fluid after 72 h, attributed to the formation and settling of agglomerates. However, unlike AlN, Ag nanoparticles form aggregates that are relatively easier to disrupt, possibly due to weaker van der Waals forces and the spherical shape of these particles.

3.3. Hybrid and tri-hybrid nanofluid

The comprehension of the stability dynamics is essential for maximising the effectiveness of nanofluids across various applications, ranging from optimising thermal management systems to advancing biomedical devices. Moving forward, the exploration of hybrid and trihybrid nanofluids, such as MWCNTs/Ag, Ag/AlN, MWCNTs/AlN, and MWCNTs/Ag/AlN, becomes imperative. These combinations harness distinct nanoparticle properties to tackle specific challenges and enhance overall performance, focusing on optimising dispersion stability, improving heat transfer efficiency, and enhancing critical attributes for advanced industrial applications. Based on the stability study, a concentration of 0.025 vol% was selected for the hybrid samples. This concentration was utilised for the preparation and further analysis of all hybrid and tri-hybrid nanofluid samples. The pH of the hybrid nanofluids tends to vary around the pH values of the individual mixing fluids. As shown in Fig. 9, for the Ag-AlN hybrid nanofluid samples, the pH values were observed to range from 9 to 9.61. A significant reduction in pH was noted as the proportion of Ag in the mixture increased. This trend suggests a direct influence of Ag concentration on the overall pH of the hybrid nanofluid, as the pH value of the Ag nanofluid was 7.35. In the nanofluid comprising a suspension of MWCNTs and Ag nanoparticles, pH values were recorded to vary from 7.68 to 7.95. Notably, these values were slightly higher than those observed for the individual MWCNTs and Ag nanoparticles. This elevation in pH indicates a potential interaction between MWCNTs and Ag nanoparticles in the hybrid suspension, possibly altering the overall pH of the fluid. In comparison to samples containing AlN, the pH values measured for MWCNTs/Ag were noted to be lower. Similar to the Ag-AlN hybrid samples, the pH values of MWCNTs-AlN hybrid samples also demonstrated a trend where the pH increased with higher proportions of AlN. Specifically, the pH varied from 9.05 for the 80/20 ratio to 9.93 for the 20/80 mixing ratio. However, these pH values were slightly higher compared to those observed in MWCNTs/Ag hybrid samples. As anticipated, the pH values

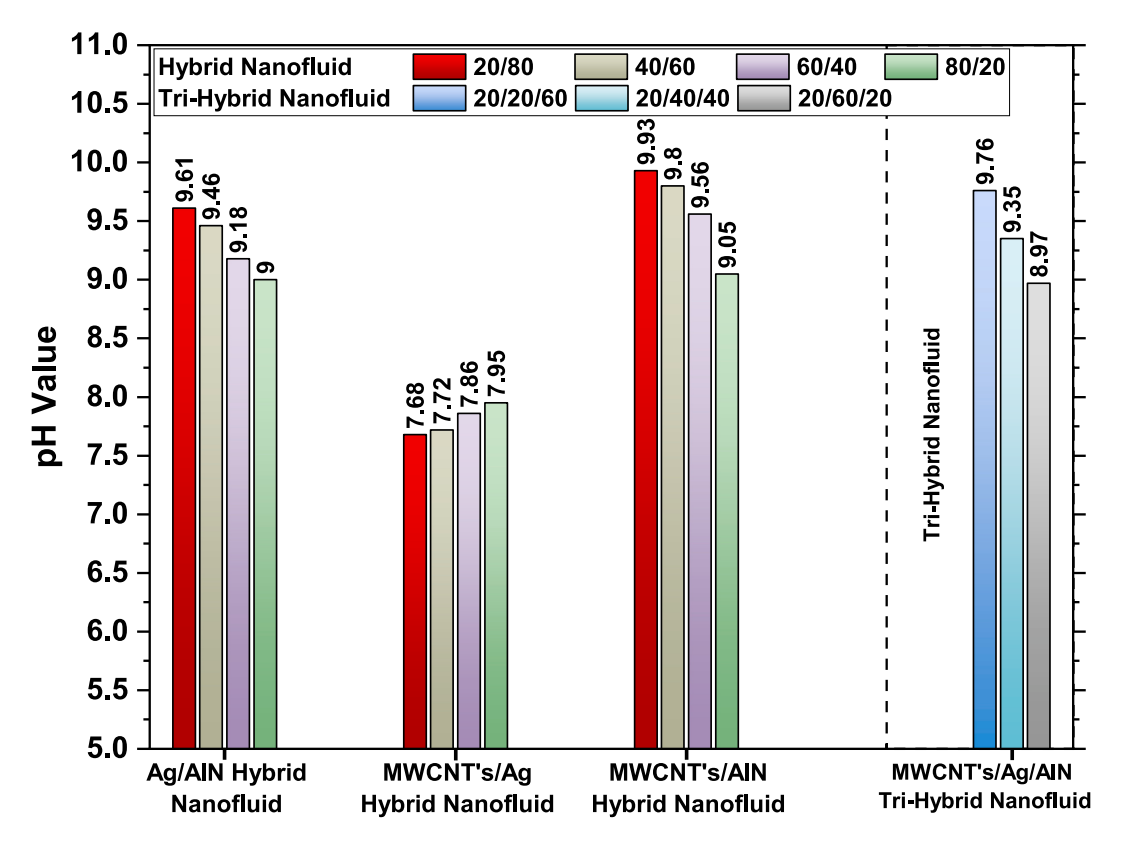


Fig. 9. pH values of hybrid and tri-hybrid nanofluids with different mixing ratios.

of the tri-hybrid nanofluid composed of MWCNTs/Ag/AlN varied with different mixing ratios. For a composition of 20 % MWCNTs, 20 % Ag, and 60 % AlN, the pH was 9.76, indicating a more basic nature due to the high AlN proportion. As the proportion of Ag increased to 40 %, with 20 % MWCNTs and 40 % AlN, the pH decreased to 9.35. This reduction indicates the influence of Ag nanoparticles, which tend to lower the pH of the solution. The pH further declined to 8.97 when the composition was adjusted to 20 % MWCNTs, 60 % Ag, and 20 % AlN. The results demonstrate that increasing the concentration of Ag nanoparticles or reducing the AlN nanoparticles' loading shifts the pH towards a more neutral value.

The study findings emphasise the profound influence of surfactants, particle types, and concentrations on pH variations in nanofluids. These pH dynamics are pivotal for improving nanofluid stability and overcoming associated challenges. This understanding not only guides the optimisation of nanofluid formulations but also advances their reliability and performance across diverse technological applications.

The hybrid nanofluid samples demonstrated improved stability due to the synergistic interactions among different particles. However, Ag/ AlN hybrid samples began to exhibit upper layer clarification after one week, attributed to particle sedimentation. Importantly, the presence of Ag nanoparticles in the hybrid samples prevented the formation of hardto-break clusters typically observed in simple AlN nanofluid samples. In the case of pure AlN nanofluids, once clusters formed, it was challenging to break them apart and re-suspend the particles uniformly, even when high-frequency sonication was applied. Conversely, in the hybrid samples, the bonding among settled particles was not as strong, which facilitated easier re-dispersion and processing of the solution. This could be attributed to the rolling effect of the spherical shape of the Ag nanoparticles, which likely prevented the formation of tightly bound clusters. The rolling effect allowed the particles to remain more loosely connected, making it easier to break them apart and achieve a uniform suspension once again. This observation underscores the significance of hybrid nanofluids and selecting a suitable combination of nanoparticles.

The ability to maintain a stable and easily re-dispersible nanofluid is crucial for practical applications, where uniform particle distribution is essential for optimal performance.

The hybrid samples of MWCNT's/Ag and MWCNT's/AlN showed better stability, retaining it for a longer period, as shown in Fig. 10. The rate of particle agglomeration was significantly lower compared to the simple and other hybrid nanofluids containing Ag and AlN nanoparticles. This reduced tendency for agglomeration and sedimentation suggests that hybrid nanofluids are less likely to experience these issues during operational conditions. Finally, the tri-hybrid nanofluid exhibited even greater stability, offering enhanced thermal characteristics. The distinct shapes and properties of the different nanoparticles in the tri-hybrid system contribute to a more effective dispersion and stability, leading to better thermal performance.

4. Characterisation

4.1. X-ray diffraction (XRD)

X-ray diffraction (XRD) is a powerful technique used to investigate the phase composition and crystallographic structure of nanoparticles such as aluminium nitride, silver, and MWCNTs. By examining the atomic arrangements within these materials, XRD provides detailed insights into their properties. Numerous research studies have employed XRD to characterise nanoparticles composed of pure or composite materials [43,44]. For this analysis, an X-ray diffractometer (Bruker - D8 Advance) with Cu-K α radiation (energy: 8.05 keV, wavelength: 1.5406 Å) was utilised. The XRD pattern for AlN nanoparticle showed several distinct peaks at specific 2 θ angles, which correspond to the diffraction from different crystallographic planes of the AlN crystal, as shown in Fig. 11(a). The peaks are indexed with Miller indices (hkl), indicating the specific planes that contribute to the diffraction peaks. The presence of sharp, well-defined peaks indicates a highly crystalline nature of the AlN nanoparticles. The pattern suggests a hexagonal crystal structure,



Fig. 10. Stability comparison of hybrid and tri-hybrid nanofluid samples.

which is the typical structure for AlN. The diffraction peaks observed at 2θ values of approximately 33° , 36° , 38° , 48.8° , 59.31° , 66° , and 71.44° correspond to the (100), (002), (101), (102), (110), (103), and (201) planes of hexagonal AlN, respectively. The lattice parameters were found to be $a=3.112\,\text{Å}$ and $c=4.982\,\text{Å}$. These values result in a unit cell volume of $V=41.8\,\text{Å}^3$ and a corresponding density of $3.26\,\text{g/cm}^3$. The results are aligned with the standard data from the Joint Committee on Powder Diffraction Standards (JCPDS), specifically JCPDS card number 25-1133, confirming the phase purity of the AlN nanoparticles being

investigated. The results also correspond with the data reported by Hsu et al. [45] for AlN. In the analysis of the XRD pattern for silver nanoparticles, the prominent peaks observed at approximately 77° , 64° , 44° and 38° were indexed to the (311), (220), (200), and (111) planes of face-cantered cubic (FCC) silver, respectively, Fig. 11(b). The lattice parameter was calculated to be 4.089 Å, while the unit cell volume was determined as 68.39 Å 3 . These values are in excellent agreement with the established data for silver nanoparticles as documented in the JCPDS card number 04–0783. Additionally, the pronounced intensity of the

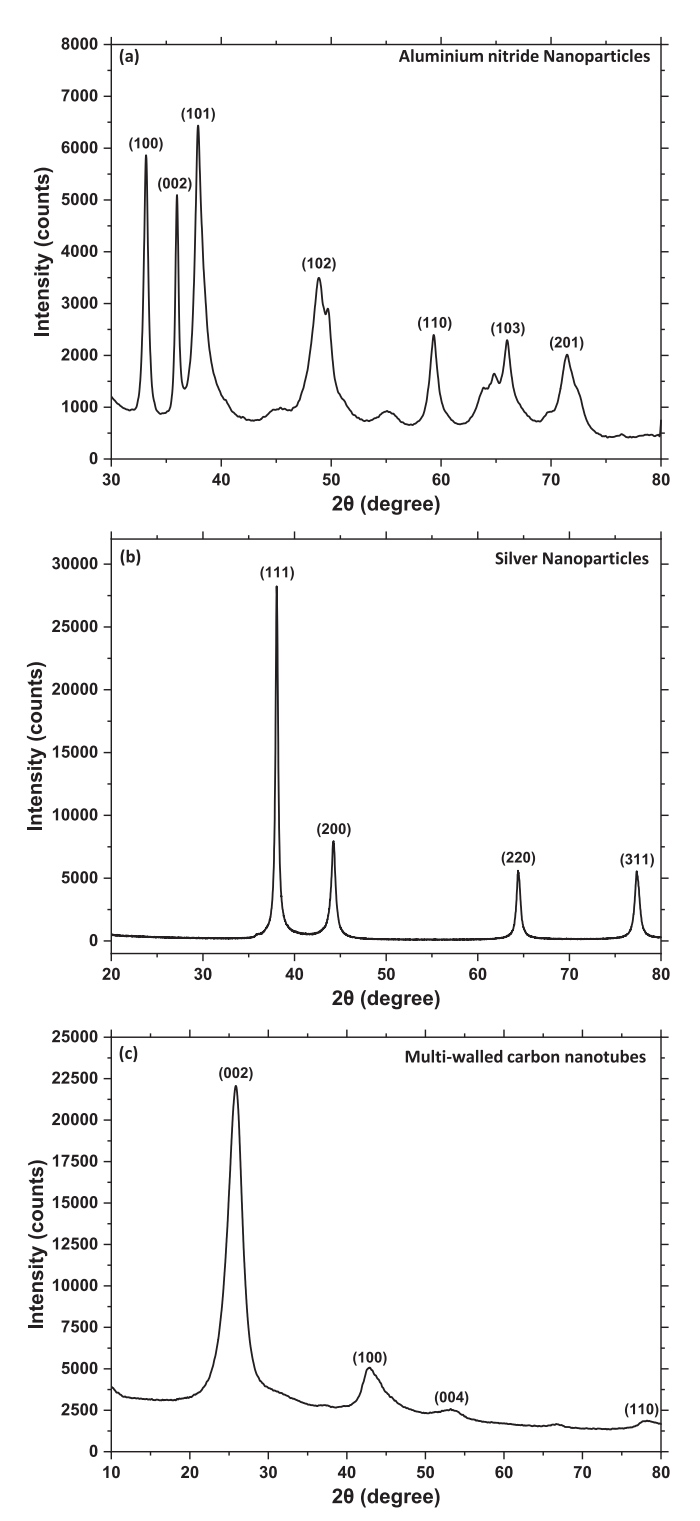


Fig. 11. X-ray diffraction (XRD) patterns for (a) Silver nanoparticles, (b) Aluminium nitride nanoparticles, and (c) multi-walled carbon nanotubes.

(111) peak suggests a preferential orientation of the silver nanoparticles, with the majority of their (111) crystal planes aligned parallel to the substrate or sample surface. The XRD pattern of MWCNTs exhibited broad peaks rather than sharp ones, indicating a relatively low degree of crystallinity. This is characteristic of MWCNTs due to their turbostratic structure, where the graphene layers have a random stacking arrangement. The most prominent peak was observed around $2\theta=25.8^\circ$, corresponding to the (002) diffraction plane, as depicted in Fig. 11(c). This peak signified the graphitic structure of the MWCNTs and provided

information about the interlayer spacing (d-spacing) between the graphene layers. Additionally, a less intense peak was often observed around $2\theta=43^\circ$, corresponding to the (100) diffraction plane, further confirming the graphitic nature of the material. The XRD pattern exhibited weaker peaks at higher angles, specifically around $2\theta=54^\circ$ and 77° . These weaker peaks corresponded to different crystallographic planes within the material. However, they were less pronounced compared to the more prominent peaks, likely due to the turbostratic nature of MWCNTs. The same pattern was observed and reported in various studies [46,47], corroborating the purity of the nanoparticles used in the current research.

The analysis revealed that AlN nanoparticles possessed a highly crystalline hexagonal structure, silver nanoparticles exhibited a face-centred cubic structure, and MWCNTs showed a typical turbostratic graphitic structure. The findings not only validated the phase purity and structural properties of the nanoparticles but also underscored the efficacy of XRD as a critical tool for detailed nanoparticle characterisation.

4.2. Transmission Electron Microscopy (TEM)

To gain deeper insights into particle morphology, the nanoparticles of silver, aluminium nitride, and multi-walled carbon nanotubes were examined using the JEOL Transmission Electron Microscopy (TEM) JEM-1400 Plus instrument [48,49]. This advanced analytical technique offers high-resolution imaging, which is essential for a detailed examination of the nanoparticles' shape, size, and structural characteristics.

Fig. 12 presents the TEM images, showcasing these three distinct types of nanoparticles under investigation in this study. Silver nanoparticles were observed to have a spherical shape with sizes ranging from 20 to 40 nm, while some particles broke down to sizes smaller than 20 nm when subjected to high-frequency waves during the sonication process. The results revealed that these nanoparticles tend to agglomerate or aggregate, forming irregular clusters. Second from the left in Fig. 12, multi-walled carbon nanotubes displayed their characteristic tubular structure, with lengths and diameters that varied in the range of 2.5–20 μm and 6–13 nm respectively. The TEM images clearly showed the elongated and intertwined nature of the MWCNTs, which contributed to their unique thermal characteristics. Aluminium nitride nanoparticles exhibited a different morphology, typically presenting as irregularly shaped particles with varying dimensions.

In the hybrid nanofluids combining MWCNTs, Ag, and AlN nanoparticles, the TEM images revealed a complex interaction between the different types of particles. The hybrid samples showed a more dispersed distribution, with the different nanoparticles maintaining their morphologies while interacting with each other. The AlN nanoparticles acted as a bridge to transfer heat between the nanotubes. In the simple MWCNTs sample, while they exhibited better thermal characteristics, the interactions between particles restricted effective heat transfer. The introduction of AlN nanoparticles helped mitigate this issue by providing pathways for heat to flow between the nanotubes, thereby enhancing overall thermal conductivity. Additionally, it was observed that some of the silver nanoparticles became embedded within the AlN matrix, further facilitating heat transfer. The presence of silver nanoparticles also played a crucial role in reducing the strong interactions between AlN particles, preventing the formation of tightly bound clusters that are difficult to break apart. This reduction in strong interactions helped maintain a more stable suspension.

AlN nanoparticles also played a crucial role in minimising the interwinding of MWCNTs and reducing the agglomeration of Ag nanoparticles. This dual functionality of AlN not only enhanced thermal conductivity but also improved the overall dispersion stability of the hybrid nanofluids. The synergistic effect of AlN, Ag, and MWCNTs in the hybrid nanofluid demonstrated a balanced interaction, which is vital for achieving optimal thermal performance and stability.

The complex interplay among these nanoparticles ensured that the thermal pathways remained efficient while preventing detrimental

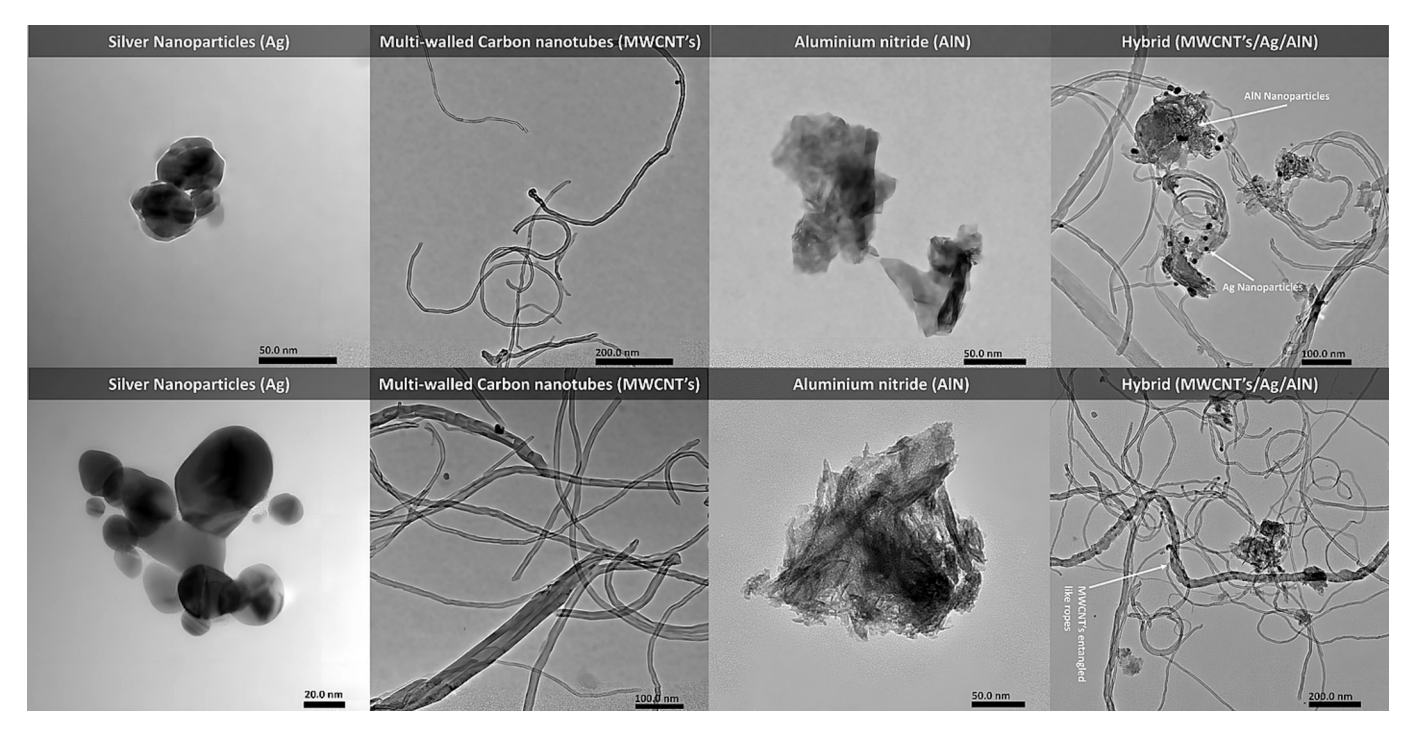


Fig. 12. TEM images displaying the morphology and agglomeration nanoparticles.

agglomeration and clustering. This behaviour highlights the importance of carefully selecting and combining different nanoparticles to maximise the benefits of hybrid nanofluids. The detailed TEM analysis provided insights into these interactions, showcasing the potential of these hybrid systems for advanced thermal management applications where both stability and high thermal conductivity are required.

4.3. Stability and particle size distribution

Zeta potential is a critical parameter that indicates the degree of repulsion (DOR) between adjacent, similarly charged particles in a dispersion. A higher absolute value of zeta potential generally suggests better stability, as it implies that the particles will repel each other more strongly, preventing aggregation and maintaining a stable suspension. However, it is important to note that zeta potential is not the sole determinant of stability. Factors such as particle morphology, density, and size also play significant roles in the long-term stability of nanofluids and must be considered alongside zeta potential when evaluating overall stability. The zeta potential values presented in Fig. 13 provide insight into the stability of the pure, hybrid, and tri-hybrid nanofluids composed of Ag, AlN, and MWCNTs.

A Malvern Zetasizer, a renowned instrument for nanomaterial analysis, was used to examine the samples [20,50]. The measurements were carried out in a specialised DTS 1070 cell, which is specifically designed for precise zeta potential measurements under controlled conditions. This cell is especially suitable for analysing emulsions and suspensions, where traditional cuvettes might not provide accurate readings. During the analysis, an electric field was applied to the nanofluid sample contained within the cell, and the movement of the particles in response to this field was observed. The velocity of these particles, which is influenced by the zeta potential, was measured, and the results were calculated using the Smoluchowski equation or similar mathematical models. The scattered light data was then processed by the Zetasizer software to determine the zeta potential of the samples.

The zeta potential values, which were measured immediately after sonication of both simple and hybrid nanofluid samples, fell within a range of -45 to -70 mV, as depicted in Fig. 13. This range is indicative of a high level of stability, with zeta potential values exceeding ± 30 mV

generally being recognized as a marker of good stability in particle suspensions. The zeta potential value for pure AlN was recorded at -48.23 mV. This value suggests good stability, as zeta potential values greater than ± 30 mV generally indicate a stable colloidal system. The negative value indicates that the surface of the AlN particles carries a negative charge in suspension. In comparison, Ag nanoparticles showed a zeta potential of $-51.9\,$ mV, indicating slightly higher stability compared to pure AlN. This suggests that Ag nanoparticles, in isolation, have a reasonably strong electrostatic repulsion, which helps in maintaining dispersion stability. However, it is important to note that Ag nanoparticles are denser than AlN, which could negatively impact their overall stability. MWCNTs had the highest zeta potential magnitude at -65.9 mV among the pure nanofluids. This indicates the greatest stability, likely due to the high surface area and unique electronic properties of MWCNTs, which can lead to significant surface charge density. Notably, while MWCNTs have a small diameter, their elongated structure can cause some tubes to become entangled, forming rope-like bundles that are challenging to break or disperse and impact stability negatively.

The zeta potential for the Ag/AlN (20/80) hybrid was -54.3 mV, reflecting a stability level comparable to the individual components but slightly enhanced due to the interaction between Ag and AlN. As the proportion of Ag increases in the hybrid (Ag/AlN 40/60 and 60/40), the zeta potential values show a slight variation, with -56.7 mV for 40/60and -49.7 mV for 60/40. The 40/60 ratio provides the highest stability within this series, likely due to an optimal balance of the electrostatic characteristics of Ag and AlN. With further increase in the Ag content (80/20), the zeta potential drops to -48.6 mV, closer to the value for pure AlN, suggesting that the higher proportion of AlN might dominate the stability behaviour. In case of MWCNTs/Ag hybrid formulation, 20/ 80 sample exhibited a zeta potential of -59.8 mV, indicating notable stability, although it was slightly less stable than pure MWCNTs. As the ratio changed to 40/60 and 60/40, the zeta potential values fluctuated, noted to be -51.9 mV for 40/60 and -55.4 mV for 60/40. These values suggested that MWCNTs significantly contributed to the dispersion stability, especially at higher concentrations. The zeta potential increased further to -60.2 mV in the 80/20 ratio, demonstrating enhanced stability as MWCNTs became more dominant. Similar to the

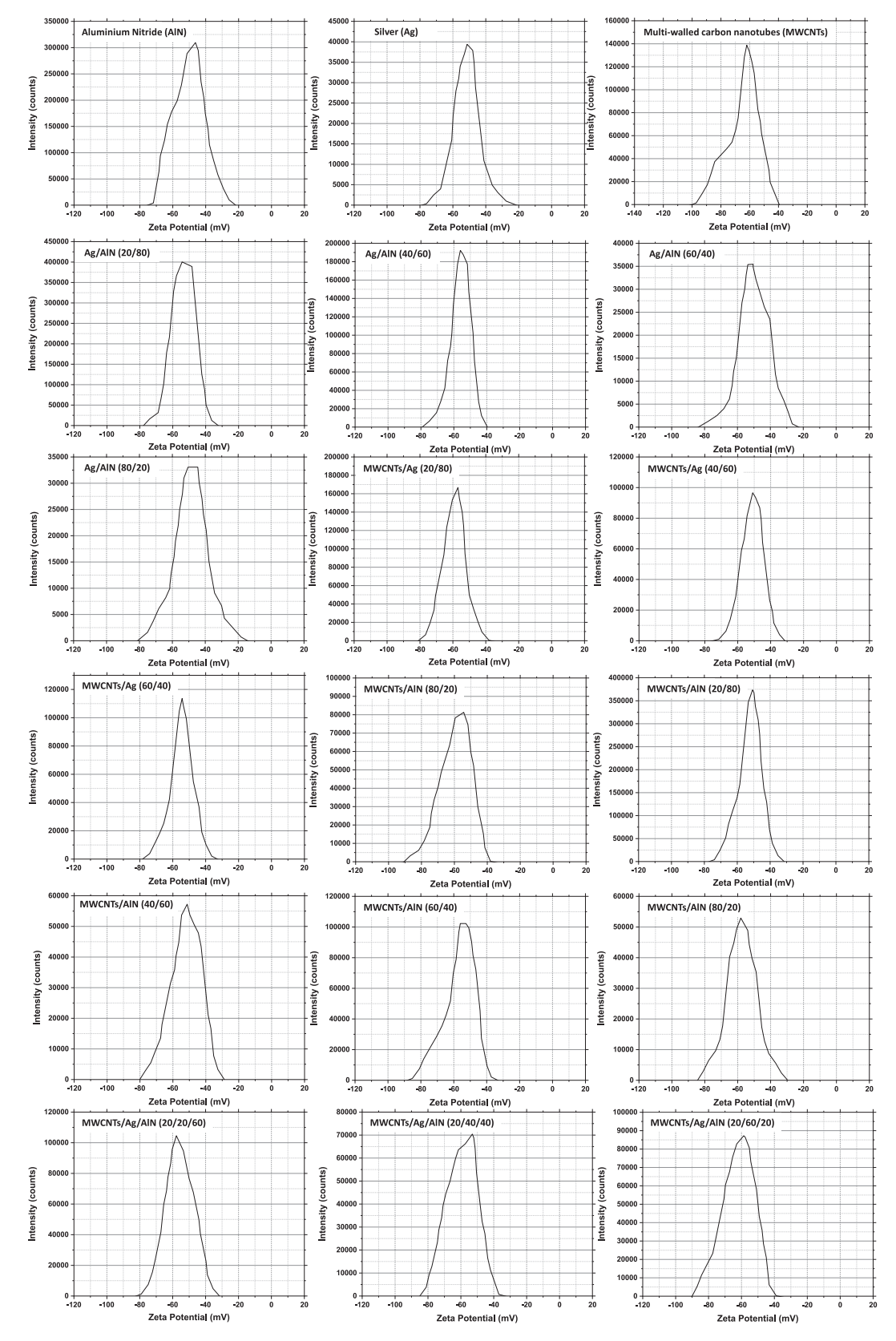


Fig. 13. Zeta potential distributions for pure, hybrid, and tri-hybrid nanofluids composed of Ag, AlN, and MWCNTs in various ratios.

MWCNTs/Ag hybrids, the zeta potential of MWCNTs/AlN formulations improved with increasing MWCNTs ratio. For the 20/80 hybrid, the zeta potential was found to be -53.1 mV, showing slightly better stability compared to pure AlN. As the proportion of MWCNTs increased in the

40/60 and 60/40 hybrids, the zeta potential rose to -52.1 mV and -57.5 mV, respectively. Among these ratios, the 60/40 hybrid exhibited the highest zeta value, highlighting the significant role of MWCNTs in enhancing colloidal stability. The value remained high recorded -56.3

 $\,$ mV for the 80/20 ratio, further demonstrating the effective stabilizing influence of MWCNTs in the hybrid nanofluids.

The tri-hybrid nanofluid with the composition 20/20/60 (MWCNTs/Ag/AlN) exhibited a zeta potential of -56.2 mV, indicating good

stability, likely due to the synergistic effects of the three nanoparticles. As the ratio changed to 20/40/40, the zeta potential increased to -59.4 mV, reflecting even higher stability due to the balanced contributions of MWCNTs and Ag. Finally, the 20/60/20 ratio showed the highest

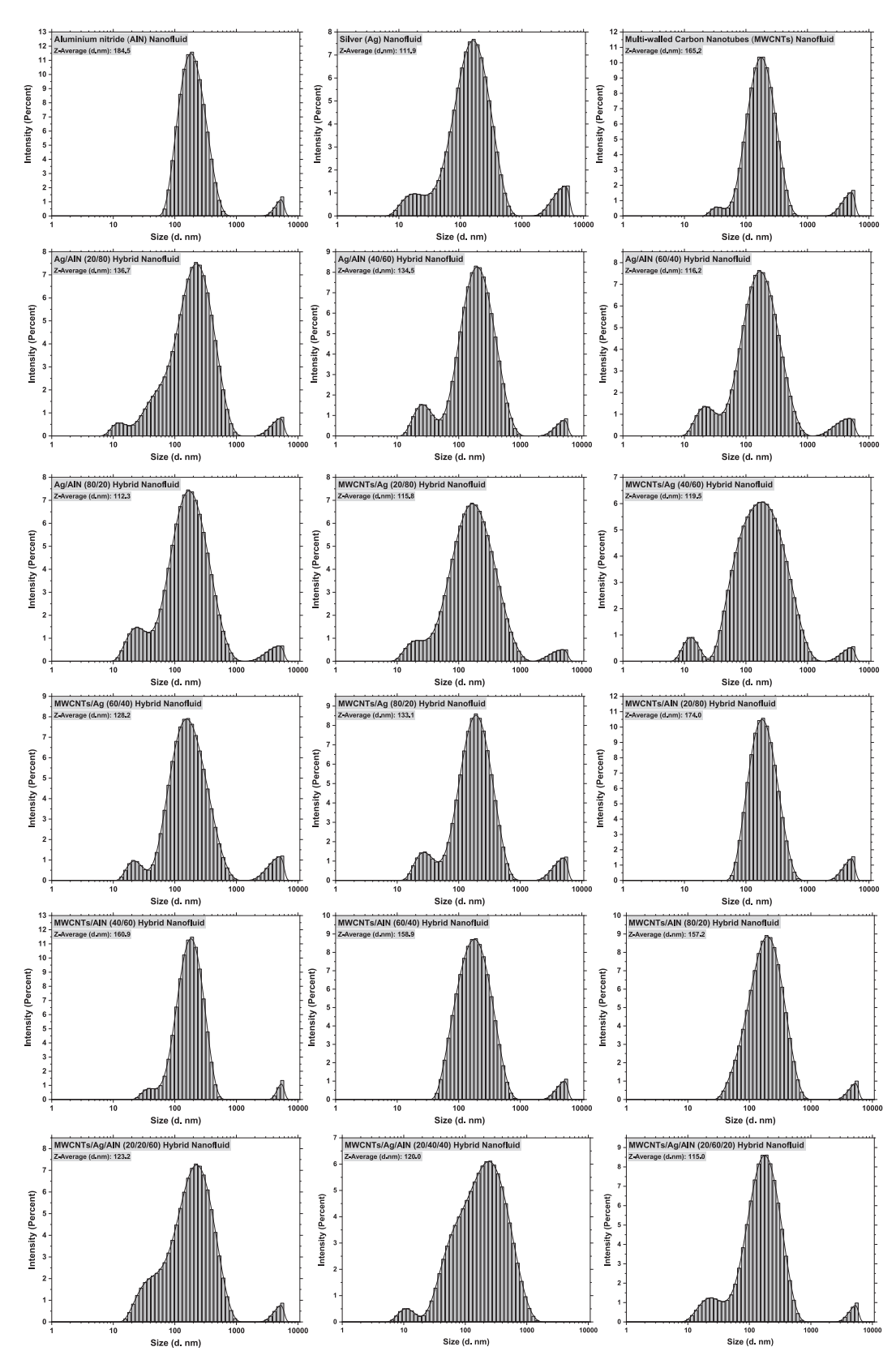


Fig. 14. Particle size distributions and Z-average values for pure, hybrid, and tri-hybrid nanofluids composed of Ag, AlN, and MWCNTs in various ratios.

stability among the tri-hybrid nanofluids with a zeta potential of -62.6 mV. This indicates that increasing the proportion of Ag, while maintaining a constant MWCNTs ratio and combining it with AlN, maximises electrostatic repulsion and effectively prevents particle aggregation. The findings concluded that carefully optimising the ratios of the constituent nanoparticles can significantly enhance the stability of nanofluids, making them more suitable for practical applications where long-term dispersion stability is critical.

The analysis of suspended particle size and agglomeration behaviour in nanofluids was also conducted using the Malvern Zetasizer, which provides insights into the stability and dispersion quality of the nanofluids. The histograms generated for each type of nanofluid indicate the particle size distribution, with the Z-average (mean) values listed for different formulations, as shown in Fig. 14. This study was carried out five days after sample preparation to assess the evolution of particle agglomeration over time. The Z-average particle size for the AlN suspension in basefluid was found to be 184.8 nm, significantly larger than its initial particle size of <100 nm. This marked increase indicates that AlN particles have a tendency to agglomerate in suspension, leading to larger clusters. In comparison to other pure nanofluids, AlN exhibited a higher Z-average value, likely due to the inherently larger size of suspended particles. The histogram reflects a relatively symmetric peak, which indicates a uniform distribution of agglomerates, with minimal formation of significantly larger aggregates. The Ag nanofluid exhibited a Z-average of 111.8 nm, which, while larger than its initial size of 10-40 nm, was still considerably smaller than that of AlN. However, considering the initial size of particles and the relatively small difference in zeta potential between Ag and AlN, the formation of agglomerates observed in the Ag samples was substantial. The histogram is slightly asymmetric, with a tail on the right, indicating the presence of some larger agglomerates. Additionally, the broader base of the histogram suggested the existence of agglomerates of varying sizes.

The MWCNT nanofluid showed a *Z*-average of 184.8 nm, similar to that of AlN. This large *Z*-average is due to the high aspect ratio of MWCNTs, which tend to form entangled networks rather than simple spherical agglomerates. The histogram indicates a somewhat broad distribution, reflecting a range of agglomerate sizes due to the complex geometry and tendency of nanotubes to entangle.

Among the nanofluids studied, the Ag nanofluid had the smallest *Z*-average, which could be attributed to its smaller initial particle size. However, relying solely on the *Z*-average to assess the stability of nanofluids is not considered to be a good approach. Despite the lower *Z*-average, the higher density of Ag nanoparticles negatively impacted stability, leading to a tendency for sedimentation. Therefore, factors such as particle density and initial size should also be considered equally when evaluating nanofluid stability. It was evident that the stability of nanofluids is not governed by a single factor but is influenced by a combination of properties. Thus, while the Ag nanofluid exhibited a lower *Z*-average, this did not necessarily mean it outperformed the MWCNT or AlN nanofluids in terms of stability.

In the case of hybrid samples, the Z-average particle sizes for the Ag/ AlN hybrids varied slightly, ranging from 136 nm to 112 nm. The Ag/ AlN (20/80) nanofluid, having the lowest Ag content, exhibited a Zaverage value of 136.7 nm, indicating the presence of larger-sized AlN nanoparticles. As the proportion of Ag increased, the Z-average particle size decreased, with the 40/60 and 60/40 ratios showing reduced average particle sizes of 134.5 nm and 116.2 nm, respectively. The Ag/ AlN (80/20) nanofluid, with the highest Ag content, achieved the smallest Z-average value of 112.3 nm, demonstrating that a higher proportion of small-sized Ag nanoparticles was effective to some extent in reducing the size of larger AlN clusters. However, compared to pure AlN, the hybrid nanofluids showed slightly better stability. In the MWCNTs/Ag hybrid nanofluid samples, the Z-average particle sizes were observed to increase as the proportion of MWCNTs increased. The MWCNTs/Ag (20/80) nanofluid, with the highest Ag content, exhibited the smallest Z-average size at 115.8 nm, indicating that a higher

proportion of Ag, combined with a lower MWCNT content, favoured the formation of smaller-sized nanoparticles. As the proportion of MWCNTs increased, the particle size also increased, with the Z-average values rising to 119.5 nm for the 40/60 ratio, 128.2 nm for the 60/40 ratio, and reaching the highest value of 133.1 nm for the 80/20 ratio. The histogram of 40/60 was slightly broader, with a wider base, reflecting a greater variation in particle sizes. For MWCNTs/AlN hybrid nanofluid samples, the Z-average particle size consistently decreased as the MWCNTs concentration increased. The MWCNTs/AlN (20/80) nanofluid, characterized by a higher proportion of AlN, exhibited the largest Z-average particle size of 174.0 nm. As the ratio of MWCNTs was increased, the particle sizes progressively reduced, with the Z-average values decreasing to 160.9 nm, 158.9 nm, and 157.2 nm for the 40/60, 60/40, and 80/20 ratios, respectively. However, the minor peaks observed towards the right end of the histograms indicate the presence of slightly larger particle agglomerates, particularly in samples with a higher AlN content. Finally, the MWCNTs/Ag/AlN tri-hybrid nanofluid samples exhibited a consistent decrease in *Z*-average particle sizes as the proportion of silver increased relative to AlN. A 20/20/60 ratio (MWCNTs/Ag/AlN) resulted in a Z-average size of 123.2 nm. With an increased Ag content to a 20/40/40 ratio, the average size was slightly reduced to 120.0 nm. Further elevation of the Ag content to a 20/60/20 ratio led to the smallest observed particle size of 115.0 nm. This trend indicates that the inclusion of higher amounts of smaller Ag nanoparticles effectively disrupts the formation of larger AlN clusters, yielding a more uniform and reduced particle size distribution.

The comparative analysis of tri-hybrid nanofluids with other pure and hybrid nanofluids reveals that the inclusion of different sized and shaped particles in the tri-hybrid solution not only helps to enhance the thermal characteristics but also results in smaller Z-average particle sizes for the agglomerates formed. This effect is particularly evident in the histogram, where the wider base indicates the presence of a diverse range of particle sizes and the varying agglomerates or structures they create. The incorporation of multiple particle types in the tri-hybrid formulation introduces heterogeneity in size and shape, which in turn weakens the attractive forces between particles. This weakening makes it easier to disrupt and redisperse the agglomerates, contributing to a more stable and uniform particle distribution.

The *Z*-average particle size measurements obtained from the Malvern Zetasizer confirm that all nanofluids experience agglomeration to some extent, though the degree varies depending on the specific composition. This study underscores the importance of understanding and controlling agglomeration in nanofluids, as it directly impacts their stability, thermal efficiency, and overall performance. By optimising the composition and particle distribution within nanofluids, researchers can develop more effective solutions for applications that require enhanced thermal management and stability.

5. Results and discussion

5.1. Thermal conductivity

Fluids thermal conductivity is a critical property that significantly influences their heat transfer characteristics across various applications. Understanding and accurately measuring this property is essential for optimising the performance of nanofluids in practical use. The current study used the Hot Disk TPS 2500S thermal analyser, which employs the transient plane source (TPS) technique to accurately and reliably measure the thermal conductivity of both water and nanofluid samples. A double spiral Kapton 7577 sensor element is used to measure the values, designed to function as both a heat source and a resistance thermometer. This dual functionality allows it to heat the nanofluid sample while simultaneously measuring the resulting temperature changes with high precision. The experimental setup consists of a TPS analyser, constant temperature bath, and a liquid sample holder, as illustrated in Fig. 15. A specially designed liquid sample holder was used to confine the fluid

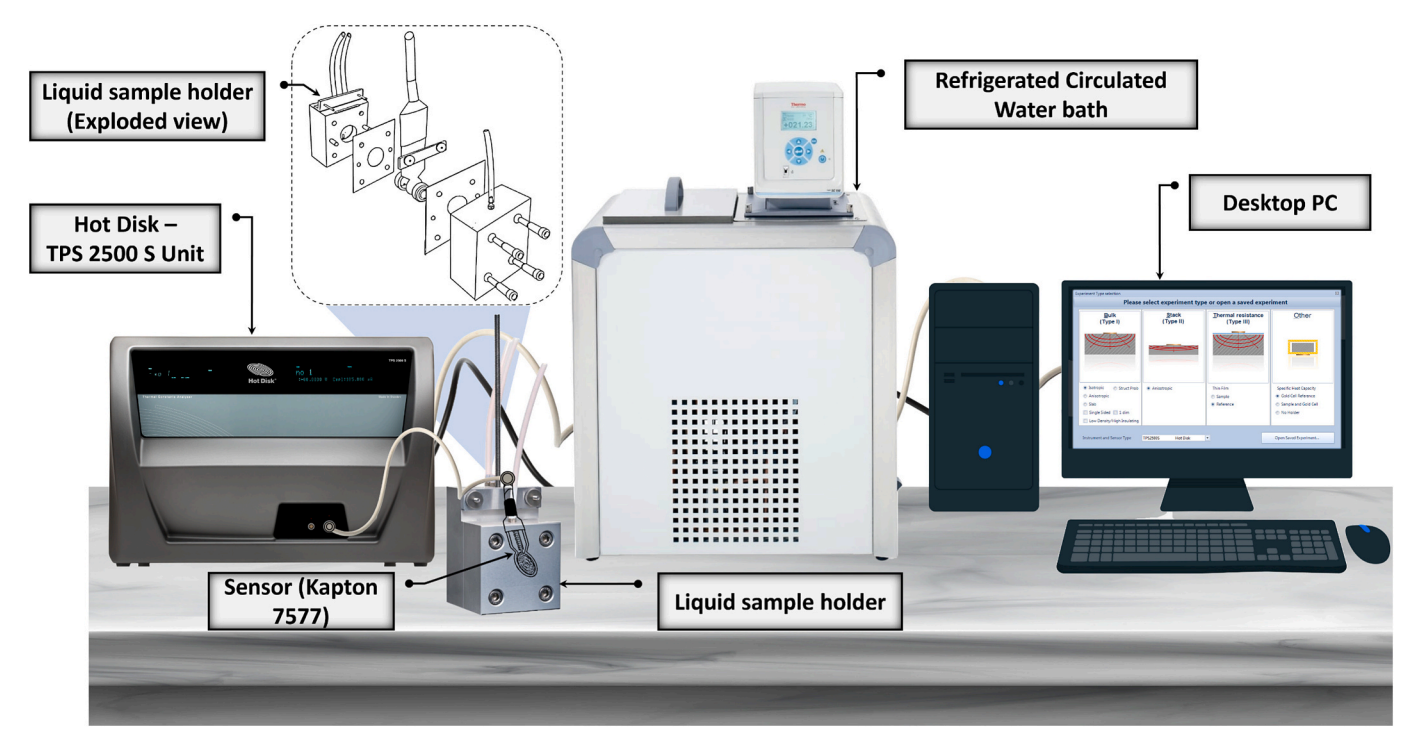


Fig. 15. Schematic representation of the experimental configuration for measuring thermal conductivity.

within a small, controlled chamber, positioning the sensor in the liquid while preventing any contact with the chamber walls. The careful placement of the sensor is essential to avoid any measurement errors that could arise from sensor-wall contact or convective effects. To maintain a stable temperature during the measurements, the liquid

sample holder was immersed in a constant temperature bath. This setup helped to ensure that the thermal conductivity readings remained unaffected by external temperature fluctuations, thereby allowing for reliable and consistent data. A heating power of 60 mW was applied with a measurement duration of 2 s. During the measurement procedure, the

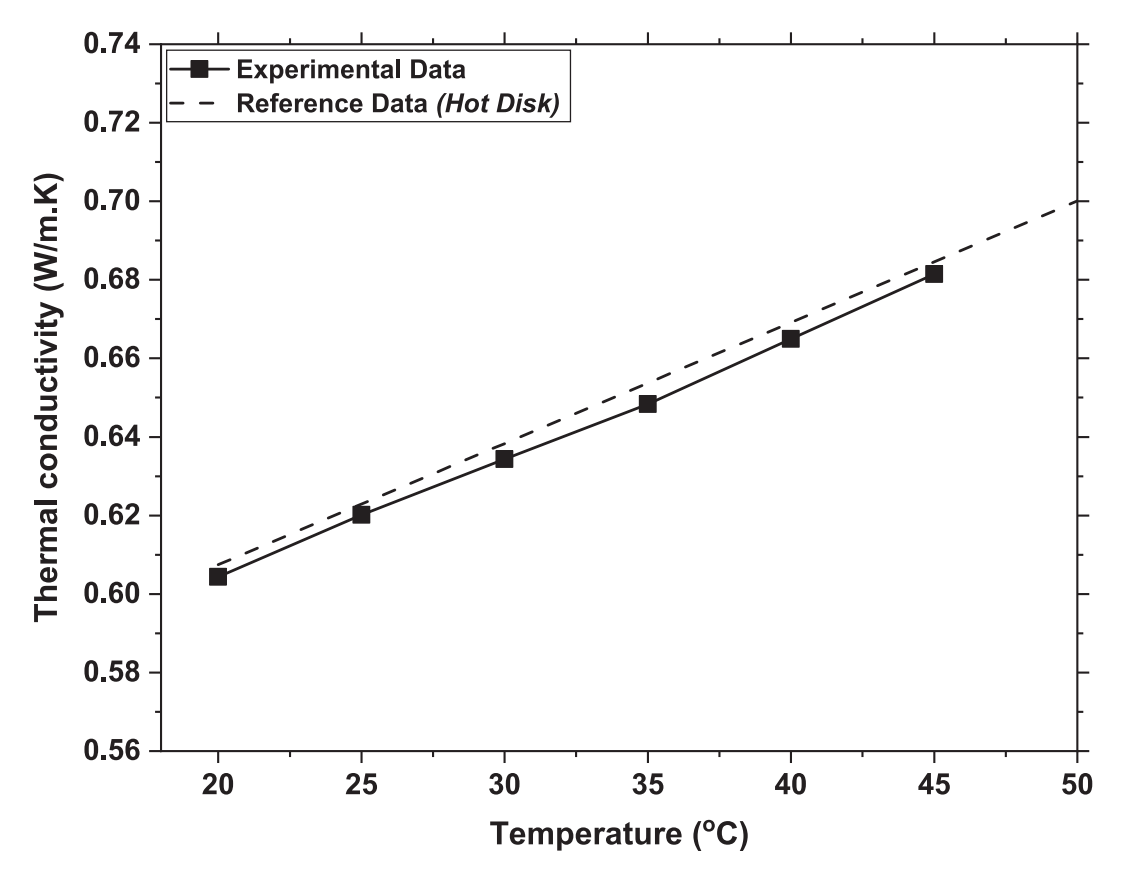


Fig. 16. Comparison of experimental thermal conductivity data for distilled water with reference data from Hot Disk across a temperature range of 20 °C to 45 °C.

Hot Disk analyser applies a heat pulse through the sensor and records the transient temperature response of the nanofluid. The analyser processes this data to determine how the temperature changes over time, ultimately calculating the sample's thermal conductivity value.

The uncertainty in thermal conductivity measurements was assessed based on the accuracy of experimental procedures and the instrument's specifications. The Hot Disk TPS 2500S thermal analyser has a manufacturer-specified maximum uncertainty of ± 5 %. However, for the fluid sample, the maximum standard deviation was measured to be less than 0.7 %, which reflects the high precision of the collected data. This low standard deviation demonstrates minimal variation between repeated measurements and remains within acceptable limits. To improve the accuracy, three measurements were recorded at each temperature point. This careful approach was designed to reduce potential errors and ensure the reliability of the results. Furthermore, system calibration was performed using a stainless-steel reference sample provided by the supplier, which yielded a standard deviation of less than 0.5 %. This suggests that the experimental setup was properly calibrated and capable of generating consistent and reliable results. Sundberg et al. [51] conducted a comparative study of thermal property measurements using different methods and found that the TPS method showed excellent repeatability, with standard deviations within sample groups better than ± 0.5 %.

The accuracy of the testing setup was validated by measuring the thermal conductivity of distilled water across a temperature range of 20 $^{\circ}\text{C}$ to 45 $^{\circ}\text{C}$, with data collected at 5 $^{\circ}\text{C}$ intervals, as demonstrated in Fig. 16. Comparison of these results with the reference values provided by Hot Disk showed close agreement, suggests that the setup is reliable. The minor variations observed are likely attributable to the natural variability in water properties.

The addition of surfactants is a common practice to enhance the suspension stability of nanoparticles [52,53]. However, selecting a suitable surfactant is crucial as some can adversely affect stability, resulting in reduced thermal conductivity of the fluid. While surfactants can significantly improve fluid stability, their effects vary with the type of particle used. An unsuitable surfactant can reduce stability, causing particles to agglomerate and settle more quickly.

A study was conducted to investigate the impact of different surfactants on the TC of prepared nanofluid samples. For this purpose, the conductivity of simple nanofluid samples prepared with 0.01 vol% nanoparticles was measured just after the sonication and after 72 h. According to the results, a significant reduction in thermal conductivity was observed in the AlN nanofluid prepared without any surfactant. The thermal conductivity decreased from 0.664 W/m·K to 0.657 W/m·K, with the enhancement dropping from 2.38 % to 1.33 %, as shown in Fig. 17. Among the surfactants tested, SDS was found to be the worst choice for AlN nanofluid, showing the most considerable reduction in thermal conductivity over time. In contrast, SDBS showed the minimum

reduction, indicating better stability. Gum Arabic was identified as a good surfactant after SDBS, while CTAB provided better stability than SDS. As anticipated, the silver nanofluid showed a notable decrease in thermal conductivity after 72 h for the sample prepared without a surfactant. However, the decline was less pronounced in samples containing CTAB and SDBS surfactants. Among these, the SDBS sample exhibited superior stability, while SDS and Gum Arabic proved to be less effective. The thermal conductivity results of MWCNT nanofluids further underscore the significant impact of surfactants on thermal properties, which vary depending on the type of particles used. In case of MWCNTs, samples prepared with SDSBS and Gum Arabic demonstrated better particle suspension stability, with only a slight reduction in thermal conductivity after 72 h. However, nanofluids prepared with other surfactants exhibited more pronounced decreases in thermal conductivity over the same period. Specifically, the thermal conductivity of the nanofluid without any surfactant was notably poor, dropping from 0.6790 W/m·K to 0.6740 W/m·K after 72 h.

The results revealed that surfactant choice greatly affects nanofluid stability and thermal conductivity. SDBS and CTAB proved most effective for AlN and silver nanofluids, showing minimal reductions in thermal conductivity. For MWCNT nanofluids, SDSBS and Gum Arabic were best at maintaining thermal properties. These findings underscore the importance of selecting the appropriate surfactant to improve nanofluid performance.

Particle concentration is another critical factor in optimising nanofluid performance [54]. To evaluate its impact, nanofluid samples containing AlN, Ag, and MWCNTs were prepared with particle concentrations ranging from 0.01 to 0.03 vol%. This range was chosen to balance enhanced thermal properties with stability, crucial for applications like electronic cooling in mini and microchannel heat sinks. Higher particle concentrations can lead to an increase in pressure drop, higher pumping power, and the risk of particle agglomeration. Agglomerated particles may cause blockages in channels, resulting in localised heating and potential damage to the system. Thus, optimising particle concentration is key to maintaining fluid stability and system performance.

The thermal conductivity has been calculated at a constant temperature of 35 $^{\circ}$ C and the results are presented in Fig. 18. While all types of nanoparticles exhibited an increase in thermal conductivity with rising concentration, however, this enhancement varied among different nanoparticle types. According to the results, MWCNT's suspended nanofluid demonstrated the highest thermal conductivity values at all tested concentrations. At 0.01 %, the thermal conductivity increased by 4.54 %, and at 0.03 %, it reached a 7.29 % enhancement. The consistent rise in thermal conductivity across all concentrations demonstrated the strong impact of MWCNTs, making them highly effective for improving thermal performance in nanofluids. This superior performance is due to the high thermal conductivity and unique structure of carbon

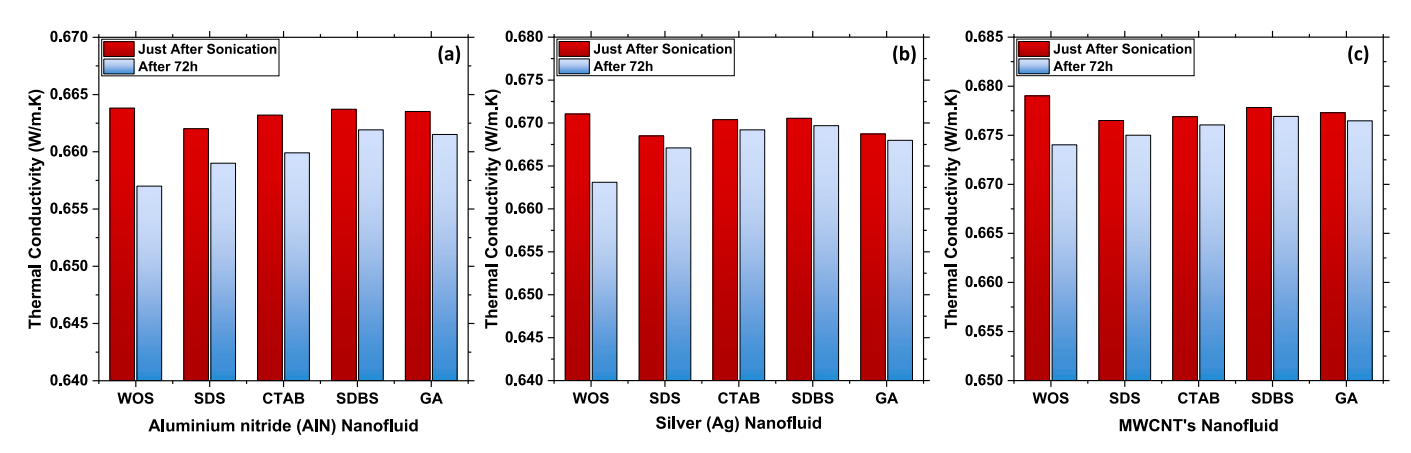


Fig. 17. Effect of surfactants on the thermal conductivity of nanofluids over a 72-h period.

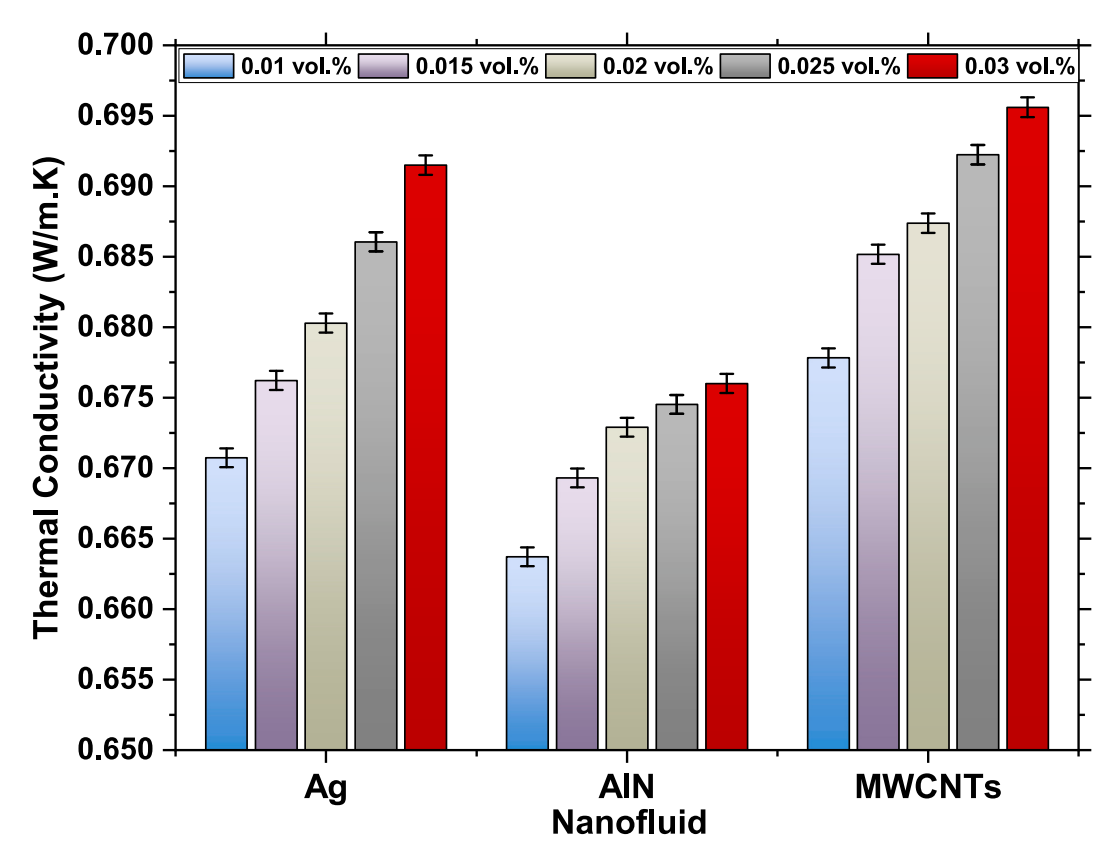


Fig. 18. Thermal conductivity of nanofluids with varying particle concentrations.

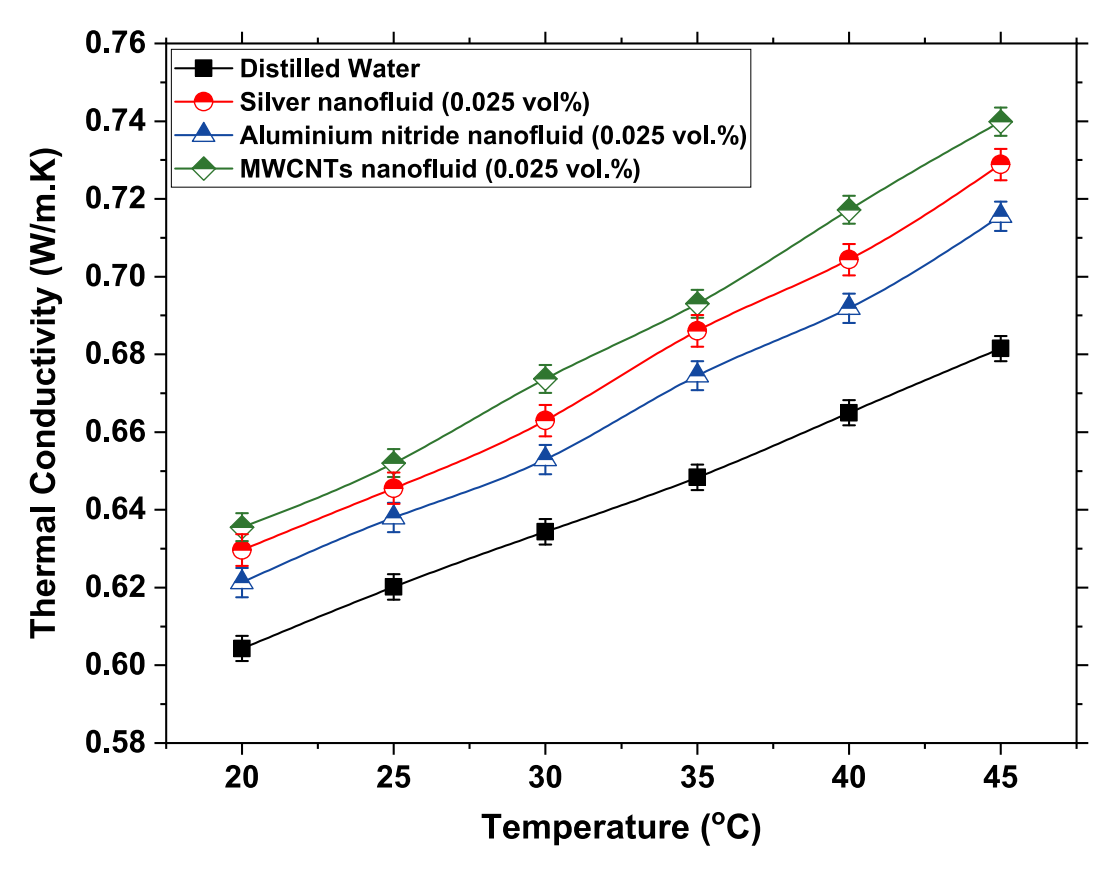


Fig. 19. Temperature-dependent thermal conductivity of distilled water and nanofluids containing Ag, AlN, and MWCNTs at 0.025 vol% concentration.

nanotubes, which enable efficient phonon transport, resulting in significant conductivity improvements even at lower concentrations. Silver nanoparticles also showed significant improvements in thermal conductivity, though their performance, while notable, was not as high as that of MWCNTs, although it was closely competitive. The enhancement ranges from 3.45 % at the lowest concentration to 6.65 % at the highest. This progressive increase in thermal conductivity with concentration underscores the effectiveness of silver nanoparticles in improving heat transfer properties. However, it is important to consider the stability of the nanofluid, as higher nanoparticle concentrations can impact dispersion and potentially affect thermal conductivity over time. Aluminium nitride nanofluids, on the other hand, exhibited a more modest increase in thermal conductivity compared to MWCNTs and Ag, due to AlN's inherently lower thermal conductivity. As the concentration of AlN nanoparticles increased from 0.01 % to 0.03 %, the thermal conductivity of the nanofluid improved steadily, with enhancements ranging from 2.37 % to 4.26 %. Although AlN did enhance thermal conductivity, its effect was less pronounced than others.

The findings emphasise the importance of optimising particle concentration to balance thermal performance with stability, as in practical applications consistent heat transfer and long-term fluid stability are crucial. Ultimately, selecting the appropriate nanoparticle and concentration is key to achieving the desired thermal performance.

Fig. 19 shows the thermal conductivity of water and various

nanofluids containing Ag, AlN, and MWCNTs suspension over a temperature range from 20 °C to 45 °C. Each nanofluid was prepared with a particle concentration of 0.025 vol%. The study found that thermal conductivity increased significantly with temperature for all samples. The increase in thermal conductivity with temperature and concentration is primarily due to improved Brownian motion of nanoparticles, which facilitates more effective micro-convection and energy exchange within the fluid. As temperature increases, particle agitation intensifies, leading to enhanced thermal energy transport across the liquid medium. This is particularly evident beyond 30 °C, where the thermal conductivity shows more pronounced growth. As nanoparticles move more freely and uniformly within the fluid, they can more effectively transfer heat through the nanofluid. This improved thermal transfer is reflected in the higher thermal conductivity observed at elevated temperatures. In heat transfer applications, this means nanofluids are more effective at higher temperatures, making them ideal for scenarios where elevated temperatures are common. Water exhibited a steady increase in thermal conductivity from 0.604 W/m·K at 20 °C to 0.681 W/m·K at 45 °C, reflecting enhanced molecular motion and reduced viscosity at higher temperatures. Silver nanofluid consistently demonstrated superior thermal conductivity compared to water, rising from 0.630 W/m·K at 20 °C to 0.729 W/m·K at 45 °C, due to the high thermal conductivity of silver particles. Aluminium nitride nanofluid also showed improved thermal conductivity over water, increasing from 0.621 W/m·K at 20 °C

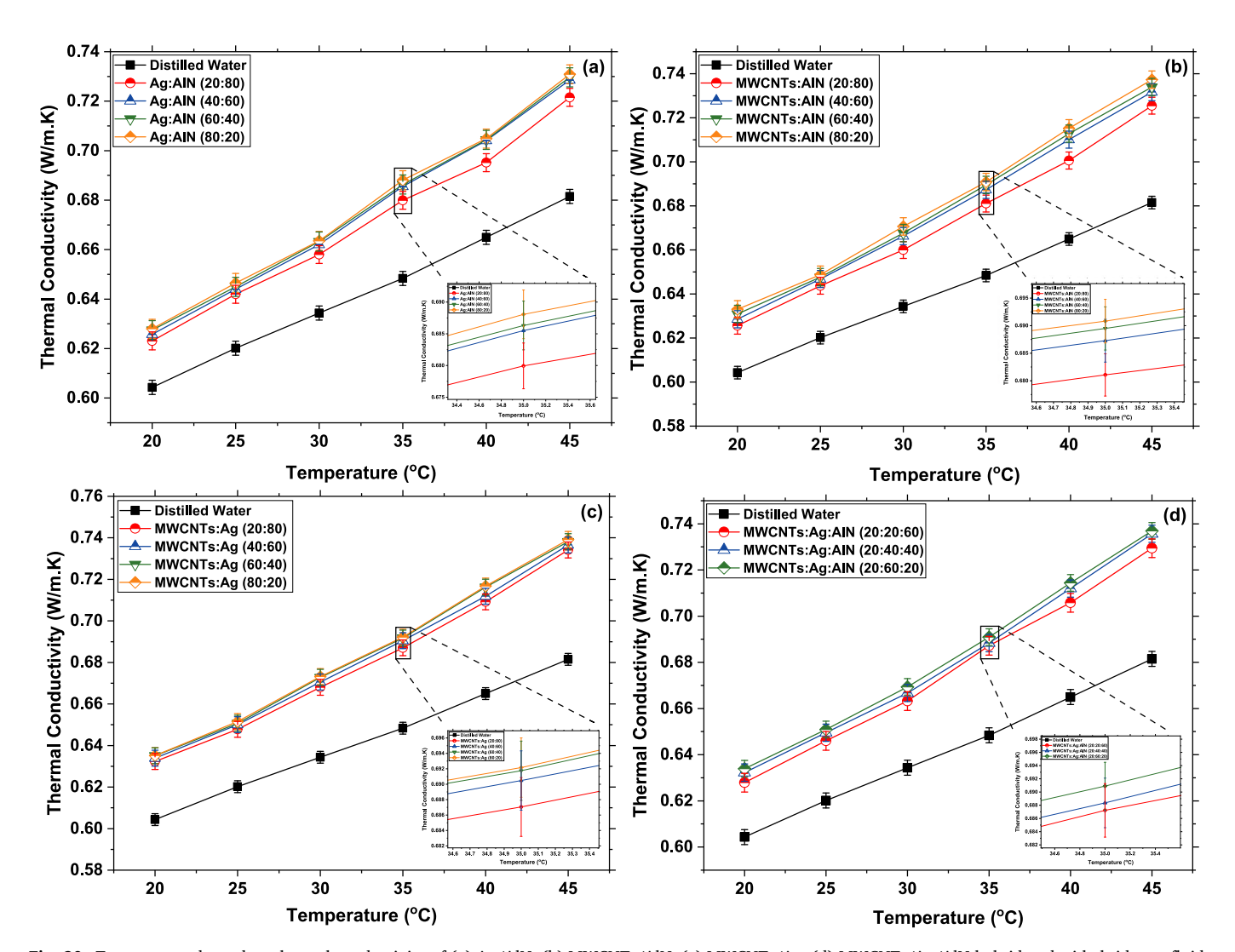


Fig. 20. Temperature-dependent thermal conductivity of (a) Ag/AlN, (b) MWCNTs/AlN, (c) MWCNTs/Ag, (d) MWCNTs/Ag/AlN hybrid and tri-hybrid nanofluids with different mixing ratios.

to 0.716 W/m·K at 45 °C, however, the enhancement was less pronounced than with silver. Among the nanofluids tested, MWCNTs exhibited the highest thermal conductivity. The thermal conductivity of MWCNTs nanofluid increased from 0.636 W/m·K at 20 °C to 0.740 W/m·K at 45 °C. The exceptional increase is attributed to the unique structural and thermal properties of the multi-walled carbon nanotubes, which provide superior heat transfer capabilities.

Fig. 20 presents the thermal conductivity values of various hybrid nanofluids, prepared with different mixing ratios of 80/20, 60/40, 40/60, and 20/80, across temperatures ranging from 20 °C to 45 °C. The outcomes demonstrated that the thermal conductivity of these hybrid samples was significantly influenced by the proportions of nanoparticles within the mixture, as well as by temperature variations. Notably, all the hybrid nanofluids demonstrated substantial enhancements in TC compared to water. The study conducted by Wanatasanappan et al. [55] reported similar trends in their investigation of Al₂O₃/CuO hybrid nanofluids, demonstrating that the thermal conductivity enhancement was a function of both particle concentration and temperature.

As depicted in Fig. 20(a), the thermal conductivity of the Ag/AlN hybrid nanofluids was evaluated across various mixing ratios. The results showed that the hybrid nanofluid prepared with a 20/80 ratio exhibited intermediate thermal conductivity values, ranging from $0.6230 \text{ W/m} \cdot \text{K}$ at $20 \,^{\circ}\text{C}$ to $0.7216 \, \text{W/m} \cdot \text{K}$ at $45 \,^{\circ}\text{C}$, falling between those of pure Ag and AlN nanofluids. As the proportion of silver increased to 40 % further improved the thermal conductivity, with values rising from $0.6257~W/m\cdot K$ at $20~^{\circ}C$ to $0.7285~W/m\cdot K$ at $45~^{\circ}C$. Despite this enhancement, thermal conductivity remained slightly lower than that of the pure Ag nanofluid, indicating that while the inclusion of Ag had a beneficial effect, it did not surpass the conductivity provided by silver alone. However, at the 60/40 mixing ratio, thermal conductivity slightly exceeded that of both the individual Ag and AlN nanofluid, with values recorded to be 0.6275 W/m·K at 20 $^{\circ}\text{C}$ and 0.7297 W/m·K at 45 $^{\circ}\text{C}$. This finding suggests a synergistic interaction between Ag and AlN at this specific ratio, where the combination of the two nanoparticles resulted in a hybrid nanofluid that outperformed its unitary counterparts. Finally, at the 80/20 ratio, the hybrid nanofluid's thermal conductivity improved further, approaching the values observed for the 60/40 hybrid sample, with thermal conductivities of 0.6280 W/m·K at 20 °C and 0.7309 W/m·K at 45 °C. These results indicate that the optimal interaction between highly conductive silver particles and AlN particles enhances nanoparticle dispersion and stability within the base fluid, leading to superior thermal performance of the hybrid nanofluid at the 60/40 and 80/20 mixing ratios.

The samples containing MWCNTs and AlN nanoparticles exhibited superior thermal conductivity values compared to Ag/AlN hybrid samples across all mixing ratios, due to the presence of MWCNTs, Fig. 20(b). The study found that increasing the proportion of MWCNTs in the nanofluid resulted in higher thermal conductivity values. As shown in Fig. 20(b), at 35 °C, the thermal conductivity for the 20/80 MWCNTs/ AlN mixture was 0.681068 W/mK, while the 80/20 mixture reached 0.690820 W/m·K. This observation is consistent with the known high thermal conductivity of MWCNTs, which appeared to dominate the thermal behaviour of the mixtures, enhancing their overall thermal performance. For this hybrid combination, the values varied in-between the individual thermal conductivities of MWCNTs and AlN. At 20 $^{\circ}\text{C},$ the thermal conductivity of Ag/AlN hybrid samples were recorded to be varied ranging from 0.6231 to 0.6280 W/mK, as demonstrated in Fig. 20 (a). However, the thermal conductivity values for the MWCNTs/AlN nanofluids at the same temperature ranged from 0.6256 W/mK for the 20/80 ratio to 0.6330 W/mK for the 80/20 ratio. This trend of increased thermal conductivity in nanofluids persisted as the temperature increased. By 45 $^{\circ}$ C, the thermal conductivity of Ag/AlN reached 0.7308 W/mK, whereas the values for the MWCNTs/AlN nanofluids were significantly higher, with the 80/20 mixture achieving a value of 0.7373 W/m·K. Fig. 20(c) presents the results of MWCNTs/Ag hybrid nanofluid, which delivered superior thermal conductivity compared to

Ag/AlN and MWCNTs/AlN nanofluids across all mixing ratios. This enhanced performance can be attributed to the exceptional thermal properties of both MWCNTs and Ag, along with several other influencing factors such as particle shape, Brownian motion, density, better suspension, etc. As the MWCNTs loading increased, there was a noticeable rise in thermal conductivity, with values improving from 0.7341 W/m·K at a 20/80 ratio to 0.7392 W/m·K at 80/20 ratio.

The thermal conductivity of the tri-hybrid nanofluid was observed to be slightly lower compared to the MWCNTs/Ag hybrid solution across the temperature range studied, as shown in Fig. 20(d). As the MWCNTs ratio was the same, with the increase in Ag loading, the value increased, showing an enhancement in thermal conductivity. For the sample with a 20/60/20 mixing ratio, at 20 $^{\circ}$ C, the thermal conductivity was noted to be 0.6339 W/m·K which was marginally lower than that of the MWCNTs/Ag hybrid solution with a conductivity of 0.6351 W/m·K. This trend persists at higher temperatures; for example, at 45 $^{\circ}$ C, the tri-hybrid nanofluid exhibited a thermal conductivity of 0.7369 W/m·K, which remains slightly below the 0.7391 W/m·K recorded for the MWCNTs/Ag hybrid.

The observed lower thermal conductivity in the tri-hybrid nanofluid can be attributed to the presence of AlN, which, despite its significant role in enhancing thermal pathways through its distinct shape and interaction with MWCNTs and spherical Ag particles, has a lower intrinsic thermal conductivity compared to MWCNTs. At lower temperatures, this difference is less pronounced, but as temperature increases, the thermal conductivity advantage of MWCNTs and Ag particles becomes more evident. However, the tri-hybrid nanofluid presents notable advantages in terms of long-term stability and cost-effectiveness, making it a viable alternative for applications where these factors are critical. The slightly reduced thermal conductivity must be weighed against these benefits, suggesting that the tri-hybrid formulation could be preferable in scenarios where stability and economic considerations are prioritized over marginal improvements in thermal performance.

Fig. 21 presented the thermal conductivity enhancement of various nanofluids relative to the base fluid, water. The data highlighted the varying degrees of enhancement across different compositions at 45 $^{\circ}$ C. For the simple nanofluids, AlN exhibited a moderate enhancement of 4.997 %, indicating that the inclusion of AlN nanoparticles offered a significant improvement over the base fluid. The addition of Ag nanoparticles results in a higher enhancement, with a value of 6.948 %. MWCNTs provided the greatest enhancement among the simple nanofluids, with a value of 8.566 %, consistent with their known superior thermal properties.

The hybrid nanofluids, which were combinations of two different nanomaterials, exhibited varying levels of thermal conductivity enhancement depending on the ratio of the components. The Ag/AlN hybrid nanofluid showed a progressive increase in thermal conductivity as the proportion of Ag increased: starting from 5.878 % for a 20/80 ratio and reaching 7.244 % for an 80/20 ratio. This trend highlighted the synergistic effects of combining Ag and AlN, with the thermal conductivity enhancement predominantly influenced by the higher conductive Ag component. Similarly, the MWCNTs/AlN hybrid nanofluid demonstrated increasing thermal conductivity with higher MWCNTs content, ranging from $6.455\,\%$ at a $20/80\,$ ratio to $8.191\,\%$ at an $80/20\,$ ratio. This suggested that MWCNTs dominated the enhancement due to their superior thermal conductivity properties compared to AlN. In the case of the MWCNTs/Ag hybrid nanofluid, the thermal conductivity enhancement values were higher compared to both the Ag/AlN and MWCNTs/ AlN hybrids, starting at 7.723 % for a 20/80 ratio and reaching 8.465 % for an 80/20 ratio. The close proximity of these values to those of pure MWCNTs highlighted that while silver contributed positively, the MWCNTs largely dictated the thermal conductivity performance.

Tri-hybrid nanofluids, which combined MWCNTs, Ag, and, AlN demonstrated significant enhancements in thermal conductivity, highlighting the synergistic effects of these three materials. For the 20/20/60

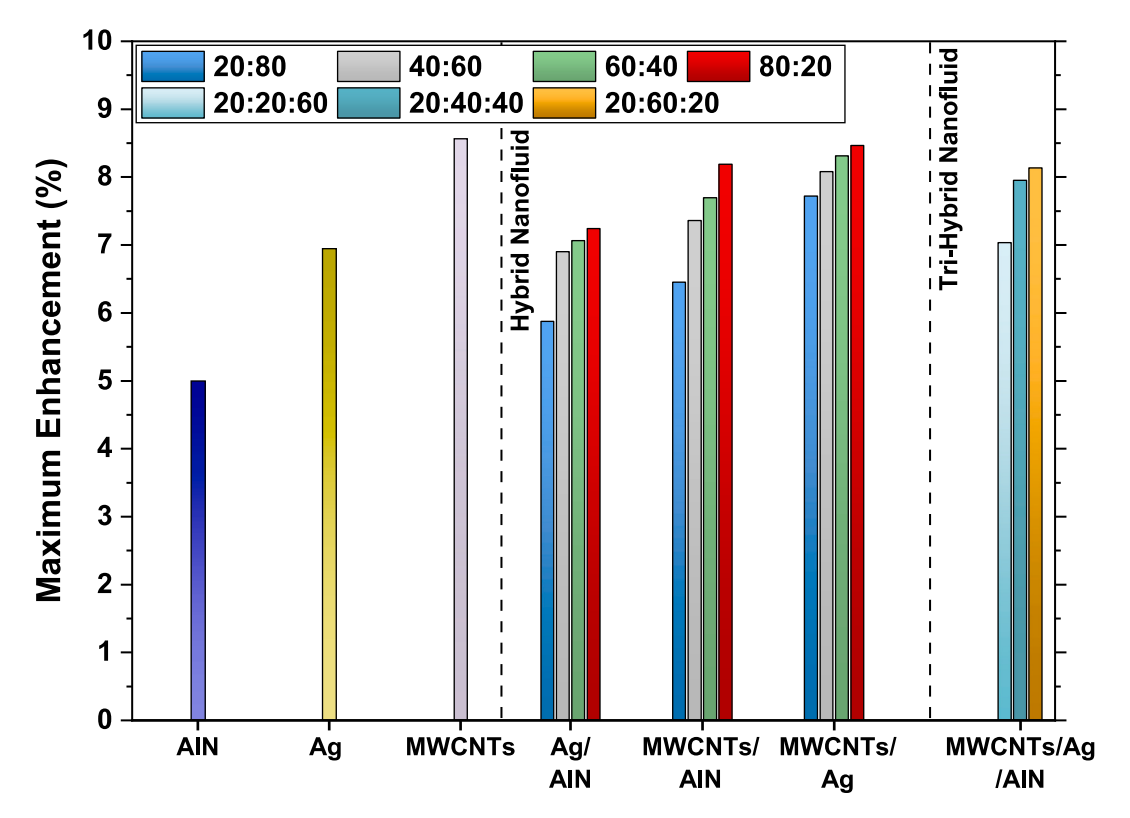


Fig. 21. Maximum thermal conductivity enhancement of simple, hybrid, and tri-hybrid nanofluids relative to the base fluid (water).

formulation, thermal conductivity enhancement was recorded to be $7.036\,\%$. As the proportion of Ag increased in the 20/40/40 and 20/60/20 formulations, thermal conductivity further improved to $7.951\,\%$ and $8.136\,\%$, respectively. This trend indicated that while MWCNTs played a pivotal role due to their inherent high thermal conductivity, the introduction of Ag and AlN further amplified the heat transfer capabilities, likely due to their excellent thermal properties and ability to create a more efficient conductive network within the fluid.

When comparing the thermal conductivity enhancements across all nanofluids, it is evident that MWCNTs play a crucial role in boosting thermal performance, whether in simple, hybrid, or tri-hybrid formulations. The simple MWCNTs nanofluid achieves the highest enhancement outperforming all other simple and hybrid combinations. However, the tri-hybrid formulation with a 20/60/20 ratio nearly matches this performance, indicating that a well-balanced combination of MWCNTs, Ag, and AlN can deliver similar results. This combination also offers additional advantages, such as improved stability, cost-effectiveness, fine-tuned properties, and suitability for specific applications.

This study underscored the importance of selecting the right

combination and ratio of nanomaterials to achieve the desired thermal conductivity enhancement. MWCNTs consistently demonstrated the highest potential for improving thermal conductivity, while the addition of Ag and AlN in hybrid and tri-hybrid formulations offered opportunities for fine-tuning the properties of the nanofluid to suit specific thermal management applications.

In the pursuit of understanding how temperature influences the thermal conductivity of various nanofluids, a comprehensive analysis was conducted using Design Expert [56]. This study carried out with a high degree of statistical rigor, aimed to develop a predictive model that accurately reflects the relationship between temperature and thermal conductivity. The quadratic model that emerged from this analysis is expressed with Eq. (2):

Thermal Conductivity
$$(k) = a + bT + 0.0000287 T^2$$
 (2)

Here, k represents the thermal conductivity, T denotes temperature, and a and b are the coefficients determined through regression analysis, as listed in Table 3. This model was developed with a confidence level of 95 %, meaning the critical p-value threshold was set at 0.05.

The significance of the model and its components were evaluated

Table 3Values of coefficients for the thermal conductivity quadratic model of various fluid samples.

Sample	a	b	Sample	a	b
DW	0.571282	0.001186	MWCNTs/AlN (60:40)	0.572631	0.002318
Ag	0.575327	0.002107	MWCNTs/AlN (80:20)	0.573279	0.002367
AlN	0.572419	0.001872	MWCNTs/Ag (20:80)	0.575753	0.002202
MWCNTs	0.576665	0.002342	MWCNTs/Ag (40:60)	0.577041	0.002239
Ag/AlN (20:80)	0.573077	0.001983	MWCNTs/Ag (60:40)	0.57665	0.002308
Ag/AlN (40:60)	0.569932	0.002234	MWCNTs/Ag (80:20)	0.576418	0.002333
Ag/AlN (60:40)	0.572001	0.002202	MWCNTs/Ag/AlN (20:20:60)	0.572785	0.002196
Ag/AlN (80:20)	0.572628	0.002213	MWCNTs/Ag/AlN (20:40:40)	0.574169	0.002281
MWCNTs/AlN (20:80)	0.57268	0.002081	MWCNTs/Ag/AlN (20:60:20)	0.576012	0.002286
MWCNTs/AlN (40:60)	0.571805	0.002283			

Table 4 ANOVA results for the thermal conductivity quadratic model.

Source	Sum of Squares (SOS)	df	Mean Square	p – value	F- value	Significance of model
Model	0.146	38	0.0038	< 1.0E-04	2149.09	Significant
Fluid-A	0.0102	18	0.0006	< 1.0E-04	318.1	
Temperature-B	0.1348	1	0.1348	< 1.0E-04	75,419.29	
AB	0.0006	18	0	< 1.0E-04	17.53	
B^2	0.0004	1	0.0004	< 1.0E-04	204.72	
Residual	0.0001	75	1.79E-06			
Mean	0.67644		\mathbb{R}^2	0.9991		
Std. Dev.	0.0013369		Predicted R ²	0.9979		
PRESS	0.0003043		Adjusted R ²	0.9986		
C.V. %	0.19764		Adeq Precision	171.0224		

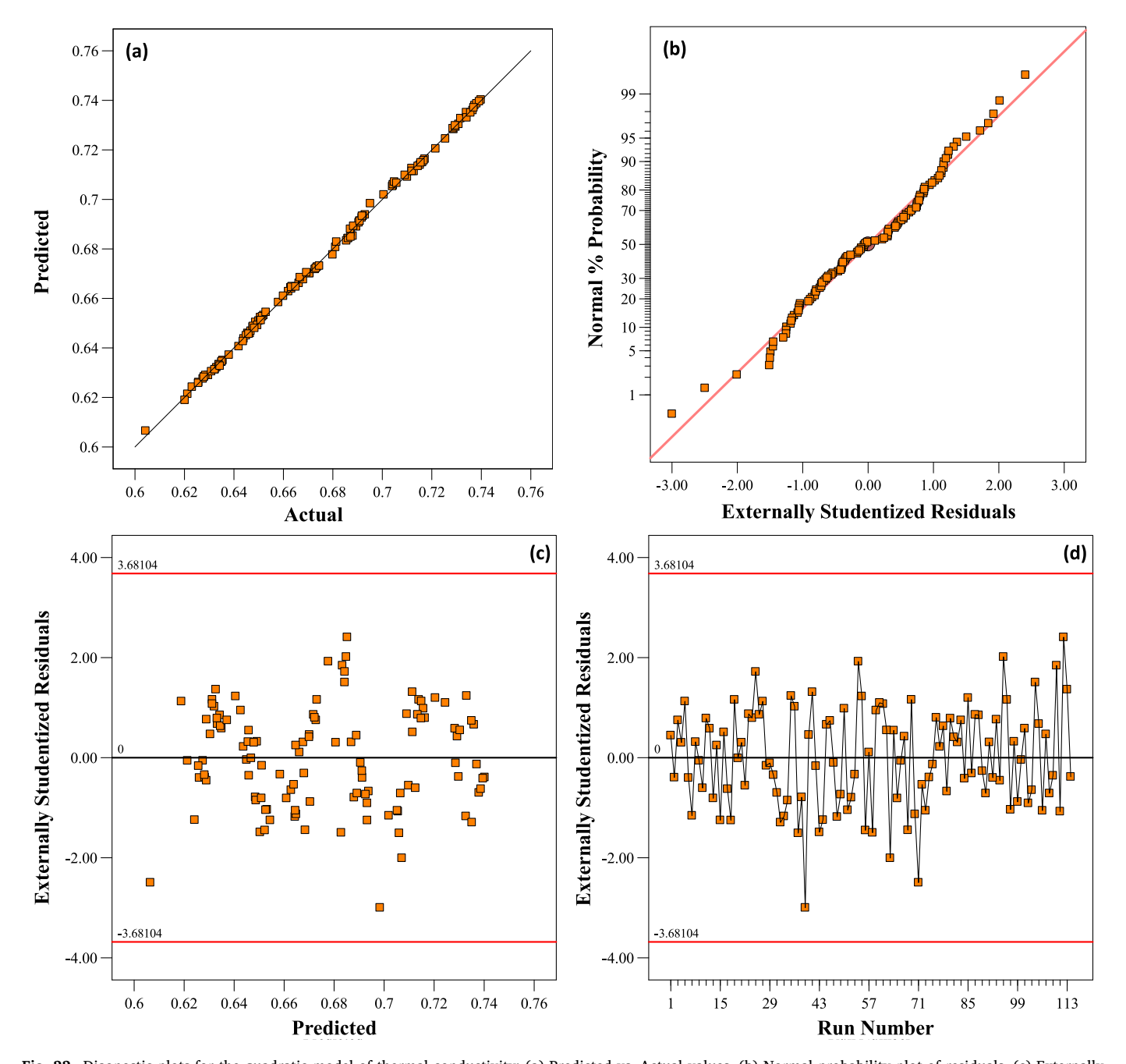


Fig. 22. Diagnostic plots for the quadratic model of thermal conductivity: (a) Predicted vs. Actual values, (b) Normal probability plot of residuals, (c) Externally Studentized Residuals vs. Predicted values, and (d) Externally Studentized Residuals vs. Run Num.

using ANOVA (Analysis of Variance), with the results summarised in the provided Table 4. The overall model was highly significant, with an F-value of 2149.09 and a p-value of less than 0.0001, indicating that the model has strong predictive power. The residual sum of squares was very small (0.0001), further demonstrating the model's accuracy. Additionally, the predicted R^2 of 0.9979 is very close to the adjusted $R,^2$ suggesting that the model has excellent predictive capability. The low coefficient of variation (C.V.%) of 0.1976 indicates high precision, and the Adeq Precision of 171.02 exceeds the threshold of 4, signifying an adequate signal.

To ensure the validity and reliability of the model, several diagnostic plots were examined. These plots are critical for assessing whether the assumptions underlying the regression analysis are met and for identifying any potential issues with the model. Fig. 22(a) compares the predicted thermal conductivity values with the actual measured values. Ideally, if the model were perfect, all points would lie exactly on the 45-degree line. According to the results, the data points were found to be closely aligned with this line, demonstrating a high degree of accuracy in the model's predictions. The close alignment suggests that the model has captured the underlying relationship between temperature and thermal conductivity effectively, with minimal deviation between predicted and observed values.

Fig. 22(b) shows the normal probability plot of residuals analysed to assess the normality of the residuals. In this plot, the residuals are plotted against the expected values from a normal distribution. The data points follow a straight line quite closely, indicating that the residuals are approximately normally distributed. As shown in Fig. 22(c), the externally studentized residuals are plotted against the predicted values of thermal conductivity. The absence of any discernible pattern in the spread of residuals suggests that points are randomly distributed, with no signs of increasing or decreasing variance. This randomness is what we expect in a well-behaved model, indicating that the model's predictions are not biased and that the residuals have constant variance. Finally, the residuals against run number plot was examined to detect any potential patterns related to the order in which the data were collected, as depicted in Fig. 22(d). The purpose of this plot is to identify if there are any time-related or sequence-related effects influencing the residuals. The residuals appear to be randomly scattered without any noticeable trend, indicating that there are no sequence-related biases affecting the model.

5.2. Viscosity

The viscosity of thermal fluid samples was assessed using the Brookfield DVNext Cone/Plate Rheometer, equipped with a CPM-40Z cone spindle and CPA-44PYZ Cup [8,28,57]. The spindle operated at 100 rpm, and each test lasted for 45 s. The spindle operated at 100 rpm, and each test lasted for 45 s. Temperature control within the testing chamber was ensured by connecting the cup to a thermal bath system through pipes. The Masterflex L/S Pump maintained continuous water circulation, stabilizing testing conditions, as illustrated in Fig. 23. A 5 ml sample was used for each experiment, following procedural guidelines. However, the level of accuracy and reproducibility is critical for obtaining reliable data, especially when assessing the performance of fluid samples under varying conditions. The DVNext rheometer offers a measurement accuracy of ± 1.0 % of its full-scale range. Moreover, the system demonstrated excellent reproducibility, with variations between repeated measurements not exceeding ± 0.2 %. This high level of accuracy and reproducibility ensured that the data collected was consistent and dependable, minimising the potential for significant variations between tests.

To ensure the reliability of the test rig, we conducted a series of viscosity measurements on distilled water at temperatures between 20 $^{\circ}$ C and 45 $^{\circ}$ C. These experimental values were then compared with established viscosity data for standard water found in the literature [58], as shown in Fig. 24. The results showed close alignment, with a mean absolute error (MAE) of 0.59 % between the experimental and reference values, confirming the accuracy and reliability of the experimental setup.

The investigation conducted at 25 °C focused on the behaviour of nanofluid samples containing 0.025 vol% particle loading. It was observed that the AlN, Ag, and MWCNTs fluids exhibited Newtonian characteristics, where shear stress increased linearly with shear rate. To achieve variation in the shear rate, spindle speeds were adjusted between 60 and 160 rpm. The results, illustrated in Fig. 25, indicate that within this range, the nanofluids of AlN, Ag, and MWCNTs maintained a consistent linear relationship between shear stress and shear rate, confirming their Newtonian behaviour. However, it is important to consider the fact that increasing the particle concentration in the fluid could potentially lead to non-Newtonian behaviour [59].

The concentration study carried out at 25 °C revealed a direct

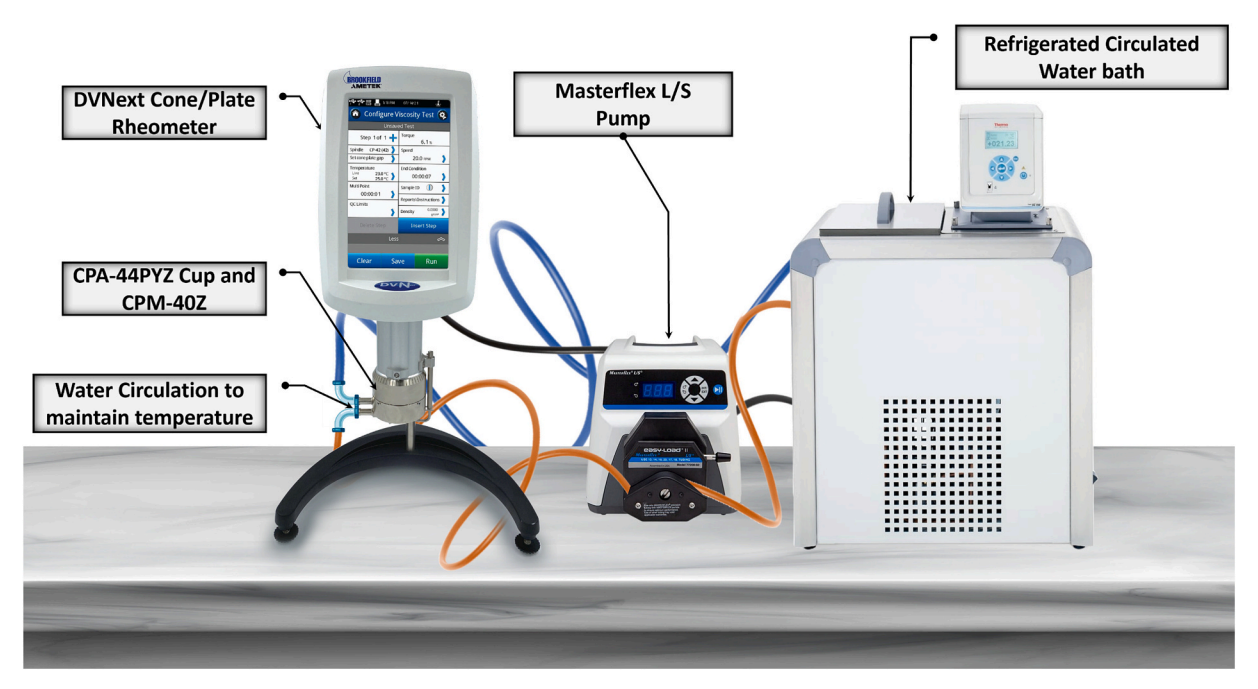


Fig. 23. Schematic diagram of the experimental setup for viscosity measurement using the Brookfield DVNext Cone/Plate Rheometer.

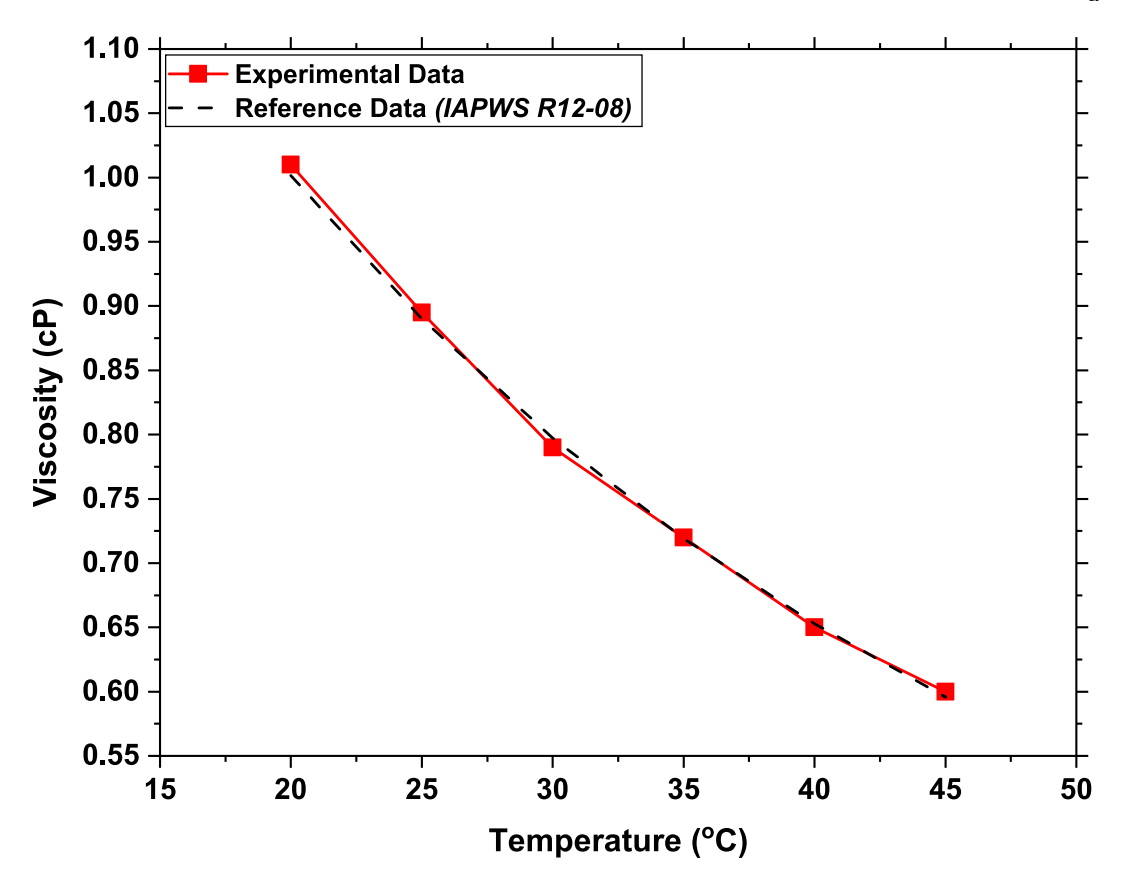


Fig. 24. Comparison of experimental viscosity measurements of distilled water with reference data (IAPWS R12-08).

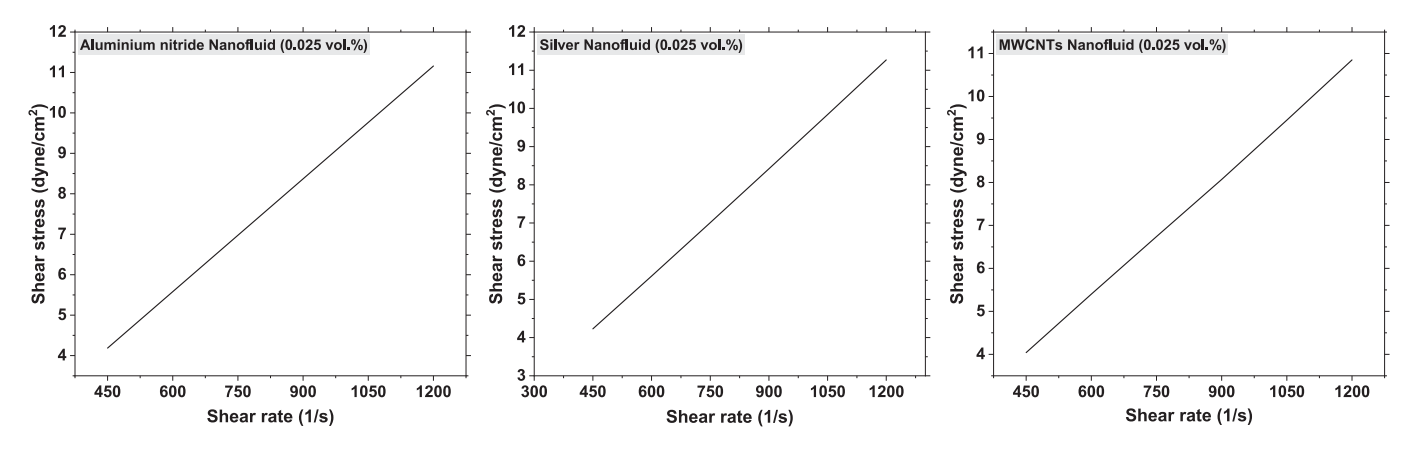


Fig. 25. Shear stress versus shear rate graphs for (a) Aluminium nitride nanofluid, (b) Silver nanofluid, and (c) MWCNTs nanofluid, with a particle loading of 0.025 vol%, demonstrating their Newtonian characteristics.

correlation between the increase in particle concentration and the rise in nanofluid viscosity, as depicted in Fig. 26. Across all three nanofluids, viscosity consistently increases as the particle concentration rises. This trend can be attributed to the fact that a higher particle load within the fluid amplifies the internal resistance to flow, leading to greater viscosity. According to the outcome, Ag nanofluid showed a gradual increase in viscosity, rising from 0.92 cP at a 0.01 vol% concentration to 0.945 cP at 0.03 vol%. The changes between each concentration step were relatively modest, reflecting a steady but notable rise in viscosity with the addition of more Ag nanoparticles. In a similar fashion, the AlN nanofluid showed a progressive increase in viscosity with higher particle concentrations. However, the viscosity values for AlN were slightly lower than those for Ag at each corresponding concentration, ranging from 0.915 cP to 0.940 cP. This indicated that AlN particles contributed

less to flow resistance compared to Ag particles.

In contrast, despite the high aspect ratio of MWCNTs and their potential for forming percolation networks, these particles exhibited lower viscosity. This was due to their lower density, better dispersion, and the rotational advantage of the tubes, which made the MWCNT-based fluid less viscous than those containing Ag or AlN. For MWCNTs, viscosity consistently increased from 0.90 cP to 0.925 cP, reflecting a steady trend but remaining lower compared to the other nanofluids.

These findings underscore the significant impact of particle concentration on the flow characteristics of nanofluids. As more particles are introduced into the fluid, they create additional frictional forces that impede the movement of the fluid layers, thereby increasing viscosity. The observed proportional increases in viscosity for each nanofluid type suggest that careful control of particle concentration is essential when

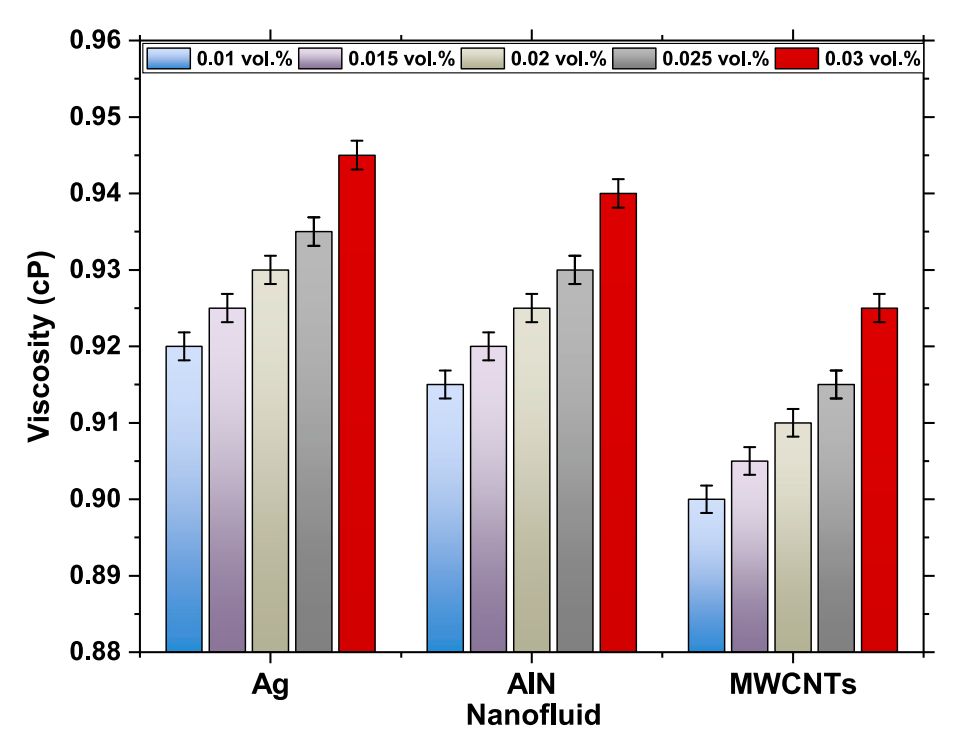


Fig. 26. Viscosity of nanofluids at different particle concentrations.

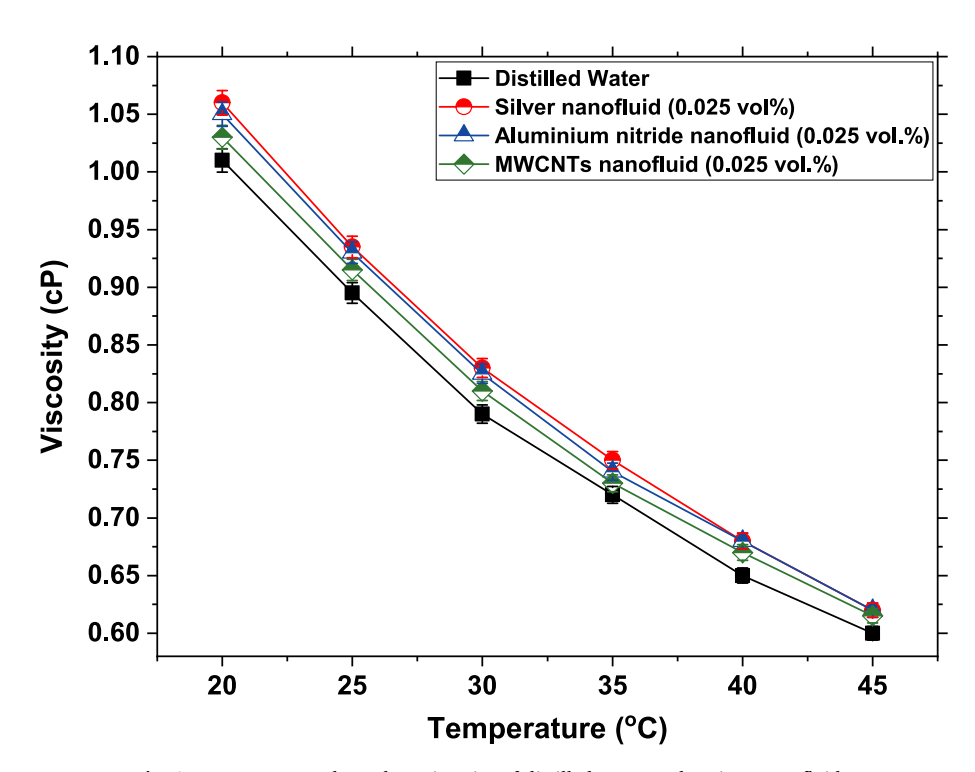


Fig. 27. Temperature-dependent viscosity of distilled water and various nanofluids.

tailoring the rheological properties of nanofluids for specific applications.

The viscosity of water and various nanofluids was plotted against temperature, as illustrated in Fig. 27. The results indicated a general trend of decreasing viscosity with increasing temperature across all fluids. Among the nanofluids, Ag nanofluid exhibited the highest viscosity enhancement compared to water, with values ranging from 1.06 cP at 20 $^{\circ}\text{C}$ to 0.62 cP at 45 $^{\circ}\text{C}$. This significant enhancement was likely due to the higher density and potential agglomeration of Ag

nanoparticles. Despite having a density three times lower than Ag, the AlN nanofluid showed viscosity values that closely approached those of the Ag nanofluid. This behaviour could be attributed to the unique morphology of AlN nanoparticles and the formation of clusters driven by strong attractive forces, which collectively augmented the viscosity. Notably, at temperatures above 35 $^{\circ}\text{C}$, the viscosity values of Ag and AlN became almost indistinguishable. This effect is particularly observed in formulations prepared with low particle concentrations. However, at higher concentrations (above 1 vol%), the difference was expected to be

more pronounced, persisting even at elevated temperatures. In contrast, the MWCNTs nanofluid showed lower viscosity values, ranging from 1.03 cP to 0.615 cP as the temperature increased from 20 $^{\circ}\text{C}$ to 45 $^{\circ}\text{C}$. Throughout the observed temperature range, the viscosity of the MWCNTs nanofluid consistently remained below that of the Ag and AlN nanofluids. The lower viscosity in the MWCNTs nanofluid can be attributed to its lower density and the "rolling effect" of the carbon nanotubes, which reduces resistance to flow. Although the formation of a percolation network, where nanotubes form a continuous network, could have contributed to a slight increase in viscosity, it remained lower than that of the Ag and AlN nanofluids.

The findings highlight the complex interplay between nanoparticle characteristics such as density, morphology, and inter-particle interactions in determining the viscosity of nanofluids. The distinct behaviours of Ag, AlN, and MWCNTs nanofluids underscore the importance of considering these factors when formulating nanofluids for specific applications, particularly those where temperature-dependent viscosity is a critical parameter.

The viscosity of the hybrid nanofluids exhibited variations dependent on both the type of particles used and their mixing ratios, as shown in Fig. 28. For the MWCNTs/AlN hybrid nanofluid with a 20/80 ratio, like pure nanofluids viscosity exhibited a temperature-dependent behaviour, decreasing from 1.05 cP at 20 °C to 0.62 cP at 45 °C. Notably, these viscosity values were found to be marginally lower than those observed for the pure AlN nanofluid, while maintaining a similar overall trend. The observed reduction in viscosity can be attributed to the inclusion of MWCNTs, which generally possess lower viscosity and contribute to minimising particle clustering, thereby reducing overall viscosity. As the AlN content decreased to 60 % and 40 %, a modest

decrease in viscosity was observed at lower temperatures. However, at elevated temperatures, the viscosity values for these ratios converged closely. For the 80/20 ratio, viscosity values ranged from 1.035 cP at $20~^\circ\text{C}$ to 0.62 cP at $45~^\circ\text{C}$. In this case, the difference in viscosity values was more noticeable; the values were closer to but higher than those of pure MWCNTs.

Fig. 28(b) presented the viscosity values for the Ag/AlN hybrid formulation, showing that its viscosity values consistently exceeded those of the MWCNTs/AlN hybrid samples across the temperature range studied. At a 20/80 mixing ratio, the fluid viscosity was noted to be 1.05 cP at 20 °C, gradually decreased to 0.62 cP at 45 °C. When the mixing ratio shifted to 40/60, the viscosity values exhibited a slight increase across all temperatures compared to the 20/80 ratio. At 20 °C, the value augmented to 1.055 cP, indicating a slight enhancement due to the increased proportion of silver. This trend continued as the temperature increased, with the viscosity slightly higher than that of the 20/80 ratio at each corresponding temperature point. By 45 °C, the viscosity aligned with the 20/80 formulation as the viscosity was observed to be 0.62 cP. indicating that the difference in viscosity between these two ratios diminished as the temperature increased. In the case of a 60/40 mixing ratio, the viscosity values were consistently the highest among all the Ag/AlN formulations. The viscosity at this ratio was noticeably higher than the other ratios, reflecting the combined effects of silver's higher density and the AlN nanoparticles' potential for forming an intricate particle network. As the temperature increased, the viscosity decreased more sharply, though it remained slightly above the other ratios and reached 0.62 cP at 45 °C, like the other mixing ratios. With a small decrease, the 80/20 mixing ratio produced viscosity values that were close to those of the 20/80 ratio, starting at 1.05 cP at 20 °C and

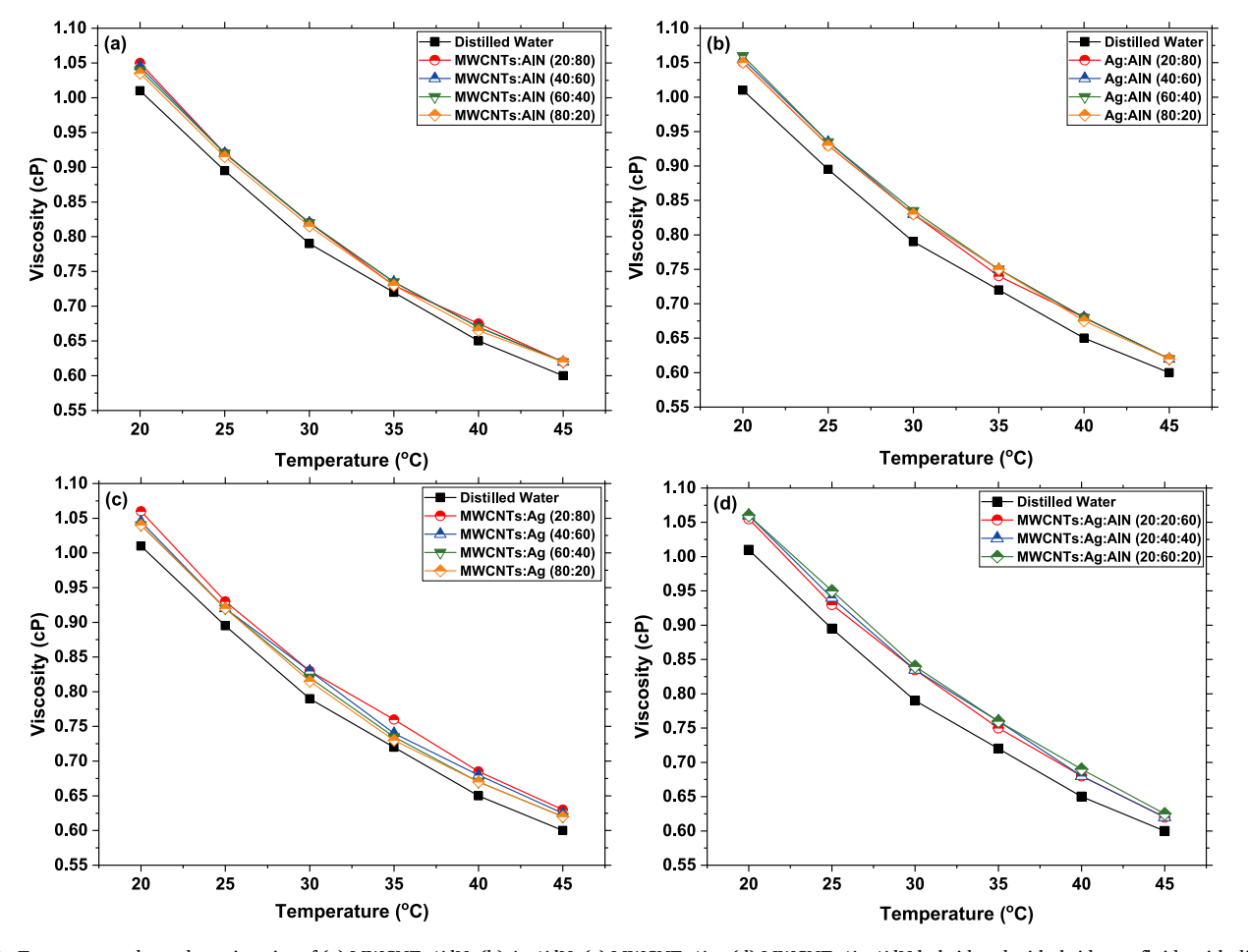


Fig. 28. Temperature-dependent viscosity of (a) MWCNTs/AlN, (b) Ag/AlN, (c) MWCNTs/Ag, (d) MWCNTs/Ag/AlN hybrid and tri-hybrid nanofluids with different mixing ratios.

gradually reducing to 0.62 cP at 45 °C.

Fig. 28(c) presented the results for the MWCNTs/Ag hybrid formulations. At a 20/80 mixing ratio, the viscosity values were observed to be the highest among the various ratios tested. The maximum viscosity value recorded was 1.06 cP at 20 °C, which decreased to 0.63 cP as the temperature increased to 45 °C. However, as the proportion of MWCNTs increased, due to the influence of low density particles, a noticeable decrease in viscosity value was observed. With a further increase in MWCNTs to a 60/40 ratio, the viscosity values decreased slightly more compared to the 40/60 ratio, reaching 1.04 cP at 20 °C and 0.62 cP at 45 °C. Finally, the 80/20 mixing ratio which had the highest MWCNTs content, exhibited the lowest viscosity values across all the MWCNTs/Ag ratios. This result indicated that the viscosity values of the 80/20 ratio were close to that of pure MWCNTs, suggesting that the influence of the silver nanoparticles was minimal at this composition.

The viscosity data for the tri-hybrid nanofluid, plotted in Fig. 28(d), revealed that the presence of particles with different shapes and the formation of complex structures or agglomerates result in slightly higher viscosity values. For the 20/20/60 formulation of MWCNTs/Ag/AlN, where the proportion of Ag is relatively low, the viscosity values were found to be close to those of pure Ag, ranging from 1.055 cP to 0.62 cP. However, when the formulation was altered to 20/40/40, the viscosity values augmented to slightly higher than those of pure Ag. Further increasing the Ag content 20/60/20 formulation resulted in even higher viscosity, reaching 1.06 cP at 20 °C and 0.625 cP at 45 °C.

Comparing these mixing ratios, the viscosity differences are most pronounced at lower temperatures. At these lower temperatures, the impact of high-density particles on viscosity was more pronounced. As the temperature increases, the viscosity values converge, particularly at 45 °C, where all mixing ratios show nearly identical viscosities. This convergence indicates that temperature plays a crucial role in the viscosity of these hybrid nanofluids. Notably, this effect is more evident in formulations with lower particle concentrations. However, with higher particle concentrations >1 vol%, the viscosity differences could remain more pronounced, even at elevated temperatures.

Fig. 29 presents a comparison of the average percentage increase in viscosity for different types of nanofluids relative to water. The results concluded that among the unitary nanofluids, Ag nanofluid exhibited the highest average percentage increase in viscosity, with an average increase of 4.43 %. This was followed by AlN nanofluid with a 3.84 % increase and MWCNTs nanofluid with a 2.89 % increase. In the case of hybrid nanofluids, formulations containing Ag and AlN generally displayed higher viscosity enhancements compared to hybrids involving MWCNTs and AlN, or MWCNTs and Ag. However, the MWCNTs/Ag 20/ 80 hybrid stood out with a significant viscosity increase of 4.98 %, likely due to the formation of an intricate percolation network or agglomerates between MWCNTs and Ag at this ratio. Notably, the Ag/AlN hybrid with a 60/40 ratio achieved a significant viscosity increase of 4.54 %. The MWCNTs/Ag/AlN ternary hybrid formulations exhibited even more pronounced effects, with the 20/60/20 ratio resulting in the highest average viscosity increase of 5.55 %, indicating a strong synergistic interaction between the three components. These findings suggested that while all nanofluids increased viscosity compared to water, the extent of this increase was strongly dependent on the specific combination and ratio of nanoparticles used, with ternary hybrids offering the most substantial enhancements. This implied potential for tailored viscosity control in heat transfer applications, where both thermal conductivity and fluid dynamics were critical considerations.

An analysis was conducted to develop a predictive model for estimating nanofluids' viscosity values as a temperature function. In this study, a cubic model was formulated to capture the non-linear relationship between viscosity and temperature, represented with Eq. (3). The inclusion of the cubic term was crucial to account for the complex behaviour of viscosity at higher temperatures, which simpler linear or quadratic models might fail to capture adequately. This equation served as the basis for further analysis, where its predictive accuracy was evaluated using various statistical measures. The model's significance was assessed by performing an ANOVA analysis, which provided a detailed evaluation of how well the model explained the variability in viscosity data. As presented in Table 5, the results indicated that the

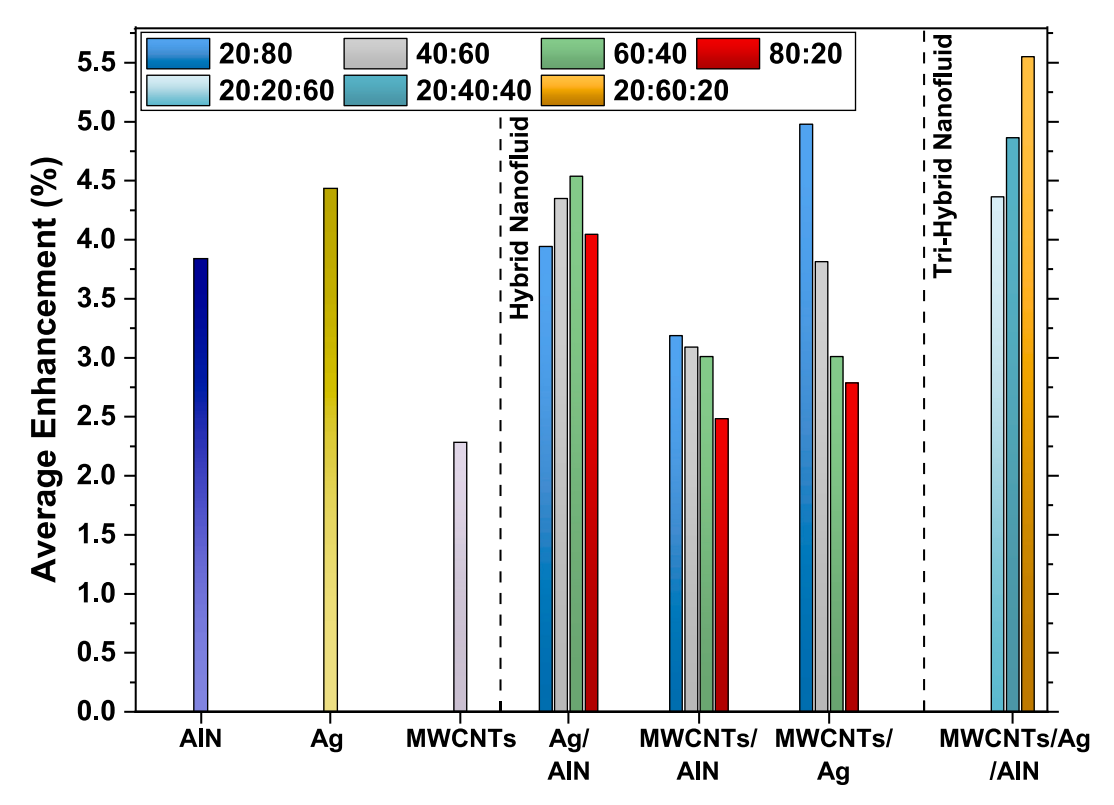


Fig. 29. Average percentage increase in viscosity for different types of nanofluids relative to water.

Table 5ANOVA results for the viscosity cubic model.

Source	Sum of Squares (SOS)	df	Mean Square	p – value	F – value	Significance of model
Model	2.47	57	0.0433	< 1.0E-04	3620.76	Significant
Fluid-A	0.0108	18	0.0006	< 1.0E-04	50.3	
Temperature-B	2.4	1	2.4	< 1.0E-04	2.01E+05	
AB	0.001	18	0.0001	< 1.0E-04	4.57	
B^2	0.0487	1	0.0487	< 1.0E-04	4074.61	
AB^2	0.0004	18	0	0.0405	1.86	
B^3	0.0003	1	0.0003	< 1.0E-04	24.72	
Residual	0.0007	56	0			
Mean	0.8057		R ²	0.9997		
Std. Dev.	0.003456		Predicted R ²	0.9987		
PRESS	0.00328		Adjusted R ²	0.9995		
C.V. %	0.4267		Adeq Precision	188.51		

model was highly significant, with a p-value <0.0001. Temperature emerged as the most influential factor, exhibiting a very high F-value and low p-value. The type of nanofluid also played a crucial role in determining viscosity, as indicated by its significance in the model. Interaction terms between fluid type and temperature, as well as the quadratic and cubic temperature terms, contributed to capturing the non-linear relationship between viscosity and temperature.

Viscosity
$$(\mu) = c - dT + e(T^2) - 3.918 \times 10^{-6} (T^3)$$
 (3)

Here, T denotes the temperature, and the coefficients c, d, and e are constants derived from the dataset. The values of these coefficients are given in Table 6.

Residual analysis demonstrated the model's robustness, as evidenced by a low residual sum of squares and an exceptionally high R² value of 0.9997. This indicates that the model accounted for almost all the variability in viscosity. Additionally, the high Adjusted R² and Predicted R² values reaffirm the model's accuracy and its capability to generalise well to new data. The Adequate Precision ratio also exceeded the minimum threshold significantly, further validating the model's reliability. Fig. 30 presents diagnostic plots that offer visual evidence of the model's effectiveness. The Predicted vs. Actual plot revealed close agreement between predicted and actual viscosity values, with points clustered along the diagonal line. This demonstrated a strong correlation between model predictions and observed data. The Normal Probability plot of residuals confirmed the residuals followed a normal distribution, which is essential for the validity of the analysis. Plots of Externally Studentized Residuals against predicted values and run number showed no discernible patterns, suggesting independent residuals with constant variance.

5.3. Density

Density is a vital thermo-physical property that plays a significant role in various applications, particularly in enhancing pumping efficiency and optimising mass flow rates. In this part of study, the densities of both base fluids and nanofluids were assessed using a DMA 35 density meter from Anton Paar at varying temperatures and concentrations or

mixing ratios for hybrid nanofluids. The meter offers an accuracy of $\pm 0.2~^{\circ}\text{C}$ for temperature and $\pm 0.001~\text{g/cm}^3$ for density measurements. Additionally, it demonstrates repeatability of $\pm 0.1~^{\circ}\text{C}$ for temperature and \pm 0.0005 g/cm 3 for density. To perform the testing, the fluid samples were poured into a sample tube submerged in a temperaturecontrolled bath, as shown in Fig. 31. This setup ensured that the temperature of the samples could be accurately maintained throughout the testing process. Sufficient time was allowed for the samples to reach thermal equilibrium, density measurements were then conducted according to a predetermined protocol. However, before proceeding with the actual density measurements and validation study, a water check was carried out following the supplier's guidelines. Additionally, density measurements were taken three times at each specified temperature, and the average of these measurements was calculated and reported. This approach of recording multiple values and averaging them is employed to enhance the accuracy and reliability of the results. The Utube measurement section, made of transparent glass, allows for visual inspection to ensure the absence of air bubbles. Validation was performed by collecting data across a temperature range from 15 °C to 45 °C, as shown in Fig. 32. The obtained experimental results were then compared with data provided by the supplier as well as with values reported in relevant scientific literature. This thorough comparison aimed to ensure the accuracy and consistency of the experimental findings. The results demonstrated a high degree of concordance with both the supplier's data and the published values, confirming the reliability and accuracy of the experimental measurements.

The density of samples prepared with varying concentrations ranging from 0.01 vol% to 0.03 vol% was evaluated at 30 °C, as presented in Fig. 33. The findings indicate that fluids containing suspensions of denser particles exhibited higher density values. Notably, the density increased with particle concentration across all types of nanoparticles. Among the tested nanofluids, the Ag nanofluid demonstrated the highest density, with values ranging from 0.9967 g/cm³ to 0.9990 g/cm³ as the concentration increased from 0.01 vol% to 0.03 vol%. AlN samples secured the second place in the list displaying a moderate increase in density, with values rising from 0.9964 g/cm³ to 0.9968 g/cm³ over the same concentration range. Finally, MWCNTs followed a similar

Table 6Coefficients of the cubic viscosity model for various fluid samples.

Sample	c	d	e	Sample	c	d	e
DW	1.75275	0.049824	0.000714	MWCNTs/AlN (60:40)	1.8085	0.051442	0.000732
Ag	1.82303	0.05091	0.000714	MWCNTs/AlN (80:20)	1.81725	0.05246	0.00075
AlN	1.81743	0.051264	0.000725	MWCNTs/Ag (20:80)	1.81668	0.05086	0.000721
MWCNTs	1.78728	0.050721	0.000725	MWCNTs/Ag (40:60)	1.79564	0.050371	0.000718
Ag/AlN (20:80)	1.80514	0.050364	0.000711	MWCNTs/Ag (60:40)	1.8085	0.051442	0.000732
Ag/AlN (40:60)	1.8	0.049607	0.000696	MWCNTs/Ag (80:20)	1.83493	0.053299	0.000761
Ag/AlN (60:40)	1.81075	0.05001	0.0007	MWCNTs/Ag/AlN (20:20:60)	1.7876	0.048853	0.000686
Ag/AlN (80:20)	1.78232	0.048767	0.000686	MWCNTs/Ag/AlN (20:40:40)	1.78257	0.047949	0.000668
MWCNTs/AlN (20:80)	1.86325	0.054689	0.000778	MWCNTs/Ag/AlN (20:60:20)	1.77332	0.047139	0.000657
MWCNTs/AlN (40:60)	1.8333	0.052924	0.000756				

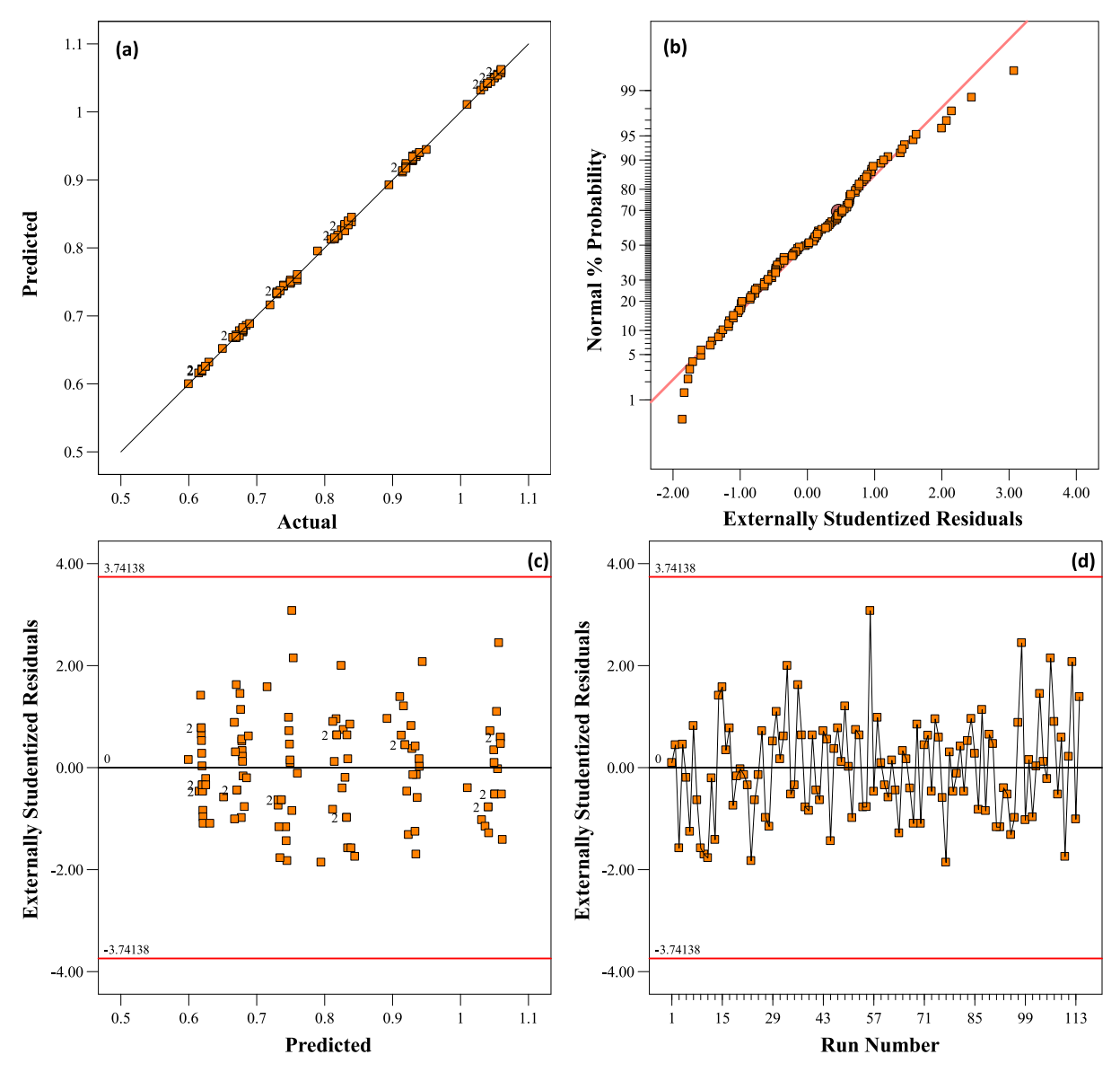


Fig. 30. Diagnostic plots for the cubic model of viscosity.

trend, with density values increased from 0.9962 g/cm 3 at 0.01 vol% to 0.9966 g/cm 3 at 0.03 vol%. However, the impact of MWCNTs on density was slightly less pronounced than that of Ag nanoparticles, due to the lower density of these particles.

As part of this study, the density of water, Ag, MWCNTs, and AlN nanofluids were measured across a temperature range of 20 °C to 45 °C, as depicted in Fig. 34. It was observed that the density of both water and nanofluids decreased with increasing temperature in a non-linear way. According to the results, for pure water, the density decreased from 0.9982 g/cm³ at 20 °C to 0.9901 g/cm³ at 45 °C.

The addition of nanoparticles resulted in higher density values compared to pure water. Silver nanofluid exhibited higher densities than pure water at all temperatures, ranging from 1.0009 g/cm³ at 20 °C to 0.9926 g/cm³ at 45 °C. Despite the decrease in density with temperature, the values remained higher due to the high density of silver nanoparticles. The smaller decrement in density with temperature, compared to water, suggested significant contributions from the silver nanoparticles. As discussed earlier, AlN nanofluid displayed a moderate density, however, with temperature rise the values ranged from 0.99935 g/cm³ at 20 °C to 0.9912 g/cm³ at 45 °C. The AlN nanofluid density was higher than that of pure water but lower than Ag nanofluid.

The MWCNTs nanofluid showed comparatively lower density values at all temperatures, ranging from $0.9988~g/cm^3$ at $20~^{\circ}C$ to $0.9907~g/cm^3$ at $45~^{\circ}C$. The results concluded that all samples exhibited a decrease in density with rising temperature, consistent with the expected thermal expansion. This observation underscores the potential of hybrid nanofluids, where selecting and combining different nanoparticles could be strategically utilised to tailor properties for specific applications, optimising performance based on desired density and thermal characteristics.

Similar to thermal conductivity and viscosity, in the case of hybrid and tri-hybrid nanofluids, the density varies based on the combination and mixing ratio of the nanoparticles, as illustrated in Fig. 35. The density results of the Ag/AlN hybrid nanofluid demonstrated that as the proportion of Ag increased, the overall density of the nanofluid also increased, with the 80/20 Ag/AlN mixture consistently exhibiting the highest density at all temperatures, as illustrated Fig. 35(a). Additionally, it was observed that across all mixing ratios, the density decreased with rising temperature. For the 20/80 mixing ratio, the density decreased from 0.9997 g/cm³ to 0.9915 g/cm³ as the temperature increased from 20 °C to 45 °C, while for the 80/20 mixture, it decreased from 1.0005 g/cm³ to 0.9924 g/cm³ over the same temperature range.

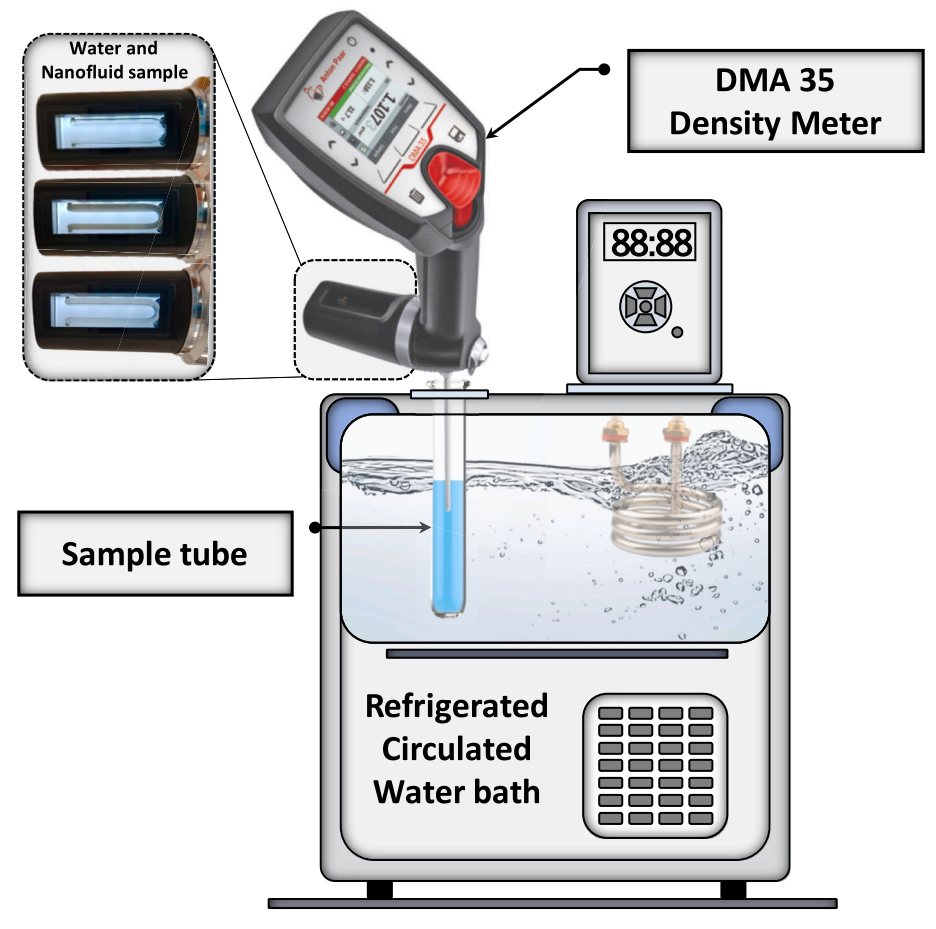


Fig. 31. Schematic representation of the experimental rig used for density measurements.

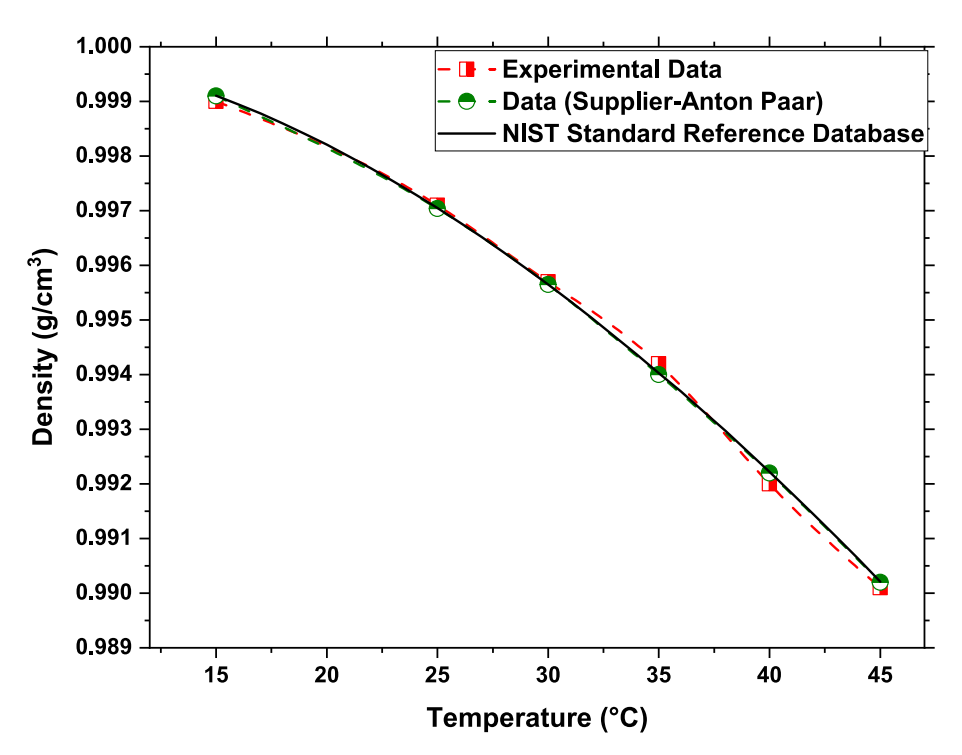


Fig. 32. Density of water compared to supplier data and NIST Standard Reference Database.

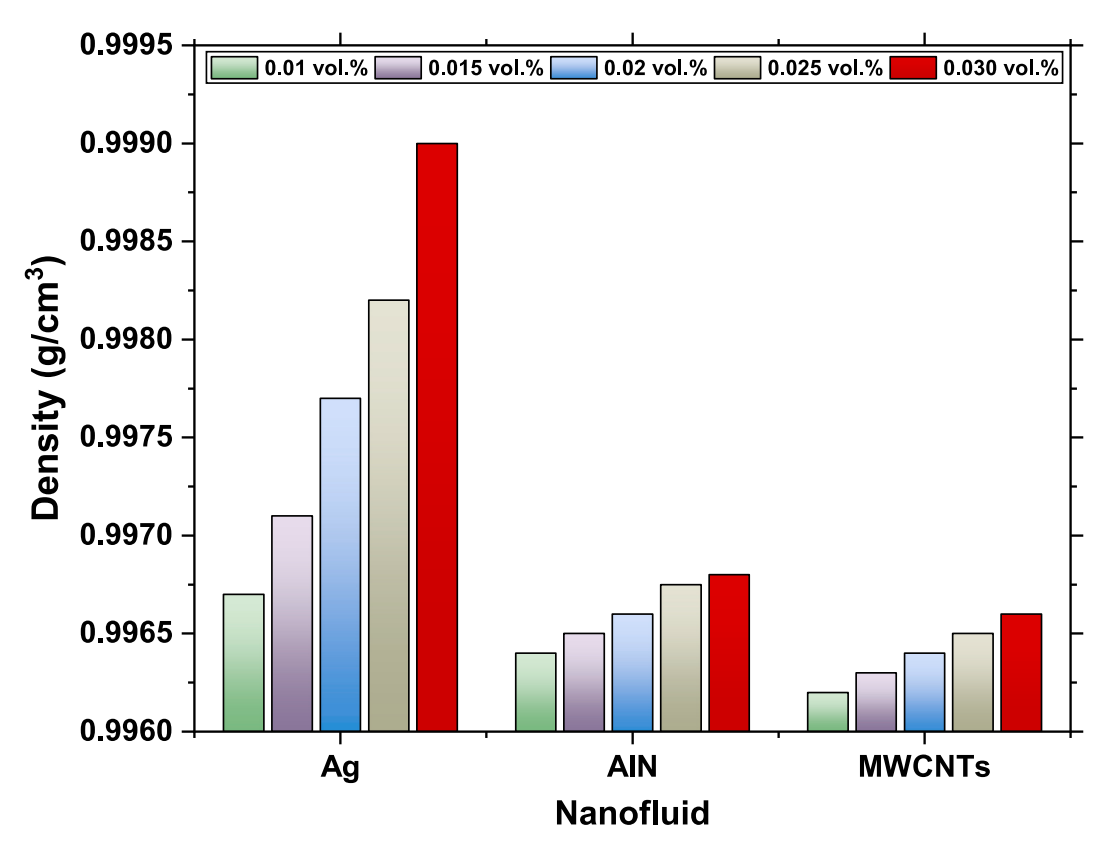


Fig. 33. Density of Ag, AlN, and MWCNTs nanofluids at various concentrations.

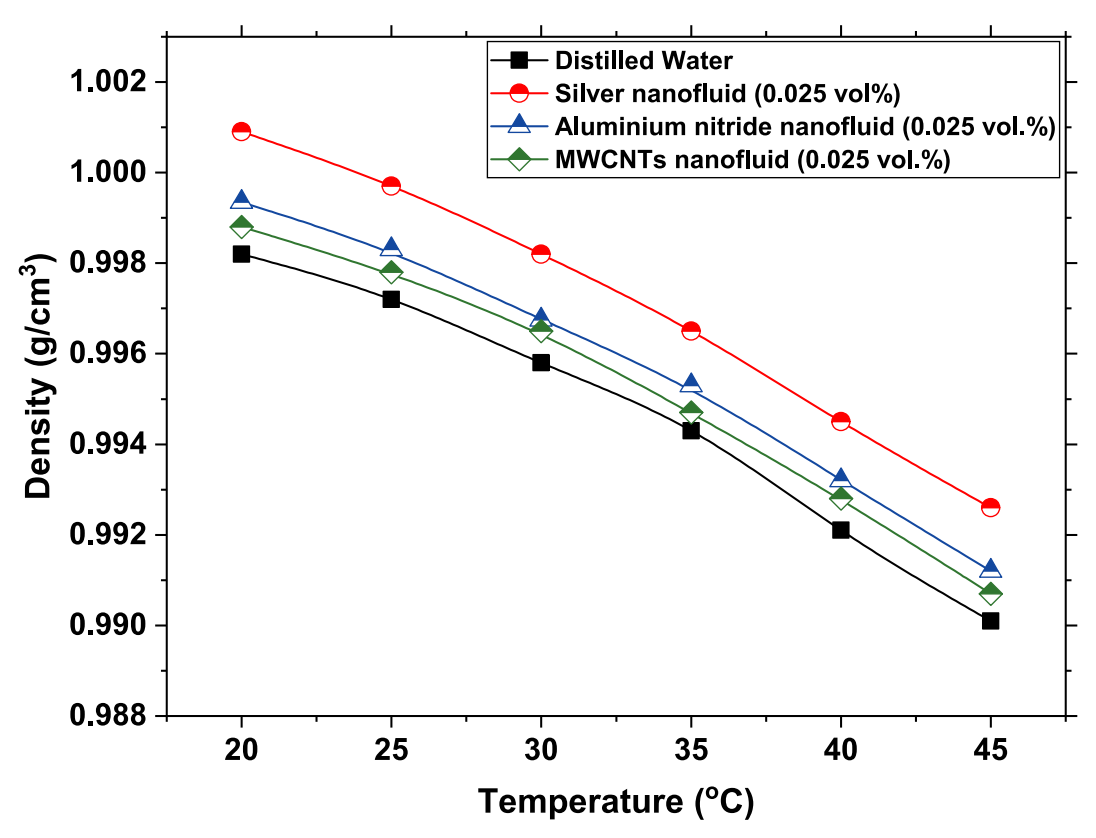


Fig. 34. Density comparison of water, Ag, AlN, and MWCNTs nanofluids across a temperature range of 20 $^{\circ}$ C to 45 $^{\circ}$ C.

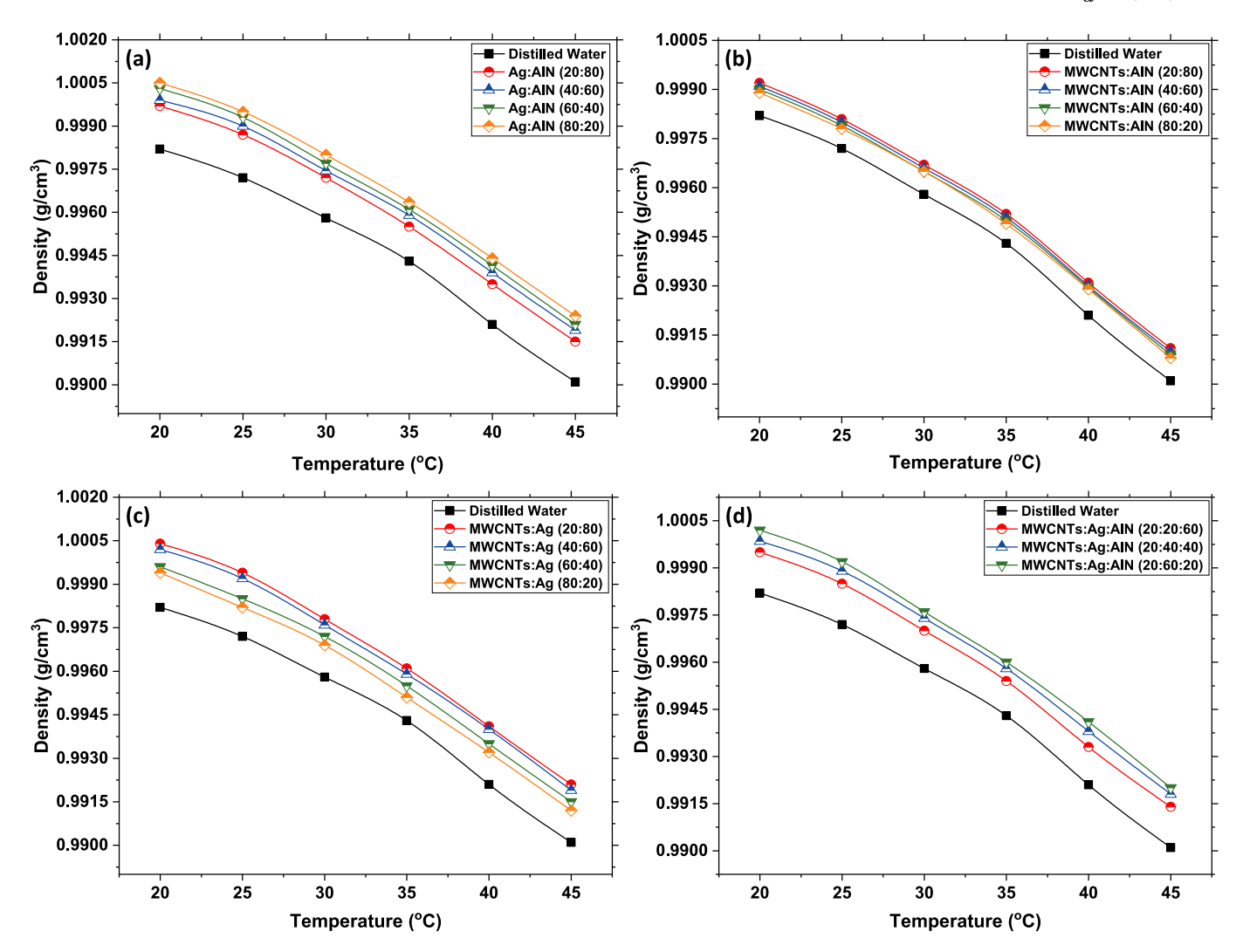


Fig. 35. Density of (a) Ag/AlN (b) MWCNTs/AlN, (c) MWCNTs/Ag, (d) MWCNTs/Ag/AlN hybrid and tri-hybrid nanofluids hybrid nanofluids at various mixing ratios across a temperature range of 20 °C to 45 °C.

The findings revealed that the rate of density decrease was slightly more pronounced in mixtures with lower Ag content, though the overall trend remained consistent, indicating a predictable thermal response across different compositions. For the MWCNTs/AlN hybrid sample, a notable decrease in density was observed with an increasing proportion of MWCNTs, as depicted in Fig. 35(b). However, this reduction was less pronounced compared to the Ag/AlN hybrid. The maximum and minimum density value was recorded to be 0.9992 g/cm³ for the 20/80 mixing ratio at 20 °C, and 0.9908 g/cm³ for the 80/20 ratio at 45 °C, respectively.

The density data for the MWCNTs-Ag hybrid nanofluid followed similar trends to those observed in other hybrid nanofluids. As the proportion of Ag in the MWCNTs-Ag hybrid sample increased, the overall density of the nanofluid also increased, with the 80/20 Ag/MWCNTs mixture showing the highest density at all temperatures, Fig. 35(c). This trend mirrored the behaviour observed in the Ag/AlN hybrids. At 20 °C, the density ranged from 1.0004 g/cm³ for the 20/80 Ag/MWCNTs mixture to 0.9994 g/cm³ for the 80/20 mixture. By 45 °C, the density values had decreased to between 0.9921 g/cm³ and 0.9912 g/cm³.

Finally, Fig. 35(d) illustrates the density results for the tri-hybrid nanofluid MWCNTs/Ag/AlN across various mixing ratios. The densities varied with the ratio of nanoparticles, at 20 $^{\circ}$ C, the 20/20/60 formulation exhibited a density of 0.9995 g/cm³, the 20/40/40 sample showed a slightly higher density of 0.99985 g/cm³, and the 20/60/20

ratio presented the highest density at $1.0002~g/cm^3$. As the temperature increased to $45~^{\circ}$ C, all formulations exhibited a consistent decrease in density, with the 20/20/60 ratio dropping to $0.9914~g/cm^3$, the 20/40/40 ratio to $0.9918~g/cm^3$, and the 20/60/20 ratio to $0.9920~g/cm^3$. The findings demonstrated that the overall trend of density reduction with rising temperature was uniform across all ratios, with the 20/40/40 mixture showing a moderate response relative to the other compositions.

Fig. 36 provided insights into the average percentage increase in density values of pure, hybrid, and tri-hybrid nanofluids relative to their base fluids. For pure fluids, the enhancements were recorded to be 0.10724 %, 0.24631 %, and 0.06033 % for AlN, Ag, and MWCNTs, respectively. In hybrid formulations, the Ag/AlN mixtures exhibited increasing density with higher Ag content, peaking at 0.22538 % for the 80/20 ratio, while the MWCNTs/AlN hybrids showed decreasing density as the proportion of AlN increased, ranging from 0.09552 % for the 20/ 80 ratio to 0.06871 % for the 80/20 ratio. As anticipated, the density of the MWCNTs/Ag hybrid samples increased with higher silver content. The mixture with a 20/80 ratio achieved the highest density of 0.20441 %, whereas the 80/20 mixture exhibited the lowest density at 0.10557 %. For the tri-hybrid MWCNTs/Ag/AlN nanofluids, the density varied with different component ratios. The 20/60/20 ratio showed the greatest increase in density at 0.19102 %, followed by the 20/40/40 ratio at 0.16506 %, and the 20/20/60 ratio at 0.124 %. Future work could explore the implications of these density changes on the thermal

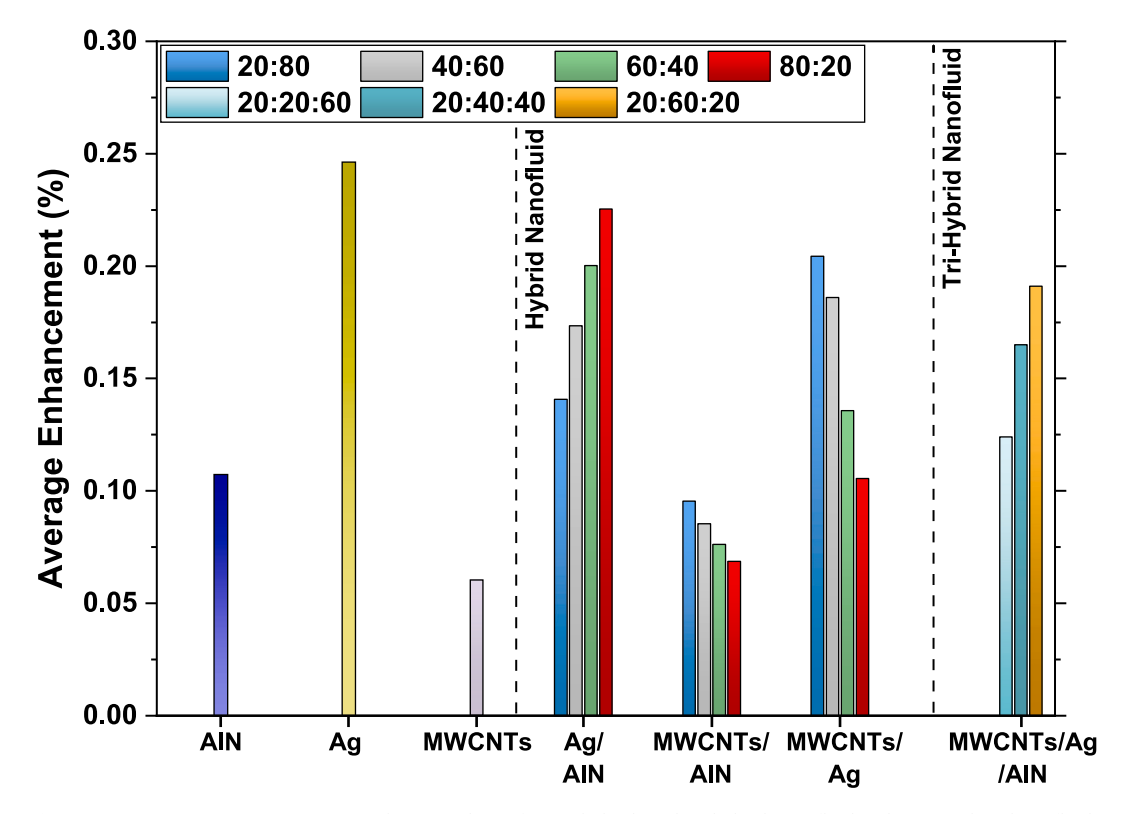


Fig. 36. Average percentage increase in density values of pure, hybrid, and tri-hybrid nanofluids relative to their base fluids.

and flow properties of the nanofluids to further optimise their practical applications.

The ANOVA analysis was conducted to develop a predictive model for calculating the density of various fluids as a function of temperature. The statistical output indicates that the model is highly significant, with a p-value of less than 0.0001 and an F-value of 3016.56. The results suggested that the model has a strong ability to predict density accurately. Additionally, the analysis revealed that both the fluid type and temperature significantly influenced density, with temperature having a particularly large effect (F-value of 1.62E+05) compared to the fluid type (F-value of 445.15). The resulting equation from the analysis for predicting density (ρ) was represented with Eq. (4).

Density
$$(\rho) = f + gT - h(T^2) + 1.00975 \times 10^{-7} (T^3)$$
 (4)

This equation captured the relationship between density and temperature, where T represented temperature, and the coefficients f, g, and h represented constants derived from the analysis, as listed in Table 7. The inclusion of both linear and non-linear terms (such as T^2 and T^3) allowed the equation to accurately model the complex temperature dependence of fluid density.

As the data presented in Table 8, the model exhibited an R² value of 0.9997, indicating that it explained 99.97 % of the variance in the density data, which demonstrated an excellent fit. The Adjusted R² of 0.9993 supported this, showing that the model remained robust even after accounting for the number of predictors. Additionally, the Predicted R² of 0.9985 suggested that the model had strong predictive power when applied to new data. The Std. Dev. was very low at 7.46248e-05, indicating minimal deviation between observed and predicted values. Furthermore, the C.V.% was 0.00749, signifying the high precision and reliability of the model. The Adequate Precision ratio of 203.42, which measures the signal-to-noise ratio, confirmed that the model provided an adequate signal for navigating the design space.

The diagnostic plots provided further insights into the model's performance, as shown in Fig. 37. The diagnostic plots provided significant insights into the model's performance. The Predicted vs. Actual plot demonstrated a strong linear relationship between the predicted and actual density values, with the points aligning almost perfectly along the diagonal. This alignment confirmed the high R² value, indicating that the model's predictions closely matched the observed data. Similarly, the Normal Probability plot of the externally studentized residuals

Table 7
ANOVA results for the cubic model of density.

Source	Sum of Squares (SOS)	df	Mean Square	p – value	F- value	Significance of model
Model	0.001	57	0	< 1.0E-04	3016.56	Significant
Fluid-A	0	18	2.48E-06	< 1.0E-04	445.15	
Temperature-B	0.0009	1	0.0009	< 1.0E-04	1.62E + 05	
AB	1.29E-07	18	7.15E-09	0.2335	1.28	
B^2	0	1	0	< 1.0E-04	2017.26	
AB^2	7.76E-08	18	4.31E-09	0.7199	0.774	
B^3	1.96E-07	1	1.96E-07	< 1.0E-04	35.22	
Residual	3.12E-07	56	5.57E-09			
Std. Dev.	7.46248e-05		R^2	0.9997		
C.V. %	0.00749		Predicted R ²	0.9985		
PRESS	1.38872e-06		Adjusted R ²	0.9993		
Mean	0.99597		Adeq Precision	203.42		

 Table 8

 Density coefficient values for different fluid samples.

Sample	f	g	h	Sample	f	g	h
DW	0.996447	0.000361	0.000016	MWCNTs/AlN (60:40)	0.997718	0.000324	0.000015
Ag	1.00107	0.000227	0.000014	MWCNTs/AlN (80:20)	0.997318	0.000345	0.000015
AlN	0.998428	0.000301	0.000015	MWCNTs/Ag (20:80)	0.999938	0.000276	0.000015
MWCNTs	0.997257	0.000347	0.000015	MWCNTs/Ag (40:60)	0.999629	0.000282	0.000015
Ag/AlN (20:80)	0.998875	0.000299	0.000015	MWCNTs/Ag (60:40)	0.99841	0.000319	0.000015
Ag/AlN (40:60)	0.99872	0.000321	0.000015	MWCNTs/Ag (80:20)	0.998854	0.000274	0.000014
Ag/AlN (60:40)	0.999666	0.000284	0.000015	MWCNTs/Ag/AlN (20:20:60)	0.998667	0.000298	0.000015
Ag/AlN (80:20)	0.999699	0.000295	0.000015	MWCNTs/Ag/AlN (20:40:40)	0.998728	0.000317	0.000015
MWCNTs/AlN (20:80)	0.997973	0.00032	0.000015	MWCNTs/Ag/AlN (20:60:20)	0.999512	0.000287	0.000015
MWCNTs/AlN (40:60)	0.997873	0.00032	0.000015	-			

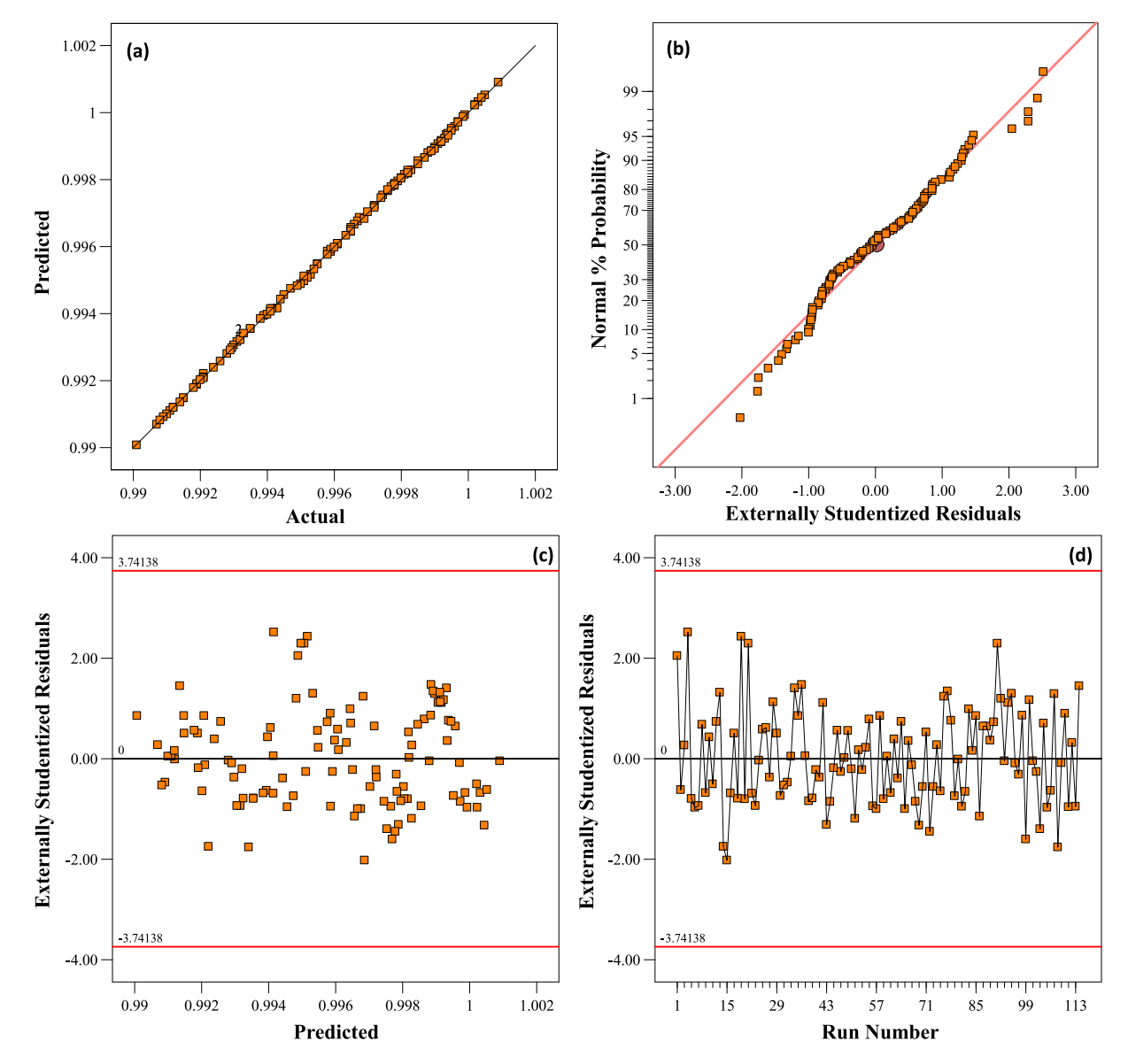


Fig. 37. Diagnostic plots for the ANOVA model of density.

showed that the residuals followed a normal distribution, as the points closely followed the straight line. This observation suggested that the errors were normally distributed, validating one of the key assumptions of ANOVA.

Further examination of the model through the Externally Studentized Residuals vs. Predicted plot revealed no patterns in the residuals, indicating that the model was well-specified without signs of heteroscedasticity. Additionally, the Externally Studentized Residuals vs. Run

Number plot displayed a random distribution of residuals throughout the sequence of data collection, which suggested the absence of time-related trends or autocorrelations that could introduce bias. Taken together, these analyses supported the conclusion that the developed model was both statistically significant and highly predictive, accurately estimating the density of the fluids studied across different temperatures.

6. Cost analysis

Cost analysis plays a crucial role in the development and application of nanofluids, as an increase in performance accompanied by a significant rise in cost is typically undesirable. In this section, we have evaluated and compared the preparation costs of various nanofluids, which include expenses related to nanoparticles, base fluids, and surfactants. However, the costs associated with laboratory resources, such as electricity used during sonication and stirring operations, are not included in this analysis since they remain constant across all samples. Additionally, the labour costs are also omitted for the same reason.

The primary contributor to the overall cost is the price of nanoparticles, underscoring the importance of selecting and optimising these materials carefully. This cost analysis also aims to encourage researchers to design more cost-effective methods for preparing nanofluids while enhancing particle suspension times. The costs for preparing 1000 ml of pure, hybrid, and tri-hybrid nanofluids with a 0.025 vol% concentration have been estimated and are presented in Fig. 38. It is important to note that while the price of MWCNTs is significantly higher than that of silver nanoparticles, the fluids were prepared based on volume percentage rather than weight percentage. This approach required a larger quantity of silver nanoparticles to achieve the same volume fraction in the fluid, resulting in final costs that are nearly the same for both fluids. Consequently, despite MWCNTs having much higher thermal conductivity, the difference in thermal conductivity between the silver and MWCNTs nanofluids was not substantial. However, the cost for silver nanofluids was calculated to be £90.27, while for MWCNTs fluids, it was £89.39. On the other hand, the cost for AlN was much lower at £15.82. The lower cost and better thermal characteristics of AlN in comparison to other nitrides and oxides were the key factors in its selection for this study, particularly for use in combination with silver and MWCNTs to prepare hybrid nanofluids.

The cost of hybrid nanofluids varied depending on the mixing ratio and the specific nanoparticles used. For Ag/AlN hybrids, the cost ranged from £30.17 to £75.38 as the proportion of silver increased from 20 % to

80 %. Similarly, the cost of MWCNTs/AlN hybrids ranged from £30.54 to £74.67, with only minor variations. Since the preparation costs for Ag and MWCNTs nanofluids were nearly identical, the cost of their hybrids also hovered around £90. In the case of tri-hybrid nanofluids, where the MWCNTs content was fixed at 20 % across all samples, the cost varied depending on the proportion of silver, ranging from £45.42 to £75.20. Based on these findings, when cost is given equal importance as thermal performance, the tri-hybrid with a 20/40/40 mixing ratio is the most cost-effective choice. However, in applications where thermal performance is a higher priority, the 20/60/20 tri-hybrid solution is recommended.

Interestingly, some hybrid nanofluids have costs comparable to trihybrids. However, tri-hybrid solutions are often preferred due to their longer-term stability and superior performance in high-flow-rate applications. This balance of cost and performance makes the tri-hybrid options particularly attractive for a wide range of practical applications.

7. Conclusion

This study has comprehensively examined the thermophysical properties of hybrid and tri-hybrid nanofluids composed of MWCNTs, AlN, and Ag, with the goal of optimising their thermal performance, stability, and cost-effectiveness for potential thermal management applications. The findings have highlighted critical aspects of nanofluid formulation, particularly the impact of volumetric ratios, cost considerations, and surfactant selection on the performance of these advanced fluids. Through meticulous experimentation, several key insights were obtained, which are summarised below.

 Among the surfactants evaluated, SDBS demonstrated superior performance in maintaining nanoparticle dispersion across all formulations, contributing to enhanced long-term stability. Additionally, the stability study revealed that hybrid and tri-hybrid nanofluids maintained more stable suspensions over time.

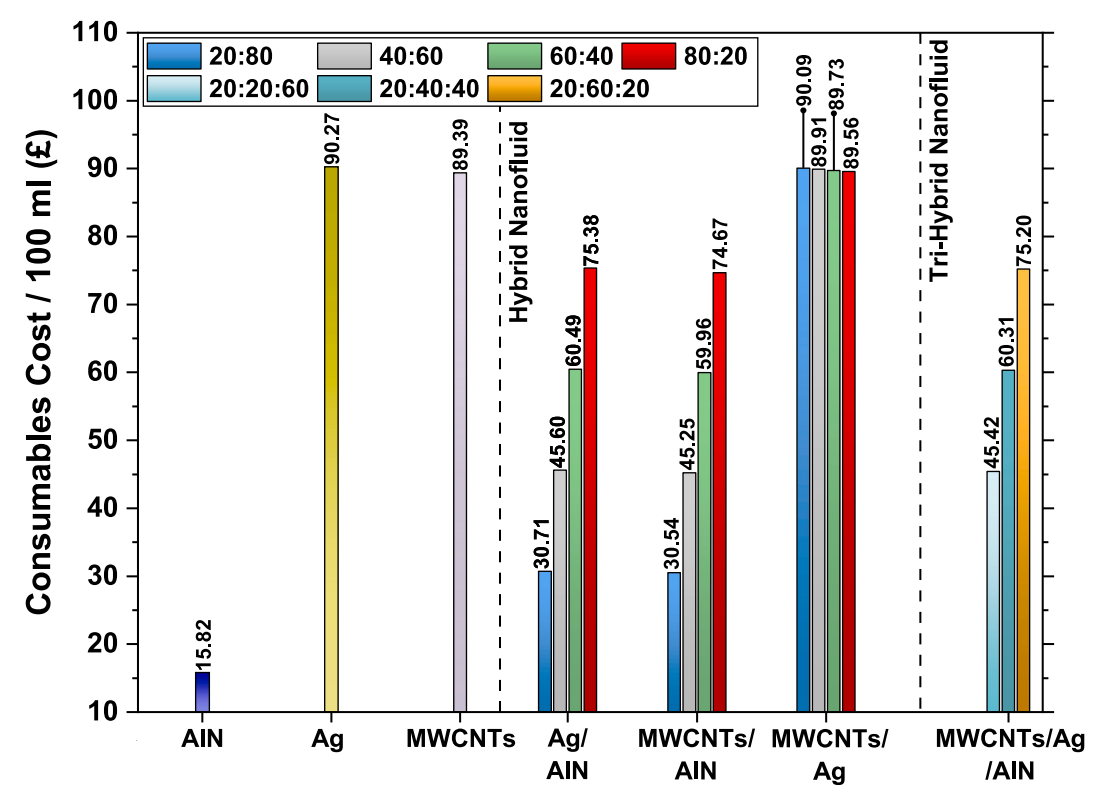


Fig. 38. Estimated costs for preparing 1000 ml of pure, hybrid, and tri-hybrid nanofluids.

- The thermal conductivity of all nanofluid samples increased significantly with temperature, with more pronounced improvements observed beyond 30 °C. Additionally, a substantial increase in thermal conductivity was observed with higher particle concentrations; however, it is crucial to select an appropriate concentration to maintain stability.
- Among mono-nanofluids, MWCNTs showed the highest improvement in thermal conductivity, achieving an 8.566 % increase, followed by silver and AlN with enhancements of 6.948 % and 4.997 %, respectively.
- Hybrid and tri-hybrid nanofluids demonstrated significant enhancements in thermal conductivity. Notably, the MWCNTs/Ag/AlN tri-hybrid nanofluid with a 20/60/20 ratio achieved a thermal conductivity enhancement of 8.14 %, alongside improved stability and acceptable cost, highlighting the synergistic benefits of combining diverse nanoparticles.
- Rheological studies confirmed that nanofluids containing AlN, Ag, and MWCNTs at a concentration of 0.025 vol% exhibited Newtonian behaviour. Their viscosity remained constant across different shear rates, which is a characteristic property of Newtonian fluids.
- Viscosity was found to decrease with increasing temperature across all nanofluid samples, consistent with typical fluid behaviour. However, a rise in nanoparticle concentration led to a proportional increase in viscosity. At temperatures beyond 40 °C, the difference in viscosity values was minimal due to the lower particle concentration, though it could be more significant for fluids prepared with higher concentrations.
- Tri-hybrid nanofluid exhibited the greatest increase in viscosity, which can be attributed to the combined effect of nanoparticles with varying shapes and sizes. Among the pure nanofluids, Ag nanofluid exhibited the highest average percentage increase of 4.43 % in viscosity, followed by AlN at 3.84 % and MWCNTs at 2.89 %. In hybrid nanofluids, the MWCNTs/Ag/AlN ternary formulation with a 20/60/20 ratio showed the most significant viscosity enhancement, with an average increase of 5.55 % compared to water.
- The density of the nanofluids increased with particle loading and decreased with rising temperature. The highest density increase was recorded for Ag nanofluids at 0.24631 %, while the maximum density for hybrid nanofluids was 0.22538 %, observed in the 80/20 Ag/ AlN formulation.
- Cost analysis revealed that although MWCNTs are the most expensive component, their exceptional thermal properties justify their use in smaller fractions, particularly in tri-hybrid configurations. Among the formulations, the tri-hybrid nanofluid with a 20/40/40 ratio emerged as the most cost-effective, providing a balanced approach between performance and economic feasibility. For applications where thermal performance is paramount, the tri-hybrid nanofluid with a 20/60/20 ratio offers the best compromise, despite its higher viscosity and cost.
- Finally, the developed models for predicting the properties as a function of temperature showed exceptional statistical reliability.
 However, to replicate results and enhance predictive accuracy, it is recommended to use particles with the same morphology and consistent preparation techniques.

This study lays the groundwork for further exploration into hybrid and tri-hybrid nanofluids, emphasizing the need for a balanced approach that optimises both performance and cost-effectiveness. Further investigations should explore the long-term stability and thermophysical performance of these nanofluids under dynamic flow and thermal cycling conditions that mimic real-world operating environments, such as those in electronic cooling systems, battery thermal management, or solar thermal collectors. Advanced characterisation techniques like in-situ TEM or SAXS could be employed to monitor nanoparticle dispersion and agglomeration over time. Moreover, machine learning models and optimisation algorithms could be integrated

to predict and fine-tune optimal nanoparticle ratios for targeted applications. The exploration of eco-friendly or biodegradable surfactants and base fluids would also enhance the sustainability of nanofluid applications. Finally, pilot-scale or field-level demonstrations should be conducted to validate the laboratory findings and assess the practical feasibility and cost-effectiveness of deploying these advanced hybrids and tri-hybrid nanofluids in industrial thermal systems.

CRediT authorship contribution statement

Hamza Babar: Writing – original draft, Visualization, Validation, Methodology, Investigation, Formal analysis, Data curation, Conceptualization. Hongwei Wu: Writing – review & editing, Supervision, Funding acquisition. Wenbin Zhang: Writing – review & editing, Supervision, Conceptualization. Muhammad Asim: Writing – review & editing, Supervision. Ali Koşar: Supervision, Methodology, Writing – review & editing.

Declaration of competing interest

The authors declare that they have no known competing financial interests or personal relationships that could have appeared to influence the work reported in this paper.

Acknowledgement

The authors gratefully acknowledge the financial support provided by the Royal Society through the International Exchanges Scheme (Grant No. IES\R3\223052) and the Engineering and Physical Sciences Research Council (EPSRC), United Kingdom (Grant No. EP/X038319/1), under the framework of the Horizon Europe Marie Skłodowska-Curie Actions (MSCA) project (Grant No. 101082394).

Data availability

Data will be made available on request.

References

- V. Rozite, E. Bertoli, B. Reidenbach, Data Centres and Data Transmission Networks. https://www.iea.org/energy-system/buildings/data-centres-and-data-transmission-networks, 2023.
- [2] IEA, Global EV Outlook. https://www.iea.org/reports/global-ev-outlook-202 3/executive-summary, 2023.
- [3] M. Bahiraei, S. Heshmatian, Application of a novel biological nanofluid in a liquid block heat sink for cooling of an electronic processor: thermal performance and irreversibility considerations, Energy Convers. Manag. 149 (2017) 155–167, https://doi.org/10.1016/j.enconman.2017.07.020.
- [4] P. Kumar, D. Chaudhary, P. Varshney, U. Varshney, S.M. Yahya, Y. Rafat, Critical review on battery thermal management and role of nanomaterial in heat transfer enhancement for electrical vehicle application, J. Energy Storage 32 (2020) 102003, https://doi.org/10.1016/j.est.2020.102003.
- [5] S. Khalatbari, P. Jalili, B. Jalili, D.D. Ganji, Investigating the improvement of heat transfer and flow characteristics of hybrid nanofluids: a comprehensive review, Proc. Inst. Mech. Eng. Part E (2025), https://doi.org/10.1177/ 09544089251318785.
- [6] H.W. Xian, N.A.C. Sidik, R. Saidur, Impact of different surfactants and ultrasonication time on the stability and thermophysical properties of hybrid nanofluids, Int. Commun. Heat Mass Transf. 110 (2020) 104389, https://doi.org/ 10.1016/j.icheatmasstransfer.2019.104389.
- [7] A.K. Tiwari, N.S. Pandya, Z. Said, H.F. Öztop, N. Abu-Hamdeh, 4S consideration (synthesis, sonication, surfactant, stability) for the thermal conductivity of CeO2 with MWCNT and water based hybrid nanofluid: an experimental assessment, Colloids Surf. A Physicochem. Eng. Asp. 610 (2021) 125918, https://doi.org/ 10.1016/j.colsurfa.2020.125918.
- [8] H. Babar, H. Wu, W. Zhang, Y. Xie, Harnessing nano-synergy: a comprehensive study of thermophysical characteristics of silver, beryllium oxide, and silicon carbide in hybrid nanofluid formulations, J. Mol. Liq. 414 (2024) 126175, https:// doi.org/10.1016/j.mollig.2024.126175.
- [9] J. Sathish Kumar, G. Senthilkumar, S. Ramachandran, Novel strategy of mixing MgO in CuO/water nanofluid for thermal conductivity improvement: experimental study, Case Stud. Therm. Eng. 52 (2023) 103723, https://doi.org/10.1016/j. csite.2023.103723.

- [10] N.S. Mane, V. Hemadri, S. Tripathi, Exploring the role of biopolymers and surfactants on the electrical conductivity of water-based CuO, Fe3O4, and hybrid nanofluids, J. Dispers. Sci. Technol. 45 (2024) 900–908, https://doi.org/10.1080/ 01932601.203.2186428
- [11] S.A. Adam, X. Ju, Z. Zhang, J. Lin, M.M. Abd El-Samie, C. Xu, Effect of temperature on the stability and optical properties of SiO2-water nanofluids for hybrid photovoltaic/thermal applications, Appl. Therm. Eng. 175 (2020) 115394, https://doi.org/10.1016/j.applthermaleng.2020.115394.
- [12] C. Duan, H. Roshani, P. Jalili, B. Jalili, I. Ahmad, Q.M. Al-Mdallal, P. Zhang, Thermal performance and entropy generation analysis of hybrid nanofluids in a 3D cylindrical microtube: implications for biomedical applications, Case Stud. Therm. Eng. 68 (2025) 105873, https://doi.org/10.1016/j.csite.2025.105873.
- [13] S.H. Hashemi Karouei, S.S.M. Ajarostaghi, M. Gorji-Bandpy, S.R. Hosseini Fard, Laminar heat transfer and fluid flow of two various hybrid nanofluids in a helical double-pipe heat exchanger equipped with an innovative curved conical turbulator, J. Therm. Anal. Calorim. 143 (2021) 1455–1466, https://doi.org/ 10.1007/s10973-020-09425-0.
- [14] V. Kumar, A. Pare, A.K. Tiwari, S.K. Ghosh, Efficacy evaluation of oxide-MWCNT water hybrid nanofluids: an experimental and artificial neural network approach, Colloids Surf. A Physicochem. Eng. Asp. 620 (2021) 126562, https://doi.org/10.1016/j.colsurfa.2021.126562.
- [15] B. Jalili, P.M. Zar, D. Liu, C.-H. Ji, P. Jalili, M.A.H. Abdelmohimen, D.D. Ganji, Thermal study of MHD hybrid nano fluids confined between two parallel sheets: shape factors analysis, Case Stud. Therm. Eng. 63 (2024) 105229, https://doi.org/ 10.1016/j.csite.2024.105229.
- [16] Z. Said, P. Sharma, L. Syam Sundar, A. Afzal, C. Li, Synthesis, stability, thermophysical properties and AI approach for predictive modelling of Fe3O4 coated MWCNT hybrid nanofluids, J. Mol. Liq. 340 (2021) 117291, https://doi. org/10.1016/j.molliq.2021.117291.
- [17] N. Van Eck, L. Waltman, Software survey: VOSviewer, a computer program for bibliometric mapping, Scientometrics 84 (2010) 523–538. https://www.vosvi ewer.com/ (accessed June 14, 2023).
- [18] A. Rehman, S. Yaqub, M. Ali, H. Nazir, N. Shahzad, S. Shakir, R. Liaquat, Z. Said, Effect of surfactants on the stability and thermophysical properties of Al203+TiO2 hybrid nanofluids, J. Mol. Liq. 391 (2023) 123350, https://doi.org/10.1016/j. mollig.2023.123350.
- [19] K. Wusiman, H. Jeong, K. Tulugan, H. Afrianto, H. Chung, Thermal performance of multi-walled carbon nanotubes (MWCNTs) in aqueous suspensions with surfactants SDBS and SDS, Int. Commun. Heat Mass Transf. 41 (2013) 28–33, https://doi.org/ 10.1016/j.icheatmasstransfer.2012.12.002.
- [20] B. Mehta, D. Subhedar, H. Panchal, K.K. Sadasivuni, Stability and thermophysical properties enhancement of Al2O3-water nanofluid using cationic CTAB surfactant, Int. J. Thermofluids 20 (2023) 100410, https://doi.org/10.1016/j. iifr.2023.100410.
- [21] M. Saraswat, R.J. Sengwa, Effects of PVP surfactant on nanosuspension stability and optical, dielectric, and rheological properties of zinc oxide nanoparticles dispersed alcohols mixture based nanofluids, J. Mol. Liq. 385 (2023) 122350, https://doi.org/10.1016/j.mollig.2023.122350.
- [22] G. Yalçın, G. Huminic, A. Huminic, H. Panchal, A.S. Dalkılıç, Investigation on the effect of surfactants on the viscosity of graphite-water-based nanofluids, J. Mol. Liq. 398 (2024) 124197, https://doi.org/10.1016/j.molliq.2024.124197.
- [23] V. Krishna Poloju, V. Khadanga, S. Mukherjee, P. Chandra Mishra, N.F. Aljuwayhel, N. Ali, Thermal conductivity and dispersion properties of SDBS decorated ternary nanofluid: impacts of surfactant inclusion, sonication time and ageing, J. Mol. Liq. 368 (2022) 120832, https://doi.org/10.1016/j.molliq.2022.120832.
- [24] A.O. Borode, N.A. Ahmed, P.A. Olubambi, M. Sharifpur, J.P. Meyer, Effect of various surfactants on the viscosity, thermal and electrical conductivity of graphene nanoplatelets nanofluid, Int. J. Thermophys. 42 (2021) 158, https://doi. org/10.1007/s10765-021-02914-w.
- [25] J. Wang, G. Li, T. Li, M. Zeng, B. Sundén, Effect of various surfactants on stability and thermophysical properties of nanofluids, J. Therm. Anal. Calorim. 143 (2021) 4057–4070, https://doi.org/10.1007/s10973-020-09381-9.
- [26] A.S. Dalkılıç, G. Yalçın, B.Ö. Küçükyıldırım, S. Öztuna, A. Akdoğan Eker, C. Jumpholkul, S. Nakkaew, S. Wongwises, Experimental study on the thermal conductivity of water-based CNT-SiO2 hybrid nanofluids, Int. Commun. Heat Mass Transf. 99 (2018) 18–25, https://doi.org/10.1016/j. icheatmasstransfer.2018.10.002.
- [27] N.N. Esfahani, D. Toghraie, M. Afrand, A new correlation for predicting the thermal conductivity of ZnO–Ag (50%–50%)/water hybrid nanofluid: an experimental study, Powder Technol. 323 (2018) 367–373, https://doi.org/ 10.1016/j.powtec.2017.10.025.
- [28] A. Dezfulizadeh, A. Aghaei, A.H. Joshaghani, M.M. Najafizadeh, An experimental study on dynamic viscosity and thermal conductivity of water-Cu-SiO2-MWCNT ternary hybrid nanofluid and the development of practical correlations, Powder Technol. 389 (2021) 215–234, https://doi.org/10.1016/j.powtec.2021.05.029.
- [29] H. Adun, D. Kavaz, M. Dagbasi, H. Umar, I. Wole-Osho, An experimental investigation of thermal conductivity and dynamic viscosity of Al2O3-ZnO-Fe3O4 ternary hybrid nanofluid and development of machine learning model, Powder Technol. 394 (2021) 1121–1140, https://doi.org/10.1016/j.powtec.2021.09.039.
- [30] M. Sepehrnia, A. Shahsavar, H. Maleki, A. Moradi, Experimental study on the dynamic viscosity of hydraulic oil HLP 68- Fe3O4-TiO2-GO ternary hybrid nanofluid and modeling utilizing machine learning technique, J. Taiwan Inst. Chem. Eng. 145 (2023) 104841, https://doi.org/10.1016/j.jtice.2023.104841.
- [31] A.M. Ajeena, I. Farkas, P. Víg, Characterization, rheological behaviour, and dynamic viscosity of ZrO2-SiC (50–50)/DW hybrid nanofluid under different temperatures and solid volume fractions: an experimental study and proposing a

- new correlation, Powder Technol. 431 (2024) 119069, https://doi.org/10.1016/j.
- [32] M. Qu, D.J. Jasim, A. Alizadeh, S. Ali Eftekhari, N. Nasajpour-Esfahani, H. Zekri, S. Salahshour, D. Toghraie, A new model for viscosity prediction for silica-alumina-MWCNT/water hybrid nanofluid using nonlinear curve fitting, engineering science and technology, an, Int. J. 50 (2024) 101604, https://doi.org/10.1016/j.iestch.2023.101604
- [33] R.K. Mande, S. Rama Raju, K.P.V.K. Varma, Thermophysical properties of TiO2/ CuO hybrid nanofluids for heat transfer applications, Mater. Res. Innov. 28 (2024) 83–93, https://doi.org/10.1080/14328917.2023.2230016.
- [34] A. Ghafouri, D. Toghraie, Experimental study on thermal conductivity of SiC-ZnO/ ethylene glycol hybrid nanofluid: proposing an optimized multivariate correlation, J. Taiwan Inst. Chem. Eng. 148 (2023) 104824, https://doi.org/10.1016/j. itice.2023.104824.
- [35] H. Babar, H.M. Ali, Towards hybrid nanofluids: preparation, thermophysical properties, applications, and challenges, J. Mol. Liq. 281 (2019) 598–633, https://doi.org/10.1016/j.mollig.2019.02.102.
- [36] A.A. Hussien, M.Z. Abdullah, N.M. Yusop, M.A. Al-Nimr, M.A. Atieh, M. Mehrali, Experiment on forced convective heat transfer enhancement using MWCNTs/GNPs hybrid nanofluid and mini-tube, Int. J. Heat Mass Transf. 115 (2017) 1121–1131, https://doi.org/10.1016/j.ijheatmasstransfer.2017.08.120
- [37] A.S. Abdelrazik, R. Saidur, F.A. Al-Sulaiman, Investigation of the performance of a hybrid PV/thermal system using water/silver nanofluid-based optical filter, Energy 215 (2021) 119172, https://doi.org/10.1016/j.energy.2020.119172.
- [38] M. Javidan, M. Gorji-Bandpy, A. Al-Araji, Investigation and simulation of parabolic trough collector with the presence of hybrid nanofluid in the finned receiver tube, Theor. Appl. Mech. Lett. 13 (2023) 100465, https://doi.org/10.1016/j. taml.2023.100465.
- [39] J. Wu, J. Zhao, J. Lei, B. Liu, Effectiveness of nanofluid on improving the performance of microchannel heat sink, Appl. Therm. Eng. 101 (2016) 402–412, https://doi.org/10.1016/j.applthermaleng.2016.01.114.
- [40] G. Żyła, J. Fal, Experimental studies on viscosity, thermal and electrical conductivity of aluminum nitride–ethylene glycol (AlN–EG) nanofluids, Thermochim. Acta 637 (2016) 11–16, https://doi.org/10.1016/j.tca.2016.05.006.
- [41] K. Kulthanan, P. Nuchkull, S. Varothai, The pH of water from various sources: an overview for recommendation for patients with atopic dermatitis, Asia Pac, Allergy 3 (2013) 155–160, https://doi.org/10.5415/apallergy.2013.3.3.155.
- [42] S. Ghosh, S. Subudhi, Developments in fuel cells and electrochemical batteries using nanoparticles and nanofluids, Energy Storage 4 (2022), https://doi.org/ 10.1002/est2.288.
- [43] Y. Feng, M. Yu, M. Meng, L. Liu, D. Rao, Cu, N codoped carbon nanosheets encapsulating ultrasmall Cu nanoparticles for enhancing selective 1,2-propanediol oxidation, J. Energy Chem. 91 (2024) 27–35, https://doi.org/10.1016/j. iechem. 2023.11.035
- [44] P.B. Maheshwary, C.C. Handa, K.R. Nemade, A comprehensive study of effect of concentration, particle size and particle shape on thermal conductivity of titania/ water based nanofluid, Appl. Therm. Eng. 119 (2017) 79–88, https://doi.org/ 10.1016/j.applthermaleng.2017.03.054.
- [45] H.-C. Hsu, G.-M. Hsu, Y. Lai, Z.C. Feng, S.-Y. Tseng, A. Lundskog, U. Forsberg, E. Janzén, K.-H. Chen, L.-C. Chen, Polarized and diameter-dependent Raman scattering from individual aluminum nitride nanowires: the antenna and cavity effects, Appl. Phys. Lett. 101 (2012), https://doi.org/10.1063/1.4753798.
- [46] M.A. Hayat, Y. Yang, L. Li, M. Bevilacqua, Y. Chen, Preparation and thermophysical characterisation analysis of potential nano-phase transition materials for thermal energy storage applications, J. Mol. Liq. 376 (2023) 121464, https://doi.org/10.1016/j.molliq.2023.121464.
- [47] R. Atchudan, A. Pandurangan, J. Joo, Effects of nanofillers on the thermomechanical properties and chemical resistivity of epoxy nanocomposites, J. Nanosci. Nanotechnol. 15 (2015) 4255-4267, https://doi.org/10.1166/inn.2015.9706
- [48] K.R. Kumar, A.H. Shaik, Synthesis, thermophysical characterization and thermal performance analysis of novel Cu-MXene hybrid nanofluids for efficient coolant applications, RSC Adv. 13 (2023) 29536–29560, https://doi.org/10.1039/ D3RA05429B.
- [49] A.G.N. Sofiah, M. Samykano, K. Sudhakar, Z. Said, A.K. Pandey, Copper oxide/ polyaniline nanocomposites-blended in palm oil hybrid nanofluid: Thermophysical behavior evaluation, J. Mol. Liq. 375 (2023) 121303, https://doi.org/10.1016/j. mollio.2023.121303.
- [50] R. Tahmasebi-Boldaji, S. Ghazanfari, H. Rajabi Kuyakhi, N. Tahmasebi Boldaji, M. Torki, Experimental investigation of ultrasonic cycle/magnetic stirrer (UC/MS) effect on water/α -AI2O3 nanofluid stability and thermal conductivity and its ANFIS/PSO modeling, Res. Eng. Des. 19 (2023) 101284, https://doi.org/10.1016/ i.ripagg. 2023. 101284
- [51] J. Sundberg, G.A. Innova, L. Hälldahl, Comparison of Thermal Properties Measured by Different Methods, Swedish Nuclear Fuel and Waste Management Co (No. SKB-R-03-18). www.skb.se, 2003.
- [52] P. Kumar Kanti, P. Sharma, K.V. Sharma, M.P. Maiya, The effect of pH on stability and thermal performance of graphene oxide and copper oxide hybrid nanofluids for heat transfer applications: application of novel machine learning technique, J. Energy Chem. 82 (2023) 359–374, https://doi.org/10.1016/j. iechem. 2023 d4 001
- [53] Z. Said, L.S. Sundar, A.K. Tiwari, H.M. Ali, M. Sheikholeslami, E. Bellos, H. Babar, Recent advances on the fundamental physical phenomena behind stability, dynamic motion, thermophysical properties, heat transport, applications, and challenges of nanofluids, Phys. Rep. 946 (2022) 1–94, https://doi.org/10.1016/j. physrep.2021.07.002.

- [54] H. Babar, H. Wu, W. Zhang, T.R. Shah, D. McCluskey, C. Zhou, The promise of nanofluids: a bibliometric journey through advanced heat transfer fluids in heat exchanger tubes, Adv. Colloid Interf. Sci. 325 (2024) 103112, https://doi.org/ 10.1016/j.cis.2024.103112.
- [55] V.V. Wanatasanappan, M.Z. Abdullah, P. Gunnasegaran, Thermophysical properties of Al2O3-CuO hybrid nanofluid at different nanoparticle mixture ratio: an experimental approach, J. Mol. Liq. 313 (2020) 113458, https://doi.org/ 10.1016/j.molliq.2020.113458.
- [56] M. Hemmat Esfe, S. Saedodin, M. Biglari, H. Rostamian, Experimental investigation of thermal conductivity of CNTs-Al2O3/water: a statistical approach, Int. Commun. Heat Mass Transf. 69 (2015) 29–33, https://doi.org/10.1016/j. icheatmasstransfer.2015.10.005.
- [57] K. Ajith, A.S. Pillai, I.V. Muthu Vijayan Enoch, M. Sharifpur, A.B. Solomon, J. P. Meyer, Effect of the non-electrically conductive spindle on the viscosity measurements of nanofluids subjected to the magnetic field, Colloids Surf. A Physicochem. Eng. Asp. 628 (2021), https://doi.org/10.1016/j.colsurfa.2021.127252.
- [58] IAPWS, R12–08: Viscosity of Ordinary Water. http://www.iapws.org/relg uide/viscosity.html, 2018.
- [59] M. Tawalbel, I. Shomope, A. Al-Othman, Comprehensive review on non-Newtonian nanofluids, preparation, characterization, and applications, Int. J. Thermofluids 22 (2024), https://doi.org/10.1016/j.ijft.2024.100705.